CONTROLLER DESIGN FOR A UNIVERSAL POWER INPUT BI-DIRECTIONAL BATTERY CHARGER FOR PLUG-IN ELECTRIC AND HYBRID ELECTRIC VEHICLES

EMILIO DAL SANTO

DIPARTIMENTO DI INGEGNERIA DELL'INFORMAZIONE

Corso di Laurea Magistrale in Ingegneria dell'Automazione
Facolta' di Ingegneria
Universita' degli Studi di Padova

Relatore Prof. Silverio Bolognani

Padova
Marzo 2011

SOMMARIO

I convertitori per l'alimentazione di veicoli elettrici o ibridi Plug-in, (Plug-in Hybrid Electric Vehicle, PHEV), richiedono alta potenza ed un flusso di corrente bidirezionale, con un ampio range di voltaggio in ingresso. Questa tesi presenta la progettazione di un carica batterie ideato per operare con un ingresso universale. Il convertitore AC/DC e' implementato usando una tipica struttura a due stadi. Il primo stadio include un convertitore boost con *Power Factor Correction* (PFC), per soddisfare i requisiti sul fattore di potenza e per migliorare l'efficienza del sistema. Il secondo stage e' costituito da un convertitore buck che e' direttamente collegato alle batterie. Il controllo di questo dispositivo e' implementato usando un controllore PID multi-loop per il raddrizzatore PFC, tramite il controllo *average mode* della corrente. Un semplice controllore PID e' implementato nel convertitore DC/DC ed entrambi utilizzano uno switching PWM. Viene inoltre presentato un nuovo approccio digitale per eliminare il controllore feed-forward dallo schema convenzionale, che semplifica ulteriormente la strategia di controllo. Il controllore digitale del sistema di potenza usa una strategia di switching binaria per i transistor. Essi switchano in base al segno dell'errore, usato come segnale di controllo. Una valutazione comprensiva del convertitore e' condotta per analizzare le performance e la robustezza del controllore in termini di stabilita'. L'analisi FFT e le curve *phase-plane* sono usate per derivare le regioni di stabilita' del circuito. Alcune condizioni di funzionamento instabili vengono individuate per migliorare il progetto.

TABLE OF CONTENTS

LIST OF TABLES

LIST OF FIGURES

ABSTRACT

Power electronic converters in Plug-in Hybrid Electric Vehicles (PHEV) and Electric Vehicles (EV) require high power and bidirectional power flow capabilities, with wide input voltage range. This thesis presents a battery charger designed to operate over a universal input. The converter is implemented using a basic two-stage structure. The first stage includes a Power Factor Correction (PFC) Boost converter to meet power factor requirements and improve the efficiency of the system. The second stage is comprised of a buck converter which is directly connected to the battery pack. Control of this converter has been implemented using a multi-loop PID controller for the PFC rectifier using average current control mode. A simple PID controller is implemented in the DC/DC converter and they both use Pulse Width Modulation switching. In addition, this thesis presents a new digital approach to eliminate the feed-forward controller from the conventional topology, which further simplifies the control strategy. Digital control of a power electronic system uses a binary switching strategy for the switches. High-power semiconductors switch based on the sign of the error which is used as control signal. A thorough evaluation of the converter has been conducted to assess the performance and robustness of the controller in terms of stability. FFT analysis and phase-plane plots are used in order to derive stability maps for the circuit. Unstable conditions are found and system design is improved accordingly.

CHAPTER 1

INTRODUCTION

In recent years, Hybrid Electric Vehicles (HEV) and Plug-in Hybrid Electric Vehicles (PHEV) have attracted more and more attention of automotive industry. Hybrid vehicles have several advantages over conventional car given their efficiency and capability of a better fuel economy. PHEVs combine the Internal Combustion Engine (ICE) with the ability of charging and discharging a storage pack. It can use the electricity stored while the battery charge is in a high state, allowing an all-electric range. At the same time PHEV provides a fuel tank to be used when an extended driving range is needed.

A battery charger is essential for the PHEV functioning. This power electronic circuit has two main functions. It charges the battery with a proper State Of Charge (SOC) in *recharge mode* of operation. The other operation mode is called *inverter mode*, which means that the battery energy is transferred back to the grid. Also supplying AC electricity for on-board loads is possible. Therefore the battery charger consists in a multi-converter system capable of bi-directional power flow.

In multi-converter systems many power electronic converters such as AC/DC rectifiers, DC/DC choppers, and DC/AC inverters are used as sources, loads, or distribution networks to provide power in different magnitudes and forms. Recent advancements in semi-conductor technology have enhanced the use of these converters in Plug-In Hybrid Vehicles applications [57]. A multi-stage conversion is considered a common choice for a battery charger circuit in [29] and [22]. It includes a rectification stage and is usually cascaded with an output regulator.

Several bi-directional AC/DC converter topologies can be used as the PHEV battery charger [38]. The specific configuration chosen depends on the requirement

of the applications in terms of efficiency, reliability, cost, volume and weight. Two main strategies involve an AC/DC bi-directional converter which can be separated from the driving system. The other one combines the motor driving inverter with the converter as an integrated PHEV motor driving system. Several research papers have been written on the design and the analysis of the converters, especially on a stand-alone basis [73].

Basic structure consists in the cascade of a AC/DC rectifier and a DC/DC converter placed between the battery and the high voltage bus. This thesis includes an example of a bi-directional circuit that can be used with Plug-in Hybrid Electric Vehicles. These power electronic circuits can be also integrated with existing gasoline or electric vehicles to provide plug-in features.

Control circuits also represent a fundamental component of considered system. It is responsible to provide a regulated and flat current at the output to charge the battery pack. Power Factor Regulation also needs to be done for the input current in order to maximize the efficiency of the system. A new control approach is analyzed with the goal to simplify the hardware structure. In fact, classical analog control techniques need a complicated implementation. It usually consists in a multi-loop controller for the PFC circuit, including a feed-forward compensator [26]. DC/DC converter stage on the other hand uses only a single PID regulator. Therefore a new approach needs to be developed in order to simplify the design of the control circuit while assuring good performances and stable operation. A novel digital control provides a reliable and robust solution for this application.

Stable behavior of the system has to be assured by the controller. Circuit design and the choice of critical components are responsible for the good performances in terms of stability. Whereas a separated stability analysis is usually conducted for each converter stage, a unified approach is preferable. Complete systems stability

analysis has to be performed accordingly to some practical criteria.

A stable system with desired response is obtained with the use of the novel digital controller. Performed research work results to be essential to provide a safe and reliable system. Its stable and sustainable operation are of primary importance for critical power electronic circuits such as in Plug-in Hybrid Electric Vehicles.

This thesis has been organized as follows. In the second chapter, a brief introduction on the application and on its recent developments has been done. PHEV concept is introduced and standard control methods are explained. A complete literature overview is provided on the most significant research topics that have been conducted. Power electronic converters design is analyzed and various control strategies are reviewed, considering their performances and robustness. Importance of the bi-directional multi-converter battery charge is underlined and various configurations are presented.

The third chapter describes in details the circuit adopted for the battery charger application. A complete analysis is done for the components of each converter as well as for the overall circuits. Buck converter and Boost converter are combined together in order to obtain the Buck-Boost topology and its bi-directional version. A Power Factor Correction circuit is developed to meet stringent requirements of this application. Its bi-directional version is then combined together with the DC/DC converter in the overall model. A two-stage bi-directional battery charger is then described and its differential equations are derived. Parametrical models are derived and different mathematical representations of the circuit are provided. The state space model of combined circuit is used in this thesis as the primary analysis tool to investigate the control design and the stability of the system.

Chapter four introduces a new approach in the control strategy involving a

digital design. Digital control techniques are analyzed and their advantages over analog regulators are shown. Digital control takes advantage of its flexible structure and of its ease of implementation in modern integrated circuits. A novel approach is here presented and its performances are shown. A detailed comparison with the classical PID regulator is also performed. Related issues and practical solutions, along with other possible implementations are presented for the control design.

In chapter five, a detailed stability analysis is presented. Classical tools are used in order to investigate the stability of the system through a practical approach. Instability conditions are described and detected in the operating conditions of the circuit. Unstable regions are identified with respect to circuits critical components values. Circuit design and the choice of critical components are thus explained with the use of stability analysis tools. The performance of the new controller design is compared with the classical analog control in terms of stability. Robustness of the controller is investigated through the simulation of a variation in the input voltage or in the load, and its performances are commented.

Chapter six discusses obtained results showing all the advantages of proposed configuration. Analysis results are explained and summarized in this chapter. Need for future works is discussed, including a further simplification in the controller. Also a mathematical confirmation of practical results obtained has to be done. Derived mathematical model in all its different configurations can be adopted for a more rigorous stability analysis.

CHAPTER 2
AN OVERVIEW ON PHEV POWER ELECTRONIC CONVERTERS

Primarily due to an increasing environmental consciousness and a fuel price lift over the last few years, Plug-in Hybrid Electric Vehicle market and research interest has widely grown. Plug-in Hybrid Electric Vehicles are vehicles that combine an internal combustion engine and an electric operating energy system, including batteries and power electronics circuits. In particular, two specific and fundamental circuits have been analyzed and will be modeled in this thesis, the AC/DC inverter and the DC/DC converter, placed between the external universal AC outlet and the battery pack. Integrated converters need to be bi-directional, in order to let the energy flow in either direction. Electrical energy can be either stored to the battery pack, from an external power supply or through regenerative braking, or used to supply power to an electrical motor or on board devices.

A thorough research has been conducted on these topics, including design considerations and simulations of single phase bi-directional AC/DC inverter with boost Power Factor Correction system, bi-directional DC/DC switching converters and battery evaluation, suitable for high power Plug-in Hybrid Electric Vehicle applications.

2.1 Plug-in Hybrid Electric Vehicle

Plug-in hybrid-electric vehicles have recently emerged as a promising technology that uses electricity to displace a significant fraction of petroleum consumption.

A plug-in hybrid electric vehicle (PHEV) is a hybrid vehicle with the ability to recharge its energy storage system with electricity from an off-board source, such as the electric utility grid. Similarly to traditional hybrid electric vehicles, it has both an electric motor and an internal combustion engine. The vehicle can then drive in a charge-depleting (CD) mode that reduces the system batteries' state-of-

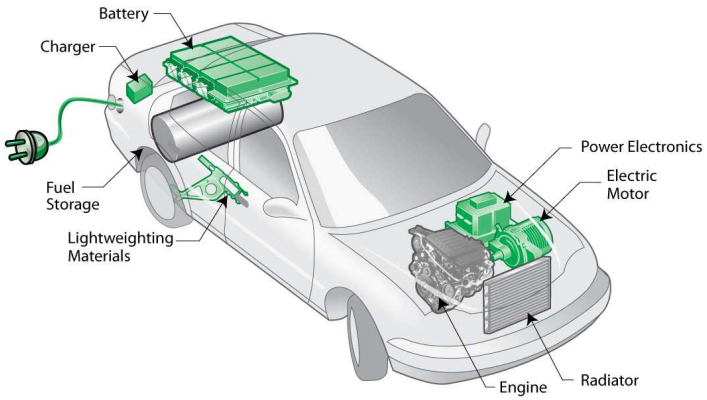

Figure 2.1. Plug-in Hybrid Electric Vehicle schematic view, picture courtesy of Argonne National Laboratory.

charge (SOC), thereby using electricity to displace liquid fuel that would otherwise be consumed. This liquid fuel is typically petroleum (gasoline or diesel), although PHEVs can also use alternatives such as biofuels or hydrogen [38]. PHEV batteries typically have larger capacity than those in HEVs so as to increase the potential for petroleum displacement and all-electric range capabilities.

Compared to conventional vehicles, PHEVs can reduce air pollution, minimize dependence on petroleum and fossil fuels, and lower greenhouse gas emissions that contribute to global warming. In fact, PHEVs can avoid use of any fossil fuel during their all-electric range if their batteries are charged from nuclear or renewable sources of energy. In addition to reducing gasoline consumption, they have the potential to also reduce total energy expenses. Existing commercial hybrid vehicles have proven to be successful components of the transportation system in the US and abroad. Plug-in hybrid electric vehicles (PHEV) can contribute significantly to transportation system efficiency by introducing vehicles that, within a limited range, can operate entirely in an electric mode and be powered by the electricity grid. Conventional Hybrid Electric Vehicles (HEVs) are already starting to create great benefits to US energy including consumption and security. Based on EPA data, the most energy

efficient existing hybrids cut gasoline consumption by around 40 percent compared with similar conventional cars. But PHEVs typically replace half of the remaining gasoline consumption with electricity. Thus PHEVs could reduce the consumption of liquid fuels by at least 70 percent compared with conventional cars.

One of the basic yet important components of a PHEV is its drive train, which include the electrical motor drive, storage device (battery pack), control electronics, inverter and battery charging circuit. In particular, the power electronic converter is responsible of the power flow from the electrical source to the load and vice versa, allowing the charging and the discharging of the battery. This basic component will be here analyzed in details, and an efficient control system will be designed and discussed.

Plug-in Hybrid Electric Vehicles and electric cars may allow for more efficient use of existing sources of electric energy, which most of the time is unused or is available as an operating reserve of power in the storage system. This assumes that vehicles are charged primarily during off peak periods, or equipped with technology to shut off charging during periods of peak demand. Another advantage of a plug-in vehicle is their potential ability to help the grid during peak loads. This is accomplished with vehicle-to-grid technology chargers [57]. Such vehicles take advantage of excess battery capacity to send power back into the grid and then recharge during off peak times using cheaper power. Such vehicles are actually advantageous to utilities as well as their owners. Even if such vehicles mat led to an increase in the use of night time electricity they would also out electricity demand which is typically higher in the day time. This would represent a greater return on capital for electricity infrastructure.

2.2 Bi-directional Converters

Bidirectional converters are nowadays widely used in various applications, and are among the most studied Power Electronic's circuits. Applications such as electric vehicles, photovoltaic systems, UPS power supplies, general battery based storage systems and various industrial fields require the development of bi-directional converters in order to allow power flow in either direction. They are usually employed as interface circuits for the different voltage level buses and have several advantages. Among all, saving space, reduction of weight and cost of the power systems with respect to standard unidirectional circuits. One of the most common applications is a battery charger circuit, in which both charging (i.e. energy storage), and discharging (energy consumption) methods are implemented, through bi-directional power conversion. Various topologies have been studied, accordingly to specific requirements, based on power capabilities, isolation, input/output relations and conversion type, number of stages and phases.

Unidirectional converters can be classified into two basic categories, according to voltage conversion type, DC/DC converter and the AC/DC converter, respectively including a DC voltage power source, or an AC voltage input, and providing a different output value of DC voltage. Classic topologies include Buck DC/DC converters, in which the output voltage is smaller than the input value, boost circuit in which output voltage is greater than the input, and buck-boost converters, in which the output can be either smaller or greater than the input. Similarly AC rectification can be made, through buck rectifiers or boost rectifiers. Bi-directional power flow requires those standard circuits to be modified to accommodate two alternate power sources and loads and bi-directional operations, thus using DC/DC bi-directional buck-boost converter and buck-boost AC/DC rectifiers. These two basic topologies can be also combined together in order to obtain a multiple stage converter, usually

using a cascaded converter system. Whereas unidirectional circuits have been widely discussed, bi-directional circuits still form an active research field [30].

In the cases where isolation is required, most of the existing bi-directional converters are of the flyback-forward topologies [11]. These buck and boost derived converters include a transformer in the circuit which provides electrical isolation between the input and the output ports. Built in transformers electrically isolate the input of the converter from its output. Not only they owe all the advantages of high frequency operation, small size and weight of the transformer, but also provide more flexibility in an eventual multiple output contexts [63]. In fact isolated topology allows multi-inputs and multi-outputs configurations using multi-winding transformers that connect multiple sources having different voltage levels, or give a greater flexibility in outputs.

For high-efficiency and high-power applications such as PHEVs, which do not require magnetic coupling, standard Bi-directional switching conversion is adopted. In such systems the load is directly connected to the grid through a conversion circuit.

Researchers have analyzed several PWM switching techniques, to eliminate transition responses and to provide soft-switching [56] using auxiliary and complex circuits, in order to increase the system's overall efficiency. Moreover, all these switching converters can provide voltage regulation as well as protection in case of power outages. In addition they also show excellent performance in terms of suppressing incoming line transient and harmonic disturbances.

2.3 AC/DC Converters

The first stage of the power electronic system for PHEV applications consists in the PWM Rectifier circuit with Power Factor Correction (PFC). This classic switching converter is mainly studied in its unidirectional topology [62] for standard

applications, to provide highly stable DC voltage at the output while maintaining a high power factor at the input. This converter is extremely useful in several power conversion devices [55] and also meets quality specifications and guidelines to regulate power quality. One of main issues of non-power factor corrected circuits is the harmonic distortion that is injected back into the mains power line. Furthermore in the United States and Europe, Federal Communications Commission (FCC) and European Association for Electrical, Electronic, and Information Technologies, have lately worked together to introduce a series of strict standards to govern conducted-noise emissions and maximum conducted noise limits. For this reason an active control circuit needs to be implemented.

PWM unidirectional inverter includes a diode rectifier circuit at the input, to convert sinusoidal $90 - 240\,VAC$, $50 - 60\,Hz$ universal voltage input into a DC rectified voltage waveform. AC/DC circuit also requires a switching boost converter, which regulates output voltage to an almost constant value, higher than the input. An inverter is a device that converts DC current from the output of DC/DC converter or the battery into AC which can be used for electric motor drives, and vice versa. It is typically comprised of a power module including high power semiconductor devices with high current capabilities as BJTs or MOSFETs, sensors, filters and a control system that regulates the switching scheme.

Considering the specific PHEV requirements, where power is drawn from the AC side to feed the battery, DC rectified power may also be used for the electrical motor or the on board electrical system, as well for vehicle-to-grid applications. For this specific use a bi-directional circuit needs to be chosen, and furthermore the bridge diode rectifier is modified into an H-bridge configuration, for power reversal capabilities. The presence of current harmonics results in several problems, and reduces power losses and decrease efficiency. Thus the current drawn from the input

inductance needs to be shaped, by only a scaling factor of the AC voltage waveform. A closed loop control [64] can be implemented as before using a voltage control loop, with voltage feed-forward compensator. It thus generates the constant output signal, while an inner current shaping regulator generates a near sinusoidal current waveform.

Circuit design based on recent results for High Current Battery Chargers for PHEVs [44] requires a calculated choice of critical components such as the inductor, based on theoretical analysis which is verifies by simulations results of this specific circuit.

Several control strategies and topologies have been studied in [7] and [28] and researchers have attempted to obtain desired performance of the system and suitable waveforms for input current and output voltage in standard operating conditions.

Furthermore a deep analysis is done for the performance of the converter, emphasizing input and output waveforms and improvements due to an appropriate design or control. Faulty conditions and their effects on the shape of the waveforms are then studied and concretized in the design of more robust control system and fault tolerant circuit.

2.4 DC/DC Converters

DC/DC bi-directional converter forms another basic circuit for PHEV chargers. This converter requires high power capabilities and works as a Buck-Boost topology, as mentioned. Its bi-directional energy flow allows also both the charging of the battery pack, and its discharge through the opposite direction, supplying energy back to the system.

It has a simple structure that is derived from basic Buck and Boost topologies, which are as now well-known and suited for this kind of applications. PWM switching converter is adapted for high power handling and simply in a cascade configuration

with the AC/DC rectifier explained above. Bi-directional buck-boost converter works as a buck circuit, producing an almost constant output voltage across the battery, reducing high input voltage from the inverter stage. In the opposite direction, with energy flowing from the load to the input side, it operates as a boost converter thus increasing the voltage and allowing battery discharge.

Modeling difficulties which make space state differential equations derivation quite complicated are related to non-linear and time varying nature of switching converters. Time-variant matrix structure, represented in the scheme of figure 2.2, may requires the use of Space State Averaging technique, in order to eliminate the time dependence.

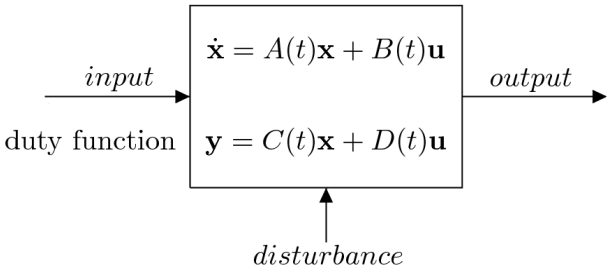

Figure 2.2. Non-linear time-invariant state space scheme.

In this thesis, functioning of this converter is analyzed and differential equations of its space state model are derived in order to simulate its behavior using MATLAB®. As for the other converters, modeling of the converter and simulation are indispensable tools. They are used to investigate further circuit responses under specific conditions.

2.5 Battery Model

One of the most important components of the power electronic circuit in PHEV drive trains are batteries, which are connected at the DC side output of the converter. Battery packs are portable sources of electrical energy that can be converted to me-

chanical energy by the electric motor. Similarly stored power can be used to feed on-board electrical equipment such as electric power steering, air conditioning system, light, pumps etc. There are many types of batteries specifically suited for Hybrid Electric Vehicle applications, including Nickel Iron, Nickel Cadmium, Nickel Metal Hydride, Lithium Polymer and other metal-air batteries.

Many factors characterize battery quality and specific performance criteria, and form interesting research topics, including: energy density, specific power, typical voltage, Ampere hour efficiency, energy efficiency, commercial availability, cost, operating temperature, self-discharge rates, life cycles and physical duration. Several studies are now focusing on developing a detailed model for a battery pack [10]. These researches involve consideration on the variation of battery load with respect to its temperature and its state of charge, realistic charge and discharge rates, analyzing battery geometry, optimum temperature of operation, along with suitable charging methods.

In this thesis a very simple model of battery is used, considering an ideal series of a DC voltage generator and a resistance. Other following research work will further investigate the modeling of a battery pack specifically suited for this high current charger.

2.6 Design Consideration and Modeling

Several papers have addressed design considerations for PHEVs' battery chargers, including practical comparative evaluations of different cascaded configurations. In standard literature, the two stages of system have been often studied separately and have led to a partial analysis of stability issues. In fact, many articles have considered the cascaded DC/DC converter for output voltage regulation as an equivalent resistive load, which dissipates the same power. Due to a complex interaction between

these two circuits, the dynamic behavior of this nonlinear system and stability issues need a thorough investigation.

In terms of stability, the operation of overall circuit results more restricted than that for PFC circuit with a constant resistive load, and further considerations are to be done. A new controller design has to be developed according to analysis results. The effects of the interaction between the two stages, shown in [24] are verified for this model. In fact, the DC/DC converter stage represents a constant power load, equivalent to a negative resistance seen from the PFC stage only when its output is perfectly regulated. In practice, since the PFC Boost regulator - is almost always cascaded with a voltage regulator - especially for medium to high power ranges, it is useful consider the overall cascaded structure of the power supply. Another particularly important issue is the choice of inductive and capacitive components in the circuits, including the AC side inductor, bi-directional buck-boost inductor and output capacitors.

This thesis considers the development of a converter capable of operating for universal voltage input. This range is defined nominally from $90\,V$ to $240\,V$ and a constant battery voltage of $48\,V$. It must be noted that this choice leads to some important considerations on the value of the DC bus voltage level. Maximum intermediate DC bus voltage level is set to $400\,V$ between the PFC rectifier and the DC/DC converter. This choice along with the modulation index calculation, which has been widely discussed in literature [75], maximizes overall system efficiency.

Further design specifications along with the ratings of circuit components consider both mathematical and a practical approach [3], based on the investigation of the performances of the circuit. Values of critical components have been evaluated in order to optimize the system response as well as its robustness, noise immunity and stability.

2.7 Control Techniques

One of the most important topics in the design is the control circuit, involving both the bi-directional PFC inverter and the DC/DC converter, to be robust and fault-tolerant. A simple yet effective typology of controllers is presented in this design using a Proportional, Integral and Derivative (PID) regulator. This control strategy assures desired response while providing quick tuning capabilities and a not very complex structure.

The PFC converter circuit uses a more complex control algorithm, including a few different regulators loops. This is due to its need of simultaneously regulate the output DC voltage and shaping input current in order to correct the power factor. In this circuit the external control loop is designed for voltage regulation. DC reference and actual sensed signal are used as inputs to produce a control output such that the DC value remains constant regardless variations of the load, supplied AC voltage or output current drawn. The voltage controller also produces a reference signal for the inner current loop, which controls the shape of input current. Output voltage is controlled by a simple PI regulator, in which a signal proportional to voltage error and to its integral is generated. When the input of the voltage error compensator increases, signal generated by PWM circuit also increases. Therefore for an increase in output terminal voltage, the inner current regulation loop reduces the current proportionally to keep the input power constant. In fact, this internal current error compensator uses sensed current and regulated voltage signal to determine the reference. Control loop error is thus determined by the difference between calculated reference signal and actual inductor current and is processed by a PID controller. This regulation system forces the inductor current to follow the reference sinusoidal waveform.

It must be mentioned that in the control strategy implemented, the current control loop should run at a much faster rate compared to the voltage loop in order

to correctly shape the input sinusoidal waveform and thus requires a relatively small bandwidth. The current controller produces a signal which is then elaborated through a PWM generator, in order to produce the appropriate duty cycle value for the gate signal of circuit MOSFETs. If the voltage decreases, also reference signal for input current decreases, thus resulting in a lower drawn power. However, in order to maintain a constant output power in correspondence of a reduced input, current reference should proportionally decrease [7]. A voltage feed-forward compensator maintains the output power constant and determined only by the load, regardless of input variations. Its operating principle averages the input voltage and divides input reference current by its squared value.

Control of bi-directional buck-boost DC/DC converters result in a simpler structure, as compared to the multi-control loop for PFC Circuits, with just one PI regulator. Proportional and integral actions are used in a feedback error loop for output current, which is compared with desired battery current reference. The output of the regulator is then used to obtain a PWM signal to generate switching signals for the MOSFETs.

2.8 Stability Issues

Power electronic circuits such as switching converters, are commonly realized using a closed loop control system, e.g. PID controller in order to minimize the error between actual and commanded response. The Converter can be implemented SimPower System toolbox in MATLAB® Simulink, which allows multiple control strategies, including direct circuit approach and more flexible digital/discrete design. Behavior of the system can be similarly described through its circuit-based representation as well as its space state model, using differential equations. Equivalently, input-output relation can be expressed in terms of Transfer Function, as a rational function of the output and the input of the system.

Stability of a control system is often extremely important and is generally a primary issue in the engineering of a system. It is usually related to the response of the system to various inputs or disturbances. Stability analysis of power converters is quite difficult due to some intrinsic features of the systems. Variation of model parameters, such as input voltage or change in load resistance, as well as structure changes in mode of operations (Continuous mode or Discontinuous mode), gives the system a complex non-linear model.

Stability analysis of the system can be performed both for its open and closed loop configurations. Using various techniques it is possible to identify instability issues, constraints in operating conditions, and performance under faulty conditions of operation. Frequency analysis, which includes methods such as Routh-Hurwitz stability criterion or Bode plot and Nyquist diagram have been preferred in many publications [37], while often regarding unidirectional systems [45] or linearized models [40]. In particular, stability issues for bi-directional circuits, need to be analyzed in both power flows directions, since common ways to improve the stability usually affect other direction. Similarly, while each bi-directional converter in the power system is designed and optimized separately, when the converters are cascaded, the system may reveal to be unstable [68].

Other stability analysis techniques consider for example Middlebrook Impedance Criterion [31], or linearization of the system around particular load conditions, and Lyapunov theory of the state space model using state feedback control to stabilize the converter.

CHAPTER 3

CONVERTER DESIGN

Charging the battery of a Plug-in Hybrid Vehicle from the AC outlet requires relatively high power capabilities. Allowing a universal input voltage range and inverse power flow for discharging operation of for in-grid applications, are also important features. This chapter will provide a detailed description of the circuits used in the battery charger implementation. Their behavior and dynamic response is analyzed through the derivation of differential equations and simulating their response in the MATLAB® Simulink environment. Figure 3.1 shows a typical two-stage cascaded converter topology as it is used in [73]. This is a typical choice for PHEV battery charger circuits. The basic scheme of this configuration consists of two cascaded bi-directional power electronic converters, an AC/DC rectifier/inverter and a DC/DC converter respectively. The converter output is required to obtain a smooth controlled current in order to charge the energy storage device, which requires stables conditions and a flat waveform. Given its relatively simple structure and well known design and control issues, as often described in literature [7], a PFC boost circuit is is the most commonly used circuit. It is found to have the most suitable configuration for this application, requiring high efficiencies and power factor correction at the input. The second stage switching converter is typically needed to eliminate the ripple at the DC bus voltage, which is typically at twice the input frequency and to regulate the output current for the large input voltage range. In this project a simple bi-directional buck-boost circuit has been chosen.

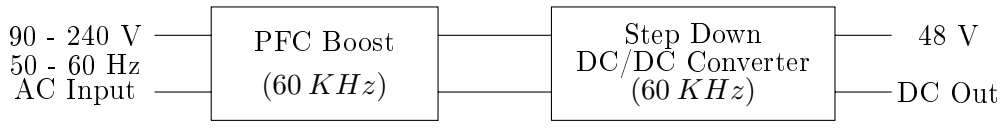

Figure 3.1. Basic block representation of the circuit schematic.

This chapter also describes the controller implementation, using a classical approach of a simple analog control circuit, both for the AC/DC and DC/DC converter. A multi-loop regulator is used to control the DC bus voltage and the shape of the input inductor current, whereas a single controller is implemented for the second stage output current regulation.

For each converter a simple ideal model is derived and its mathematical equations are calculated, considering the dynamic behavior of continuous conduction mode of operation. Furthermore, a more detailed circuit design includes ESR resistors and ON switches resistors and provides more realistic simulation results.

3.1 Boost Converter

The boost converter used here is described in continuous conduction mode of operation. It is a basic DC/DC converter that is used to get higher output voltage than the input voltage V_{in}. This high efficiency step-up DC/DC switching converter, connected to a DC power source is able to change the output DC value to a higher voltage level V_{out}. Boost converter uses a switch, typically a BJT or a MOSFET, to modulate the voltage into an inductor. It has a simple circuit which contains two switching components: a diode and a transistor. The inductor and the capacitive filter manage the energy conversion and reduce the ripple in the output current and voltage. The main operating principle can be explained as follows: the switch is positioned such that the input source charges the inductor, while the capacitor at the output maintains the output voltage using energy stored across its plates. When the switch changes its state, both the DC source and the stored energy supply power to the load, hence the output voltage boosts. When switch is closed the inductor absorbs energy from the input and the circuit is separated into two parts. This configuration allows the output signal to be completely independent of input values, as output voltage depends only on the energy stored while keeping rated power constant. This

circuit is described in greater detail later in the thesis.

This section analyzes ideal boost converter, its voltage and current relationships, and derives a state space model for the circuit. A second circuit considers equivalent series resistances (ESR) of the components, and is described through state space averaging method. This more precise model is then built, making some important considerations pertaining to the choice of component values and definition of the design requirements. In the last part of the section its behavior is observed and simulated with the use of Simulink. Also a first rough controller is designed.

3.1.1 Boost Converter State-Space Model. Analysis of the Boost converter needs some general assumptions that will be considered also in the next section for the Buck model. Described circuit operates in the steady state, and all transients and impulses conditions are neglected. This implies that all voltages and currents are periodic over one switching period. The circuit is analyzed in an equilibrium state, in which the inductor current never reaches zero (Continuous Conduction Mode - CCM). Switch S has a switching frequency of f_s, and is considered to be open (switch OFF) for the time $t_{off} = (1-D)T_s$, where $T_s = 1/f_s$ is the switching period and D indicates the Duty Cycle expressed as a percentage of the commutation period during which the switch is ON. Besides the ideal switch remains closed for time $t_{on} = DT_s$. Each component in this circuit, as shown in figure 3.2, is considered ideal.

Under these ideal assumptions, the simple Boost converter circuit is presented for the two possible states of the switch. In the ON state the switch is closed and the source input results in an increase in the inductor current, whereas in the OFF state the switch is open. In this situation the only path offered to inductor current is through the diode D, the capacitor C and the load R. This results in transferring the energy accumulated by the inductor, into the capacitor. Input current is the same as the inductor current and it is not discontinuous as will be in the buck converter,

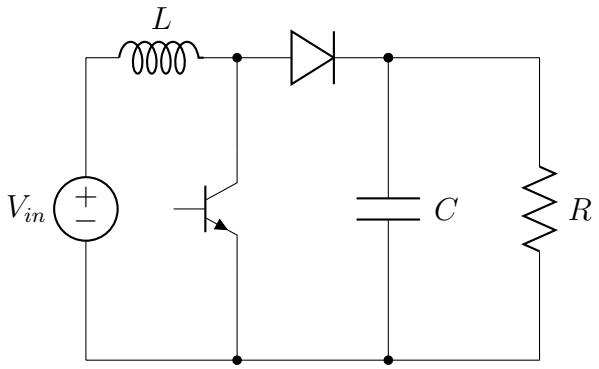

Figure 3.2. Ideal Boost circuit representation.

thus requirements on the input filter are relaxed. Two sets of equations describing the dynamics of voltage and current relationships are derived for both the closed switch circuit and the open switch circuit as follows.

Closed Switch $(u = 0)$

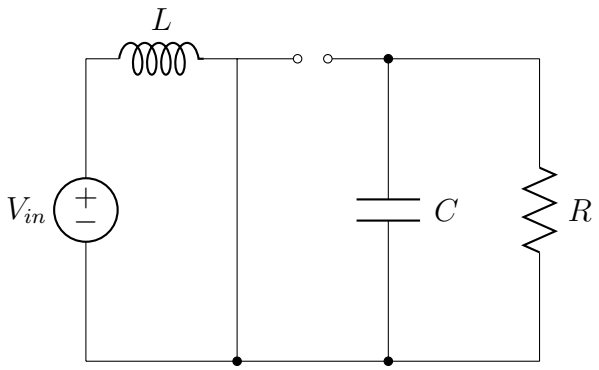

Figure 3.3. Equivalent Boost circuit representation for $S = ON$, $D = OFF$, $u = 0$.

When the switch S is closed, the diode is reverse biased and equivalent circuit is shown in figure 3.3.

Kirchhoff's voltage law around the left path containing the source, inductor and closed switch, along with Kirchhoff's current law on the leftmost upper node give

the following set of equations:

$$L\frac{di_L}{dt} - V_{in} = 0 \tag{3.1}$$

$$C\frac{dv_c}{dt} + \frac{v_c}{R} = 0 \tag{3.2}$$

These equations, describing the circuit for $u = 0$, can be written in terms of states variables v_c and i_L as

$$\frac{dv_c}{dt} = -\frac{1}{RC}\, v_c \tag{3.3}$$

$$\frac{di_L}{dt} = \frac{V_{in}}{L} \tag{3.4}$$

Open Switch $(u = 1)$

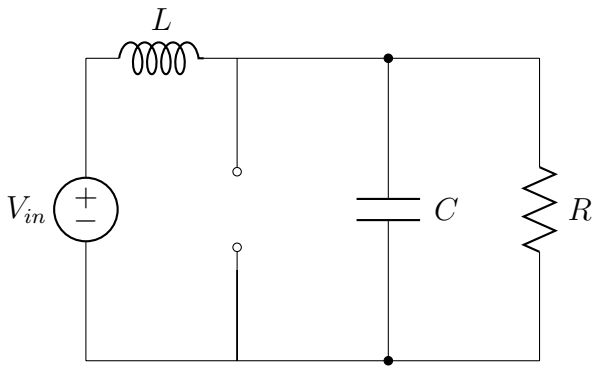

Figure 3.4. Equivalent Boost circuit representation for $S = OFF$, $D = ON$, $u = 1$.

While the switch is open, the inductor current cannot change instantaneously, so the diode D becomes forward biased to provide a path for i_L. Assuming that the output voltage V_{out} is a constant, again with Kirchhoff's voltage law around the outer loop and Kirchhoff's current load in the same node, following equations are derived.

$$V_{in} = L\frac{di_L}{dt} + v_c \tag{3.5}$$

$$i_L = i_c + i_R = C\frac{dv_c}{dt} + \frac{v_c}{R} \tag{3.6}$$

Differential equation (3.5) can be rearranged in terms of capacitor's voltage and inductor's current, and substituted in equation (3.6), leading to system equations for $u = 1$.

$$\frac{dv_c}{dt} = \frac{i_L}{C} - \frac{V_{in}}{RC} - \frac{v_c}{RC} \tag{3.7}$$

$$\frac{di_L}{dt} = \frac{V_{in}}{L} - \frac{v_c}{L} \tag{3.8}$$

These two models can be now combined together with the use of a binary input variable $u \in \{0, 1\}$ as the value of the switching input. It assumes either value $u = 0$ when the switch is closed, or the value $u = 1$ when opened, as schematized in the circuits. Equations (3.4), (3.7) and (3.5), (3.8) respectively are combined to obtain following differential global system, written using v_c and i_L state variables.

$$\frac{dv_c}{dt} = -\frac{1}{RC}\, v_c + \left[\frac{i_L}{C} - \frac{V_{in}}{RC}\right] u \tag{3.9}$$

$$\frac{di_L}{dt} = \frac{V_{in}}{L} - \frac{v_c}{L}\, u \tag{3.10}$$

3.1.2 Boost Converter State-Space Model with ESR. In previous analysis only ideal elements are considered, that is input power is transferred to the load without any losses. In real circuits, due to intrinsic properties of the materials, parasitic resistances are always present. For this reason a fraction of the input power is dissipated, producing power losses and heat. Even though some efforts need to be done in maximizing efficiency issue through a correct dimensioning of components and

a good design, it is also important to analyze the circuit considering the more general case of non-ideal components. As it has been done for the ideal Boost converter, at first complete circuit is presented, analyzing general functioning principles and then the two different switch states are discussed, deriving differential equations for the closed switch and open switch cases. The non-ideal behavior of inductor and capacitor is here modeled using Equivalent Series Resistances (ESR): R_L as inductor body resistor and R_c as capacitor body resistor. Similarly BJT switch S and diode D are modeled through an ON resistor R_s and R_D. Boost more detailed circuit is shown in figure 3.5.

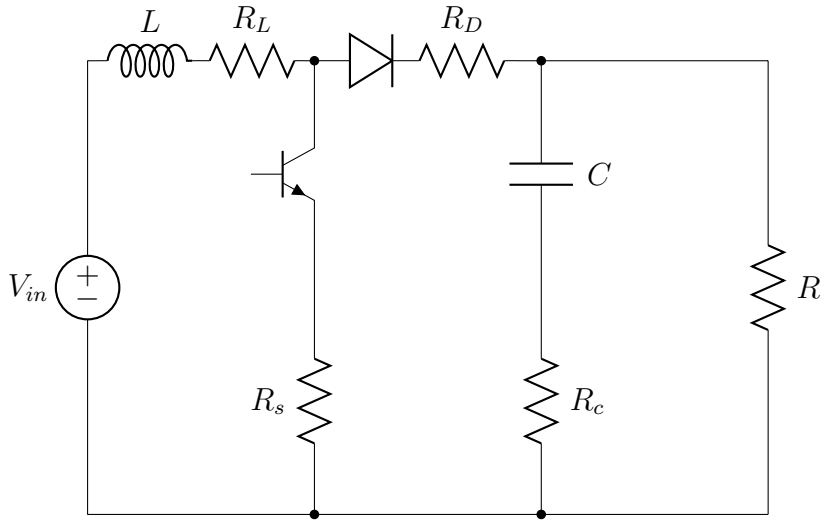

Figure 3.5. Non-Ideal Boost circuit representation.

Closed Switch $(u = 0)$

As before, when the switch is ON, diode is reversed biased and the equivalent circuit is represented in figure 3.6. Two sets of differential equations can be written for the system, considering the Kirchhoff's voltage law around the leftmost and rightmost loops respectively, as follows:

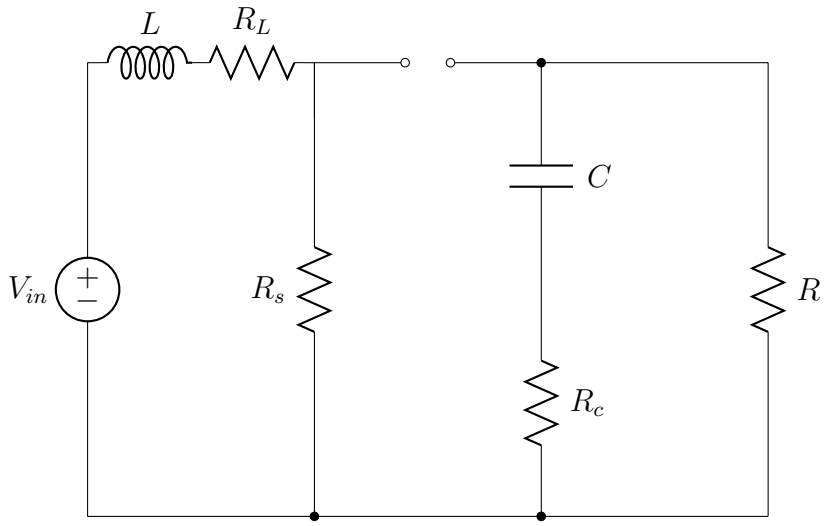

Figure 3.6. Equivalent Boost circuit representation for $S = ON$, $D = OFF$, $u = 0$.

$$V_{in} = R_L i_L + R_s i_L + v_L \tag{3.11}$$

$$V_{out} = v_c + i_c R_c \tag{3.12}$$

These equations, describing the circuit for $u = 0$, can be written in terms of states variables v_c and i_L as

$$\frac{dv_C}{dt} = -\frac{1}{C(R + R_c)}\, v_c \tag{3.13}$$

$$\frac{di_L}{dt} = -\frac{(R_L + R_s)}{L}\, i_L + \frac{V_{in}}{L} \tag{3.14}$$

Open Switch $(u = 1)$

When the switch is open $(S = OFF)$ the diode is forward biased and its internal resistance becomes R_D; equivalent circuit for the value of $u = 1$ is represented in figure 3.7. State space equations are derived from Kirchhoff's voltage law for

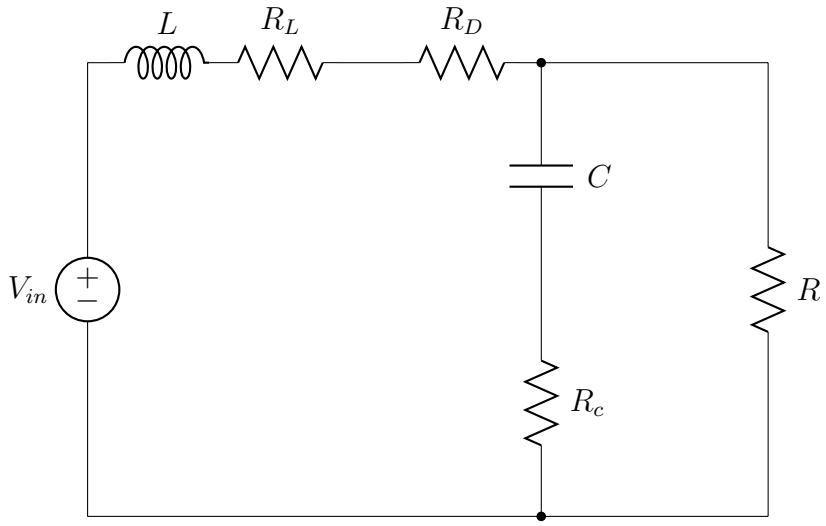

Figure 3.7. Equivalent Boost circuit representation for $S = OFF$, $D = ON$, $u = 1$.

external loop, Kirchhoff's voltage law for the rightmost loop and from Kirchhoff's current law on the upper right node as follows:

$$V_{in} = R_L i_L + v_L + R_D i_L + V_{out} \tag{3.15}$$

$$i_L = i_c + i_{out} \tag{3.16}$$

$$V_{out} = v_c + i_c R_c \tag{3.17}$$

Differential equation (3.15) and (3.16) can be rewritten in terms of inductor's current and capacitor's voltage. Equation (3.16) is substituted in equation (3.17), leading to following system equations for $u = 1$.

$$\frac{dv_C}{dt} = -\frac{1}{C(R+R_c)}\, v_c + \frac{R}{C(R+R_c)}\, i_L \tag{3.18}$$

$$\frac{di_L}{dt} = -\frac{R}{L(R+R_c)}\, v_c - \left(\frac{R_L + R_D}{L} + \frac{RR_c}{L(R+R_c)}\right) i_L + \frac{V_{in}}{L} \tag{3.19}$$

Obtained system, described by differential equations (3.13), (3.14) and (3.18), (3.19) is the equivalent state space model for boost circuit. This is characterized by

a bilinear behavior due to the nature of the control input, assuming binary values $u \in \{0, 1\}$. Global system can be written using a two set of equations. Values of diode ON resistor and switch ON resistor are assumed to be $R_s \simeq R_D$ with a very reasonable approximation, obtaining

$$\frac{dv_C}{dt} = -\frac{1}{C(R+R_c)}\, v_c + \left[\frac{R}{C(R+R_c)}\, i_L\right] u \tag{3.20}$$

$$\frac{di_L}{dt} = -\frac{R_L+R_s}{L}\, i_L + \frac{V_{in}}{L} + \left[\frac{RR_c}{L(R+R_c)}\, i_L - \frac{R}{L(R+R_c)}\, v_c\right] u \tag{3.21}$$

The highly non-linear model resulting from the combination of the two circuits can now be simplified and made suitable for simplified control analysis. The switch is replaced by replacing a continuous element, using the technique of system averaging. In particular, in following page average behavior is modeled, such as only information about low-frequency action of the converters is considered, ignoring ripple, commutations and other fast effects. For this averaged model the two switches configurations can be rearranged, considering system equations 3.13, 3.14 and 3.20, 3.21. Here the state is changing linearly from its initial value at the beginning of the switching period, until time instant $t = DT_s$. This approximation considers derivatives to be almost constant, in the condition of a triangular ripple waveform or with a high switching frequency f_s, which usually holds in reality. The value for the $\mathbf{x}$ vector, representing state variables $x_1 = v_c$ and $x_2 = i_L$, can be written as

$$\mathbf{x}(DT_s) \simeq \mathbf{x}(0) + \dot{\mathbf{x}}(0)DT_s \simeq \mathbf{x}(0) + (A_0\mathbf{x} + B_0\mathbf{u})DT_s$$

while, at time $t = T_s$, second configuration matrices are utilized as follows

$$\mathbf{x}(T_s) \simeq \mathbf{x}(DT_s) + \dot{\mathbf{x}}(DT_s)(1-D)T_s \simeq \mathbf{x}(DT_s) + (A_1\mathbf{x} + B_1\mathbf{u})(1-D)T_s$$

Therefore, global state evolution becomes

$$\mathbf{x}(T_s) \simeq \mathbf{x}(0) + [(DA_0 + D_1A_1)\mathbf{x} + (DB_0 + D_1B_1)\mathbf{u})]T_s$$

where $D_1 = 1 - D$ indicates time interval in which the second configuration is active. In equation above, averaged matrices $\bar{A} = DA_0 + D_1A_1 = DA_0 + (1 - D)A_1$ and $\bar{B} = DB_0 + D_1B_1 = DB_0 + (1 - D)B_1$ are defined, as averages of the configurations, weighted by the fraction of the duty cycle spent in every configuration. Then it is possible to simplify and produce the general form of averaged system (equation 3.22), which can be adopted also for further modeling of other converters explained later.

$$\dot{\mathbf{x}} = \bar{A}\mathbf{x} + \bar{B}\mathbf{u} \tag{3.22}$$

This approximate model gives exact results when switching period T_s is much shorter than any other time constant of the circuit. It has been proved in literature [31] that the new averaged states do track the average behavior of $\mathbf{x}$. In the infinite frequency limit the values match, avoiding the time dependence and the non-linearity typical of the switching systems.

In order to obtain a single state space system it is possible to describe the model through matrices $\bar{A}$, $\bar{B}$ and to rearrange equations using the duty ratio D. Here the dynamic of the system switches therefore between $\Sigma_0 = (A_0, B_0, C_0)$ obtained by the value $u = 0$, in the interval $D_1 = (1 - D)T_s$ and the system $\Sigma_1 = (A_1, B_1, C_1)$ when the input corresponds to $u = 1$ in the interval D_1T_s.

The two space state subsystems correspond to derived differential equations. They can then be represented using canonical model form for *State Space Linear Systems*, in which states depend on the value of the duty cycle D as percentage in the switching period T_s.

$$\bar{A} = DA_0 + (1-D)A_1 = \begin{bmatrix} -\frac{1}{C(R+R_c)} & \frac{R(1-D)}{C(R+R_c)} \\ -\frac{R(1-D)}{L(R+R_c)} & -\frac{R_L+R_s}{L} - \frac{RR_c(1-D)}{L(R+R_c)} \end{bmatrix} \tag{3.23}$$

$$\bar{B} = DB_0 + (1-D)B_1 = \begin{bmatrix} 0 \\ \frac{1}{L} \end{bmatrix} \tag{3.24}$$

3.2 Buck Converter

The Buck DC/DC converter can be used for step down operation. It reduces the input voltage V_{in} to the desired output voltage level of V_{out} suitable for example for battery charger applications. Exactly like Boost converter it is a switched-mode power supply that uses two switches (a BJT or MOSFET and a diode), an inductor and a capacitor, whereas the load can be assumed simply resistive. Although its topology is fairly simple, a buck converter can be highly efficient (easily up to 95%) and it is preferred over linear regulators.

Its operating principle takes advantage of the high commutation frequency of the switch that alternates between connecting the inductor to source voltage to store energy, and discharging the inductor into the load. Thanks to the very short transition time, and a precise choice of inductor and capacitor values output ripple is minimized and the dynamic transfer of power from the input to its output is regulated. Switching frequency is maintained constant to the value f_s, while its duty cycle is varied through a Pulse Width Modulation. In this way the ratio $D = t_{on}/T_s$ between the time t_{on} in which the switch is closed and the period $T_s = 1/f_s$ determines the desired DC level at the output. The low-pass structure of the converter, as explained in next section, guarantees a low frequency noise spectrum for this modulation scheme.

In this chapter Buck's ideal circuit is first presented and then its dynamic equations are derived with the fundamental Kirchhoff's current and voltage laws, in order to get a state space model. Non-ideal components are then used to describe a state-space model for continuous conduction mode of operation of the circuit, which is also implemented in MATLAB® Simulink. The end of the chapter analyzes its control design, evaluating choices of inductor and capacitor values and provides some simulation results.

3.2.1 Buck Converter State Space Model. Analysis of the ideal Buck converter represented in figure 3.8 requires some ideal assumptions. As before the circuit operates in the steady state, in continuous conduction mode of operation (CCM), that is inductor current is always positive and never reaches zero. Output voltage is considered almost constant V_{out}, while all components are ideal and body resistor are neglected.

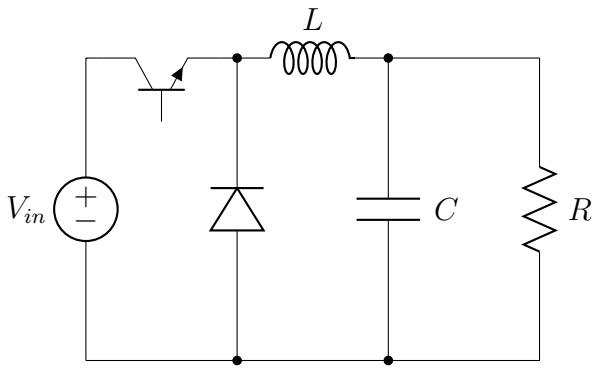

Figure 3.8. Ideal Buck circuit representation.

The switch S is closed in the interval DT_s and open for time $(1-D)T_s$. This leads to the following two equivalent circuits.

Closed Switch $(u = 0)$

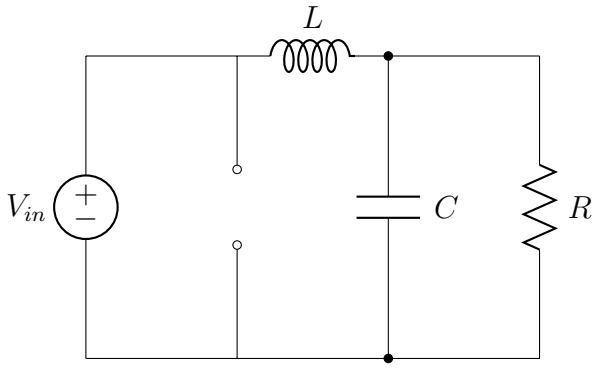

Figure 3.9. Equivalent Buck circuit representation for $S = ON$, $D = OFF$, $u = 0$.

Figure 3.9 shows equivalent Buck circuits when the switch S is closed. Diode D is reversed biased and following voltage and current relationships can be obtained using Kirchhoff's voltage law for inner and outer loops and Kirchhoff's current law for upper node

$$V_{in} = L\frac{di_L}{dt} + v_c \tag{3.25}$$

$$v_c = v_{out} \tag{3.26}$$

$$i_L = C\frac{dv_c}{dt} + i_R \tag{3.27}$$

These equations describe the circuit for $u = 0$ and can be written in terms of states variables v_c and i_L:

$$\frac{dv_c}{dt} = -\frac{1}{RC}\,v_c + \frac{1}{C}\,i_L \tag{3.28}$$

$$\frac{di_L}{dt} = -\frac{1}{L}\,v_c + \frac{V_{in}}{L} \tag{3.29}$$

Open Switch $(u = 1)$

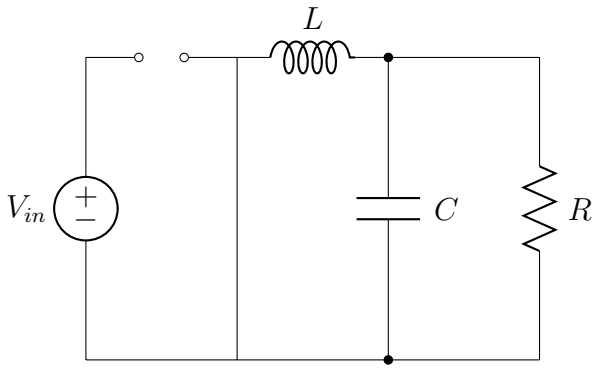

Figure 3.10. Equivalent Buck circuit representation for $S = OFF$, $D = ON$, $u = 1$.

When the switch is open the diode becomes forward biased and equivalent circuit is represented in figure 3.10. Kirchhoff's voltage law around leftmost and

rightmost loops, together with Kirchhoff's current law on upper node give the following differential equations.

$$0 = L\frac{di_L}{dt} + v_c \tag{3.30}$$

$$v_c = v_{out} \tag{3.31}$$

$$i_L = C\frac{dv_c}{dt} + i_R \tag{3.32}$$

Equations (3.30) and (3.32) can be rewritten in terms of inductor's current and capacitor's voltage. Substituting equation (3.31) following equivalent system for $u = 1$ is obtained.

$$\frac{dv_c}{dt} = -\frac{1}{RC}\,v_c + \frac{1}{C}\,i_L \tag{3.33}$$

$$\frac{di_L}{dt} = -\frac{1}{L}\,v_c + \frac{V_{in}}{L}\,u \tag{3.34}$$

3.2.2 Buck Converter State Space Model with ESR. A further step in modeling the Buck converter is assuming non-ideal components such as inductor and capacitor, as well as the diode and the switch. In its circuit representation parasitic values are schematized as equivalent series resistors (ESR): R_L, R_C, R_D and R_S, as shown in circuit schematic in figure 3.11.

Two different sets of equations are derived for the circuit with either open or closed switch, based on the binary values of u.

Closed Switch $(u = 0)$

When the non-ideal switch is closed the diode D is off, because it is reversed biased. The DC voltage source at the input supplies power to the circuit and results

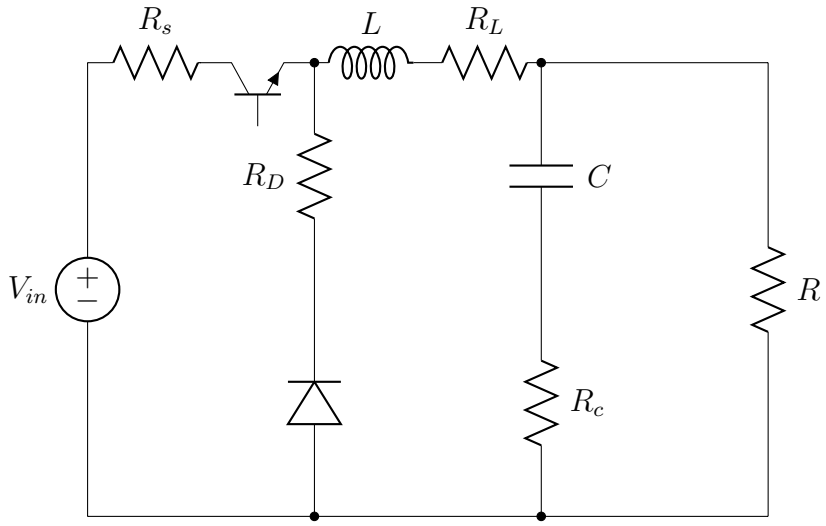

Figure 3.11. Real Buck circuit representation.

an output voltage across the resistor. Figure 3.12 shows equivalent Buck circuit for the closed switch. Writing Kirchhoff's current law for the upper node, and Kirchhoff's voltage law in the inner and outer loops we obtain

$$i_R = i_L - i_C = i_L - C\frac{dv_C}{dt} \tag{3.35}$$

$$V_{in} = L\frac{di_L}{dt} + (R_S + R_L)i_L + Ri_R \tag{3.36}$$

$$V_{in} = L\frac{di_L}{dt} + (R_S + R_L)i_L + i_C R_C + v_C \tag{3.37}$$

$$Ri_R = v_C + i_C R_C \tag{3.38}$$

Thus with some simple algebraic manipulations we get

$$\frac{dv_C}{dt} = -\frac{1}{(R + R_C)C}\, v_C + \frac{R}{(R + R_C)C}\, i_L \tag{3.39}$$

$$\frac{di_L}{dt} = -\frac{R}{(R + R_C)L}\, v_C - \left[\frac{RR_C}{(R + R_C)L} + \frac{R_L}{L} + \frac{R_S}{L}\right] i_L + \frac{V_{in}}{L} \tag{3.40}$$

These are the state space equations for the circuit, assuming i_L and v_C as state's variables.

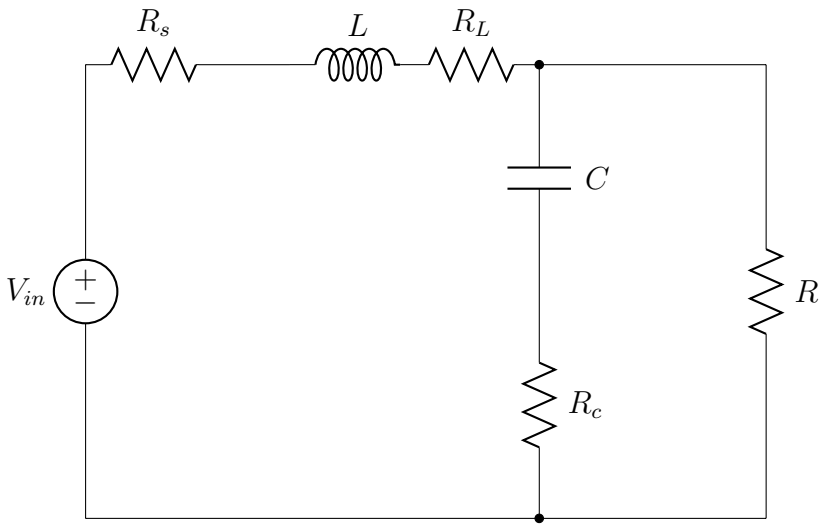

Figure 3.12. Equivalent Buck circuit representation for $S = ON$, $D = OFF$, $u = 0$.

Open Switch $(u = 1)$

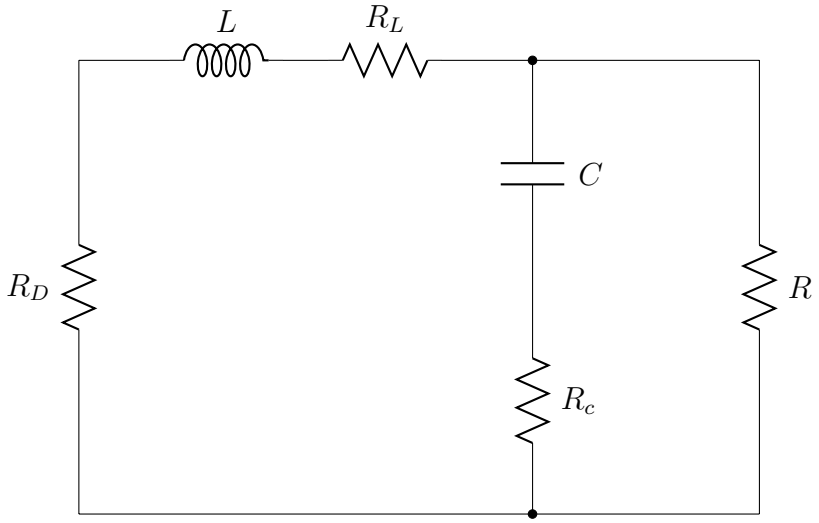

Figure 3.13. Equivalent Buck circuit representation for $S = OFF$, $D = ON$, $u = 1$.

While the switch is open the diode D becomes forward biased to carry the inductor current and the energy stored in the inductor and capacitor will discharge

through the resistor. Buck converter equivalent circuit is shown in figure 3.13. Using the same strategy this converter can be described with the following pair of differential equations:

$$\frac{dv_C}{dt} = -\frac{1}{(R+R_C)C}\, v_C + \frac{R}{(R+R_C)C}\, i_L \tag{3.41}$$

$$\frac{di_L}{dt} = -\frac{R}{(R+R_C)L}\, v_C - \left[\frac{RR_C}{(R+R_C)L} + \frac{R_L}{L} + \frac{R_D}{L}\right] i_L \tag{3.42}$$

Before combining the two pairs of equations in one single space state system, it is useful to make some considerations about real parameters, in order to simplify the system structure. As usually happens in real circuits, both diode and switch resistances are quite small, and can be considered as $R_S = R_D$. Body resistors of the inductor and the capacitor may have a significant effect on the output ripple, and on the efficiency issue for this converter, therefore they must be considered into the above model.

Using this assumptions equation (3.42) can be simplified and then combined with equation (3.37) introducing the binary input u. Along with equations (3.40-3.42) it leads to the following overall switching model:

$$\frac{dv_c}{dt} = -\frac{1}{(R+R_c)C}\, v_C + \frac{R}{(R+R_c)C}\, i_L \tag{3.43}$$

$$\frac{di_L}{dt} = -\frac{R}{(R+R_C)L}\, v_C - \left[\frac{RR_C}{(R+R_C)L} + \frac{R_L}{L} + \frac{R_D}{L}\right] i_L + \frac{V_{in}}{L}\, u \tag{3.44}$$

The switching position u is taken as input variable, assuming values in the discrete set $\{0, 1\}$.

This model can be written in the typical state space system representation. Here the input vector is given by the control input u that indicates the switch states, whereas the output vector must be calculated through equations (3.38) and (3.36) in order to get the output current and voltage of the converter. In terms of state

variables we get:

$$v_o = Ri_R = R(i_L - I_C) = R\left(i_L - \frac{v_o - v_c}{R_c}\right) \tag{3.45}$$

$$i_o = i_R = i_L - i_c = i_L - C\frac{dv_c}{dt} \tag{3.46}$$

Solving equation (3.46) produces the output voltage v_o as

$$v_o = \left(\frac{RR_c}{R+R_c}\right) i_L + \left(\frac{R}{R+R_c}\right) v_c \simeq R_c i_L + v_c \tag{3.47}$$

It can be further simplified as R_c value is usually neglectable compared to the load resistance R, obtaining a simples expression for the two outputs of the system

$$\begin{aligned} v_o &= v_c \\ i_o &= \frac{v_o}{R} = \frac{v_c}{R} \end{aligned}$$

Output matrix C, for which we have $v_o = C^T\mathbf{x}$, is valid for both switch positions and can be expressed as

$$C = \begin{bmatrix} \frac{R}{R+R_c} & \frac{RR_c}{R+R_c} \\ \frac{1}{R+R_c} & \frac{R_c}{R+R_c} \end{bmatrix}$$

Therefore final system description, for general case considering $R_c \neq 0$, is given by

$$\begin{cases} \begin{bmatrix} \dot{v}_c \\ \dot{i}_L \end{bmatrix} = \begin{bmatrix} -\frac{1}{(R+R_c)C} & \frac{R}{(R+R_c)C} \\ -\frac{R}{(R+R_c)L} & -\left[\frac{RR_C}{(R+R_C)L} + \frac{R_L}{L} + \frac{R_s}{L}\right] \end{bmatrix} \begin{bmatrix} v_c \\ i_L \end{bmatrix} + \begin{bmatrix} 0 \\ \frac{1}{L} \end{bmatrix} \begin{bmatrix} 0 \\ V_{in} \cdot u \end{bmatrix} \\ \begin{bmatrix} v_o \\ i_o \end{bmatrix} = \begin{bmatrix} \frac{R}{R+R_c} & \frac{RR_c}{R+R_c} \\ \frac{1}{R+R_c} & \frac{R_c}{R+R_c} \end{bmatrix} \begin{bmatrix} v_c \\ i_L \end{bmatrix} \end{cases}$$

A Pulse Width Modulation circuit is used to determine the switch position both in simulation and modeling. The control input signal is specified as the following duty ratio:

$$\mu(t) = \begin{cases} 1 & t_i \leq t < t_i + \mu(t_i)\, T_s \\ 0 & \mu(t_i)\, T_s \leq t < t_i + T_s \end{cases}$$

t_i is sampling instant in the fixed switching period T_s.

The model derived can be represented by a state space averaging simply letting the switch states taking values in the close interval of the real axes, $u \in [0, 1]$, and averaging the equations over the switching period T_s. State space averaging model is similar to the previous one and can be described as follows:

$$\begin{cases} \dot{\mathbf{x}} &= \bar{A}\mathbf{x} + \bar{B}\mathbf{u} \\ \mathbf{y} &= \bar{C}\mathbf{x} \end{cases}$$

In this case the input vector is $\mathbf{u} = \left[\begin{array}{c|c} 0 & V_{in} \cdot u \end{array}\right]'$, with the values of the matrices $A = \bar{A}$, $B = \bar{B}$ and $C = \bar{C}$.

3.3 Bi-directional Buck-Boost Converter

The use of a bi-directional DC/DC converter in power electronic applications allows the control and management of the power flow in both directions. It is especially suitable for battery charging applications. During charging operation of a battery a DC/DC converter is used to adjust the output current such as to follow the reference signal and maintain desired output power. A bi-directional arrangement of the converter is needed for the reversal of the power flow in order to discharge the battery or for in-grid applications. Since power can flow in both directions the output of a buck-boost can also be connected to a voltage source and thus bi-directional operation requires a direction change in output current, in order to recover the energy. In this section a traditional unidirectional form of buck-boost circuit topology is modified in order to accommodate bi-directional operations. This results in a new design of a bi-directional buck-boost system. This converter topology operates either in buck or boost mode and therefore has the ability of both step up and step down operations, as output voltage can be either higher or lower than the input voltage. To achieve bi-directional operations capability the standard circuit needs to be augmented. Two other switching elements are introduced with anti-parallel diode configuration and a new input capacitor.

3.3.1 Bi-directional Buck-Boost Space-State Model. Ideal bi-directional buck-boost circuit can be easily obtained with the combination of ideal boost and ideal buck circuits described in sections 3.1 and 3.2. The two switches S_1 and S_2 with anti-parallel diodes configuration D_1 and D_2 are here implemented using MOSFETs or BJTs and operate in an alternate complementary fashion. When switch S_1 is ON switch S_2 is OFF and vice versa. A negative current is now possible through the inductor L and enables both the increase of the voltage from the battery to the DC bus and the charging of the storage system from the hi-voltage level DC input.

As shown in the ideal bi-directional buck-boost circuit (figure 3.14) buck mode is active when switch S_1 is ON (and diode D_1 is OFF) and switch S_2 is OFF (and diode D_2 is ON). The circuit operates boost mode when switch S_1 is OFF (diode D_1 ON) and switch S_2 is ON (D_2 is OFF). Two equivalent circuits have the same representation of figure 3.2 on page 21 and scheme 3.8 on page 31. Two equivalent circuits can be represented with the introduction of an input capacitor, which can be neglected in the derivation of differential equations.

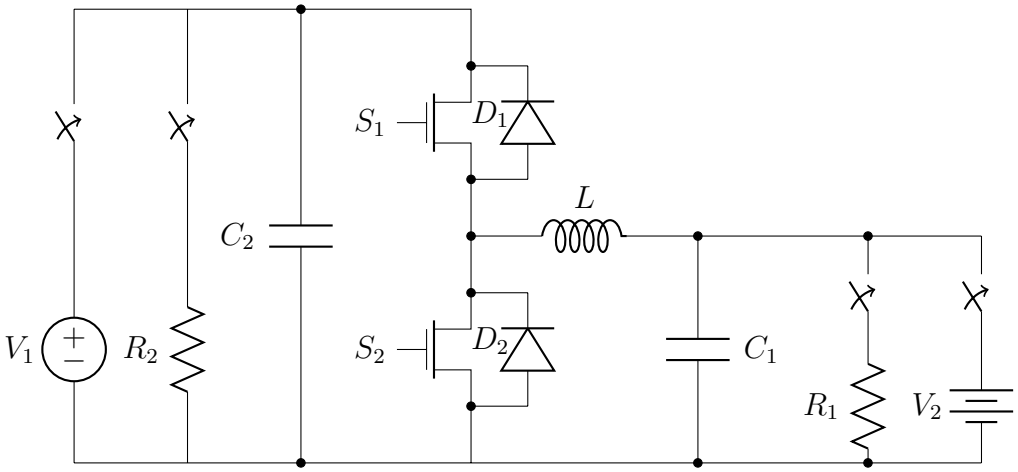

Figure 3.14. Ideal bi-directional Buck-Boost circuit representation.

Buck Mode

First circuit representation is equivalent to *buck mode*. It requires switch S_1 and diode D_2 to be ON and lead to a transfer of power from the left side to the right side of the circuit, as shown in figure 3.15. In buck mode input capacitor can be neglected since in steady state analysis input voltage charges instantaneously capacitor C_{in}. It results in an immediate input voltage V_{in} across it. This consideration simplifies drastically following differential equations as they are the same as those presented in section 3.2 for ideal buck converter.

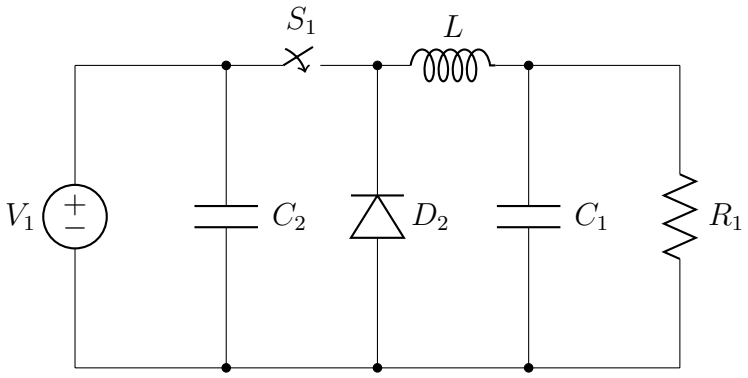

Figure 3.15. Equivalent Buck circuit representation for bi-directional circuit.

$$\frac{dv_{c,out}}{dt} = -\frac{1}{RC_{out}}\, v_{c,out} + \frac{1}{C_{out}}\, i_L \tag{3.48}$$

$$\frac{di_L}{dt} = -\frac{1}{L}\, v_{c,out} + \frac{V_{in}}{L}\, u \tag{3.49}$$

Boost Mode

Equivalently, *boost mode* circuit representation is shown in figure 3.16 and corresponds to switch S_2 and diode D_1 ON. Here which power is transferred from the *output* to the *input* with the constraint of $0 < V_{out} < V_{in}$. Output capacitor C_{out} is neglected in deriving following differential equations due to its fast charging time.

Differential equations of bi-directional buck-boost converter operating in boost mode are obtained exactly like equations 3.7 and 3.8 of ideal boost circuit representation on page 23. The circuit transfers power from the output to the input side in a revers fashion, and its behavior is described by following equations.

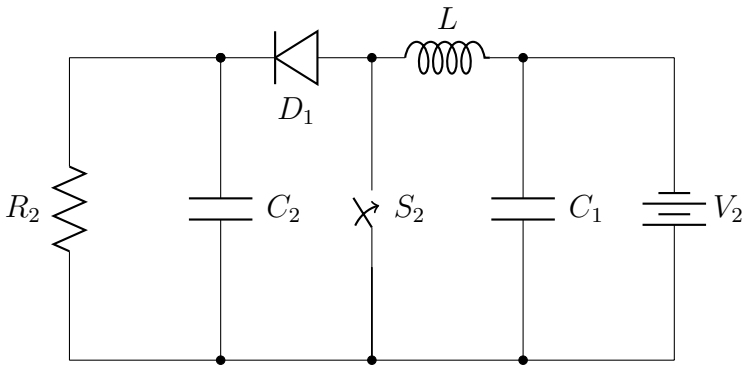

Figure 3.16. Equivalent Boost circuit representation for bi-directional circuit.

$$\frac{dv_{c_{in}}}{dt} = \frac{i_L}{C_{in}} - \frac{V_{out}}{RC_{in}} - \frac{v_{c_{in}}}{RC_{in}} \tag{3.50}$$

$$\frac{di_L}{dt} = \frac{V_{out}}{L} - \frac{v_{c_{in}}}{L} \tag{3.51}$$

These two operating modes can be grouped into a single system described by a space state representation's pair of differential equations. This new system considers four state variables, $v_{c_{in}}$, i_L and $v_{c_{out}}$, i_L that are now written respectively as v_{c_1}, i_{L_1}, v_{c_2} and i_{L_2} for simplification to indicate capacitors' voltages and inductor current.

3.3.2 Bi-directional Buck-Boost Space-State Model with ESR. As done before for buck and boost switching converters modeling, non-ideal components such as ESR and on-state resistor are now considered. A more precise model is then build using differential equations which describe its behavior in continuous conducting mode of operation. The analyzed circuit is presented in figure 3.17. This circuit includes Equivalent Series Resistor R_L, $R_{c_{in}}$ and $R_{c_{out}}$. ON resistors $R_{s_1} = R_{s_2} = R_s$ and $R_{D_1} = R_{D_2} = R_D$ are considered in the model but omitted in the figure for clarity.

Again, the circuit is analyzed for the four different states of the two switches and diodes. Differential equations are derived for buck mode (S_1 and D_2, ON) and

boost mode (S_2 and D_1, ON) of operation.

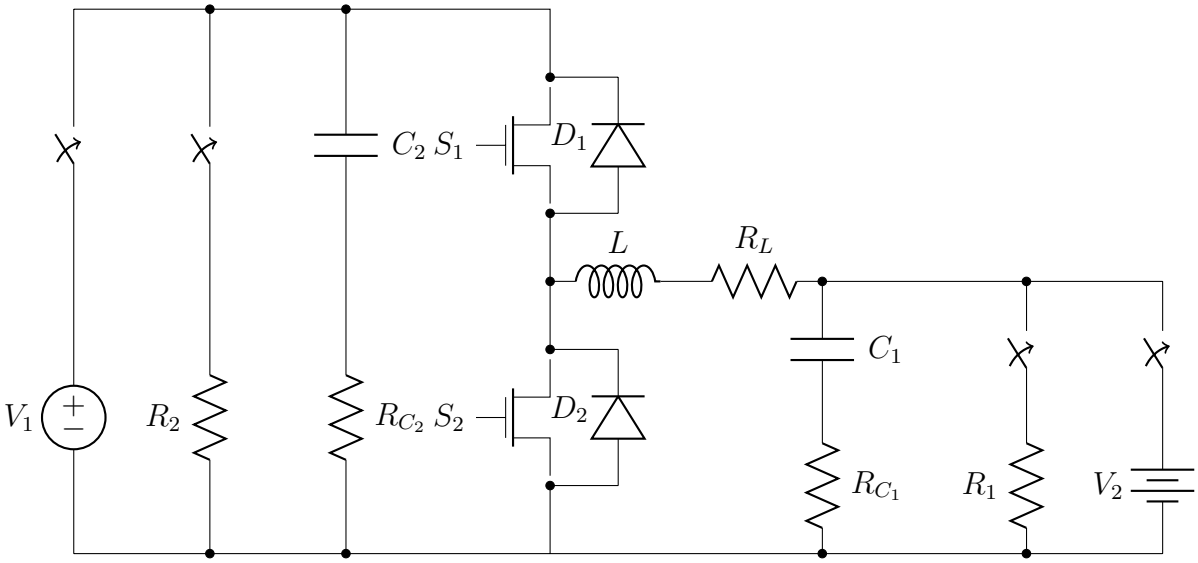

Figure 3.17. Non-Ideal bi-directional Buck-Boost circuit representation.

Buck Mode

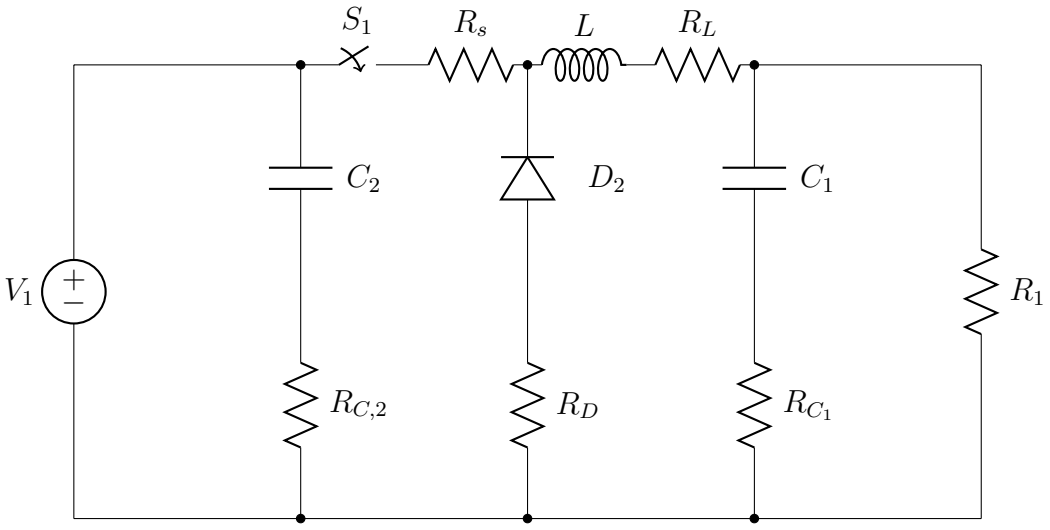

Figure 3.18. Equivalent Non-Ideal Buck mode circuit representation for bi-directional circuit.

Picture 3.18 represents equivalent circuit of bi-directional buck-boost in buck mode of operation. Input capacitor $C_{in} = C_1$ along with its ESR resistor R_{c_1} are assumed to be negligiThis chapter will provide a detailed description of the circuits used in the battery charger implementation. Their behavior and dynamic response is analyzed through the derivation of differential equations and simulating their response in the MATLAB® Simulink environment. Its space state equations are the same as those derived for non-ideal buck converter in section 3.2. Considering $v_{c_2} = v_{c_{out}}$ and i_L as state variables,

$$\frac{dv_{c_2}}{dt} = -\frac{1}{C_2(R+R_{c_2})}\, v_{c_2} + \left[\frac{R}{C_2(R+R_{c_2})}\, i_L\right] u \tag{3.52}$$

$$\frac{di_L}{dt} = -\frac{R_L+R_s}{L}\, i_L + \frac{V_{in}}{L} + \left[\frac{RR_{c_2}}{L(R+R_{c_2})}\, i_L - \frac{R}{L(R+R_{c_2})}\, v_{c_2}\right] u \tag{3.53}$$

Boost Mode

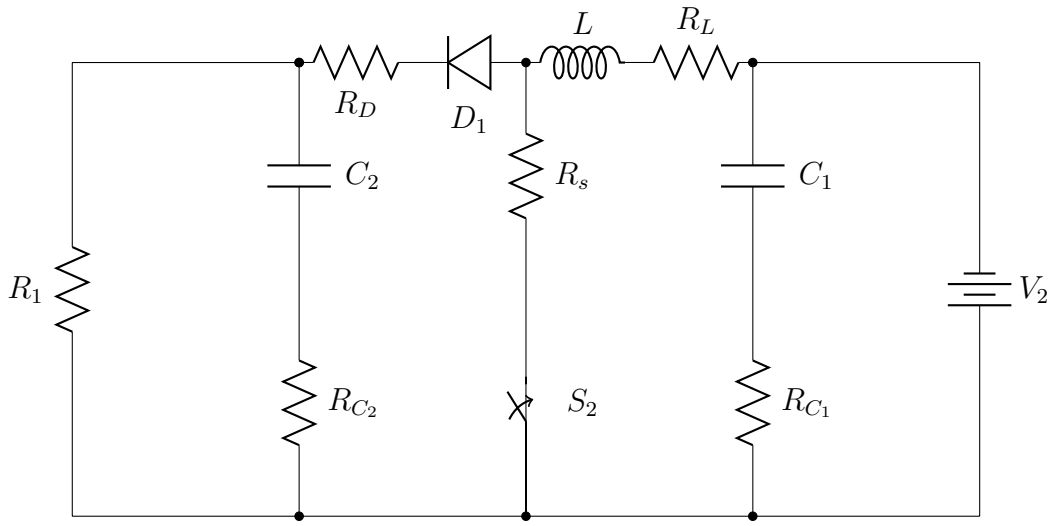

Figure 3.19. Equivalent Non-Ideal Boost mode circuit representation for bi-directional circuit.

In boost mode of operation, general bi-directional buck-boost circuit is represented in figure 3.17. It is considered when switch S_2 and diode D_1 are both ON, implying S_1 and D_2 to be OFF. Equivalent circuit representation is given in figure

3.19. It is almost identical to the non-ideal boost circuit described in section 3.1.2. Only basic differences are the inversion of input and output ports and the presence of the capacitor C_1 with its Equivalent Series Resistor R_{C_1}. The capacitor at the input of the boost circuit can be neglected since steady state behavior is studied. Following equations can be derived.

$$\frac{dv_{C_2}}{dt} = -\frac{1}{C_2(R+R_{C_2})}\, v_{C_2} + \left[\frac{R}{C_2(R+R_{C_2})}\, i_L\right] u \tag{3.54}$$

$$\frac{di_L}{dt} = -\frac{R_L+R_s}{L}\, i_L + \frac{V_2}{L} + \left[\frac{RR_{C_1}}{L(R+R_{C_1})}\, i_L - \frac{R}{L(R+R_{C_1})}\, v_{C_1}\right] u \tag{3.55}$$

3.3.3 Design Considerations. One fundamental step of the design of the circuit and the overall system is the ratings of the components of the converter. Significant research has been done considering rigorous mathematical approaches [43], which usually work better for ideal models, as well as more practical techniques by examining the *real* system response.

Critical components have been identified in this system. They are extremely important in terms of stability and robustness of the system and in terms of cost, reliability and size. Major issues are related to the energy storage components of the system that are the inductor and the capacitors. All following equations provide a guideline for the design of the converter and have been analyzed in details in [3]. Here they are used as a fundamental basis for the sizing of components.

First critical element, especially for battery charger circuits, is the output current ripple. It has to be limited according to manufacturer specifications in order not to damage the storage pack. Assuming a constant output voltage V_2 determined by battery voltage the peak-to-peak ripple on the output current is given by the ripple on the inductor L as follows:

$$\Delta I_L = \frac{V_{in} d_{DC}(1 - d_{DC})}{f_s L} = \frac{V_2 - \frac{V_2^2}{V_{in}}}{f_s L} \tag{3.56}$$

In equation 3.56 f_s indicates the switching frequency and d_{DC} the instantaneous value of the duty cycle of the DC/DC converter. The input-output relation of the buck circuit is used to simplify final expression. Magnitude of V_{in}, either the input voltage of the converter or the voltage output of the previous stage, influences the amplitude of the output current ripple and increase its value proportionally. On the other hand, increasing the switching frequency will decrease the amplitude of the ripple, whereas the inductor value assumes an important role in the design, decreasing ΔI_L for high values. Considering a constant output voltage value V_2 for the battery a tradeoff between the switching frequency f_s and the value of the inductance has to be found. A large inductor, while desirable to decrease the output ripple amplitude, will become larger and heavier. Moreover, the converter will be working with relatively low duty cycles values in order to satisfy output battery voltage. The increase of the switching frequency will affect the overall efficiency of the converter due to increased switching losses. High switching of the high current I_L will also cause significant EMI issues that will affect the performance of the circuit together with eventual other stages.

3.3.4 Simulink Model and Simulations. The bi-directional Buck-Boost circuit is implemented in MATLAB® Simulink environment and its behavior is simulated. Further stability analysis and control design are performed. Circuit presented in figure 3.17 is modeled using the SimPower System toolbox, including Equivalent Series Resistances and non-ideal elements as switching devices. MOSFET semiconductors consider internal resistance R_{on} and include a diode in anti-parallel configuration. On the other hand, manual switches are used for commuting between the two modes of operation, the buck converter and the boost converter respectively. The metal-oxide

semiconductor field-effect transistor (MOSFET) is a semiconductor device controllable by the gate signal ($g > 0$). The MOSFET device is connected in parallel with an internal diode that turns on when the MOSFET device is reverse biased ($V_{ds} < 0$) and no gate signal is applied ($g = 0$). The model is simulated by an ideal switch controlled by a logical binary signal ($g > 0\, or\, g = 0$) coming from the controller.

The MOSFET device turns on when a positive signal is applied at the gate input ($g > 0$) whether the drain-source voltage is positive or negative. If no signal is applied at the gate input ($g = 0$), only the internal diode conducts when voltage exceeds its forward voltage V_f. With a positive or negative current flowing through the device the MOSFET turns off when the gate input becomes zero. If the current is negative and flowing in the internal diode (no gate signal or $g = 0$) the switch turns off when the current becomes zero. In the ON state voltage across MOSFET becomes instead $V_{ds} = R_{on} \cdot I$ when a positive signal is applied at the gate input.

Also passive elements like capacitors and inductors are modeled including their series resistance. DC voltage sources are considered to be ideal. Battery, at the rightmost end of the circuit, is simply modeled as a resistor, or a constant DC voltage source. Storage pack State of Charge (SOC), temperature varying parameters and charging/discharging characteristics are neglected.

Buck-boost converter is controlled using a current feedback for output current. Its error is calculated through following equation,

$$i_e = i^*_{out} - i_{out} \tag{3.57}$$

and is processed by a simple Proportional Integral (PI) controller that eliminates steady-state error. PI regulator functioning is described by following expression; current error i_e is multiplied by a constant proportional gain K_I and integrated (integral

term):

$$i_{PI} = K_P \cdot i_e + K_I \cdot \int i_e. \tag{3.58}$$

Output of PI controller is then used to create the binary pattern of the switches, which is used as a gate signal for both MOSFETs. Pulse sequence is thus reversed, using the logical NOT operator, in order to guarantee the alternate functioning of the switches, either ON switch (short circuit) or OFF switch (reversed diode). PWM is generated through a comparator between the current PI signal i_{PI} which is logically compared with a pulsating saw-tooth waveform. This repeating frequency, at f_s, indicates the switching frequency of the converter.

Even if for designed circuit a bi-directional behavior is simulated, some realistic constraints have to be verified. In order to guarantee a universal input voltage, a different approach has to be considered for a practical implementation. Voltage conversion between the battery level and the DC bus value has to be done with shown DC/DC converter. However, due to practical issues, boost converter gain should not exceed three. Stability problems and other issues related to components can be caused by higher gains. Therefore, simulations provided are given only for the $110\,V$ grid voltage.

Some design considerations can be done in order to adapt the behavior of the circuit to a wider operating range in the inverse power flow. A larger voltage can be considered for the battery pack, thus limiting the gain of the DC/DC bi-directional buck-boost in boost mode of operation. Furthermore, an isolated topology can be used to increase the voltage level with the use of a transformer. Future works may include some considerations on different specifications for the system in order to optimize the bi-directional power flow.

Significative simulation results are shown in figures 3.20 and 3.21, where output voltage and inductor current are given for both ways of functioning. PID controllers previously commented are used, whereas also a digital approach as will be explained later is of easy implementation.

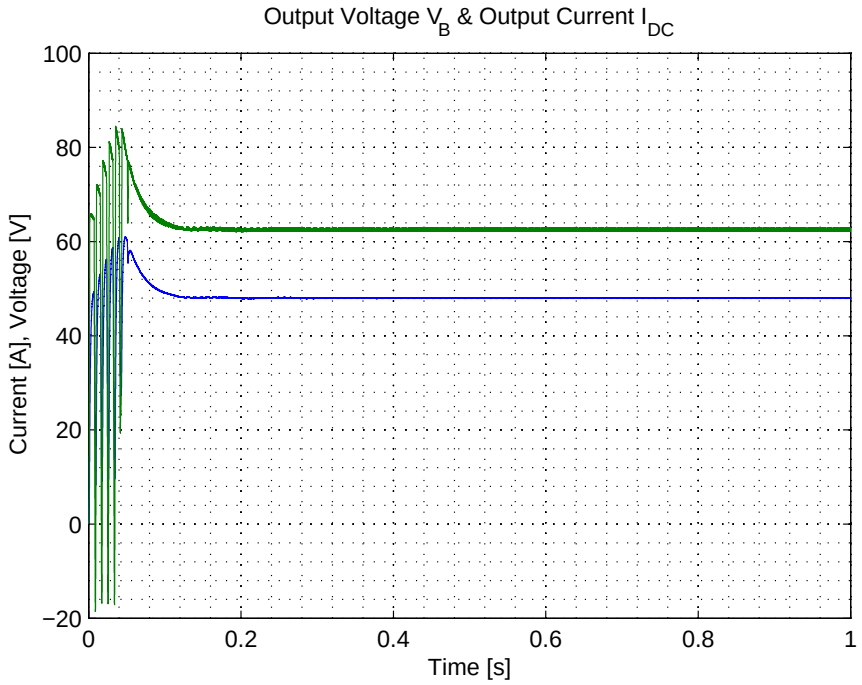

Figure 3.20. Output voltage and current of Buck-Boost converter, in Buck mode of operation.

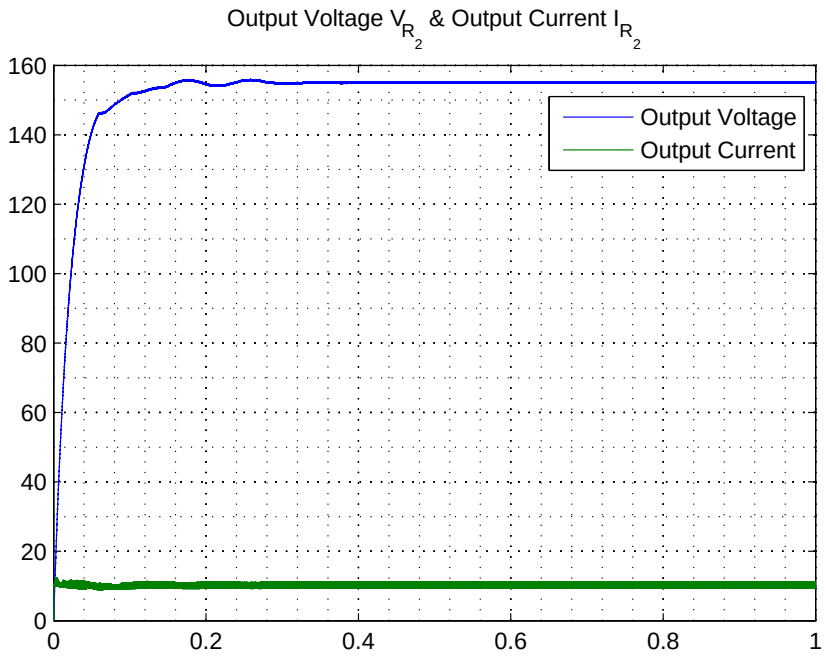

Figure 3.21. Output voltage and current of Buck-Boost converter, in Boost mode of operation.

3.4 Boost Rectifier and Power Factor Correction

Basic Switching Mode Power Supply design requires, other than the rectifier stage, a Power Factor Correction circuit. Power factor is defined as the ratio, usually expressed in percentage, of the average power flowing to the load, to apparent power

$$pf = \frac{P}{S} = \frac{P}{V_{rms} I_{rms}} = cos(\phi) \tag{3.59}$$

The last expression holds for sinusoidal AC circuits and ϕ is the phase angle between current and voltage sinusoidal waveforms. Non-linear loads such as rectifiers or switching circuits produce a large *Total Harmonic Distortion*. It is modeled as noise that distorts the sinusoidal wave shape of the current coming from the AC source. This results in apparent power that can be greater than the real power, and consequently a low Power Factor. Power Factor Correction (PFC) allows thus power distribution to operate efficiently. It minimizes losses and maximizes the real power available from the line. Ideally a PFC circuit appears purely resistive to its source and consequently the reactive power drawn from the device is zero. This implies that the input current must differ from the sinusoidal source voltage by only a scaling factor and must be exactly in phase with it. In case of purely reactive loads power factor can be corrected. It is possible to add either an inductor, in the case of a capacitive load, or a capacitor in the case of an inductive load. On the other hand, for non-linear load like the full wave bridge rectifier at the input port a passive PFC filter is not efficient. In fact, for this design purpose the preferable type of PFC is active Power Factor Correction since it provides a lighter and more effective power factor control. An active PFC circuit is an electronic system that controls the input current of the load so that the current waveform is proportional to the main voltage waveform. It keeps power factor as close as possible to unity ($\phi = 0$) and reaches high efficiencies. Active PFC circuit chosen design is composed by a full bridge diode rectifier followed by a switching boost regulator. It operates at a high frequency f_s and it is capable

of a wide range of input voltage.

The choice for the active power electronic converter for current shaping, is based on practical considerations about this peculiar design. Electrical isolation between the utility input line and the output of the power supply is not needed. It is also desirable to stabilize the DC voltage at the input of the bi-directional Buck-Boost converter optimizing the universal input feature. Since power flow in this device can be bi-directional some peculiar technical solutions must be used for the Boost step-up converter in this application.

3.4.1 Input Rectifier. The first stage in this model design is the bridge rectifier. Given universal AC input voltage, a simple full wave rectifier converts sinusoidal input to purely DC voltage. It uses four diodes in a bridge configuration to provide the same polarity of output voltage for both polarities of input voltage, as shown in figure 3.22.

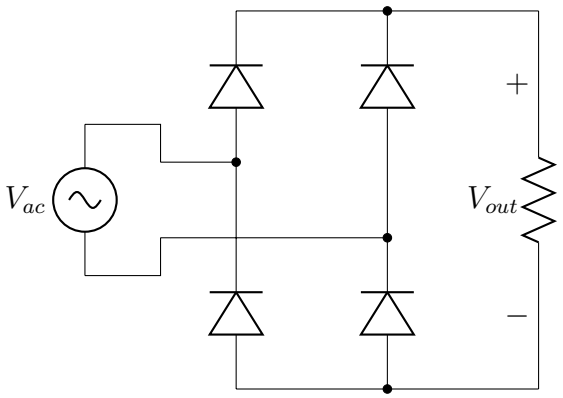

Figure 3.22. Full Wave Bridge Rectifier circuit representation.

As a feature of this power supply universal input from nominally $90V$ to $240V$ passes through the simple circuit represented above. It consists in 4 diodes connected in a typical bridge configuration on a resistive load. Output voltage is alternatively the positive or negative voltage coming from the input. Similarly output current is

rectified by the circuit and it is therefore scaled by a $\sqrt{2}$ factor. Equations for the full wave bridge rectifier represent output voltage across a general resistive load as shown in the circuit schematic. As follows:

$$v_{out}(\omega t) = \begin{cases} V_m sin(\omega t) & 0 \leq \omega t \leq \pi \\ -V_m sin(\omega t) & \pi \leq \omega t \leq 2\pi \end{cases}$$

Value of average output DC voltage can be calculated by following equation:

$$V_{out} = \frac{1}{\pi} \int_0^{\pi} V_m sin(\omega t)\, d(\omega t) = \frac{2V_m}{\pi} \tag{3.60}$$

The rectifier produces an unregulated DC voltage that is sent to the DC/DC boost step-up converter. The current drawn from this rectifier circuit occurs in short pulses around the AC voltage peaks. These pulses have significant high frequency energy that reduces the power factor. In next paragraph a Power Factor Correction circuit will be designed.

3.4.2 Active Power Factor Correction Circuit. A boost step-up converter is used together with a full wave bridge rectifier for current shaping. Basic principle of operation of the circuit is represented in the scheme of figure 3.1 and it is straightforward. At the utility input the current is desired to be sinusoidal and in phase with V_{in}. Full bridge rectifier output voltage and current waveforms are given by the rectified version of the input scaled of a $\sqrt{2}$ factor.

In the step-up converter circuit is shown in figure 3.23. Some general assumptions are necessary before proceeding with the analysis: output capacitor C is considered to be fairly large, in order to get an almost constant DC output voltage v_{out}. Input power of the ideal circuit equals output power on instantaneous basis.

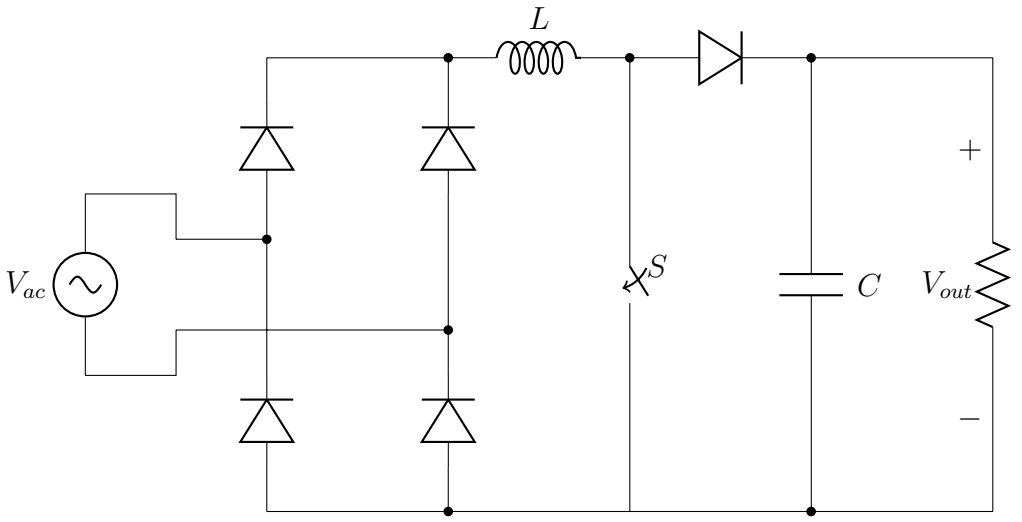

Figure 3.23. Power Factor Correction circuit representation.

Because the input current of the step-up converter is to be shaped it operates in current-regulated mode. Feedback control measures both the input voltage and the current. It also adjusts the switching duty cycle to produce an in-phase voltage and input current. Current mode control keeps a constant switching frequency to obtain that inductor current i_L reaches the reference. Controlling the ON time t_{ON} in the switch S the current in the inductance increases as the input voltage increases. Switching frequency of the boost converter is required to be much higher than the line frequency. For this application it is set to $f_s = 60\,KHz$ allowing the inductor to be very small and light. Feedback control is done measuring output voltage that is maintained almost at a constant value V_{out}. Normally, the DC output voltage is set to $10 - 20\,V$ higher than maximum input voltage. Thus the universal input power supply application meets a $90 - 240\,Vrms$ input voltage at $50 - 60\,Hz$ and a DC output voltage. Input of the DC/DC converter that equals the DC bus voltage is set at the maximum value of $V_{out} = 400V$ depending on the input amplitude. A real-time calculation algorithm is developed specifically to calculate the modulation index and the bus voltage value.

Another advantage of the PFC circuit in this power supply is that there is no hold-up capacitor directly across the bridge rectifier. It is instead postponed to the output of the circuit where high frequency of operation permits a lower value and therefore a smaller component.

3.4.3 Bi-directional Buck-Boost Power Factor Correction. As before, a bi-directional circuit is now derived. Thus the converter operates in both directions, as an AC/DC boost converter and as a DC/AC rectifier for a battery charge depleting mode. Diode rectifier previously illustrated is now substituted with an H-bridge rectifier, that lets energy flow in either direction. It is shown in circuit of figure 3.24. With suitable control, this circuit can operate as the boost PWM rectifier explained above. It is connected to an AC source whose waveform is rectified and boosted to a suitable value, while power factor is hold to a value of around 95%. With the use of the switches the output load can be switched to a constant DC voltage supply and the AC input can work as a linear load. This reversed functioning mode allows power to flow from the DC side to the AC side of the circuit to send energy to the drive. Voltage converter of figure provides excellent control over power flow in both directions. It can operate as an AC/DC converter to generate regulated DC voltage at a high power factor and the power flow can be easily reversed to operate the converter as a DC/AC inverter.

This section describes a first ideal circuit. Its differential equation of a space state model are derived and a non-ideal AC/DC converter considering ESR and ON resistor is built and analyzed.

3.4.3.1 H-Bridge PWM Rectifier. H-bridge circuit is used in the bi-directional buck-boost Power Factor Correction circuit as a reversible rectifier. It is capable of operating as both a PWM boost converter and a DC/AC inverter, through the alternate use of the switches. Two configurations are allowed, considering that only

two opposite switches are turned ON at the same time and that the current can flow in either direction. Thus the basic operating mode of an H-bridge is fairly simple: if $S3$ and $S4$ are turned on the left side of the circuit is connected to ground, while the right side is connected to the power supply. Current starts flowing through the bridge that energizes in the forward direction and results in an output voltage in the load. If $S1$ and $S2$ are turned on the converse takes place and the load gets energized in the reverse direction. It results thus in a negative current through the rectifier branch.

This simple circuit (figure 3.24) is composed of a series of four solid-state switches such as BJTs or MOSFETs with anti-parallel diodes configuration. The switches are fed by a sinusoidal AC input voltage and applied to an equivalent resistive load.

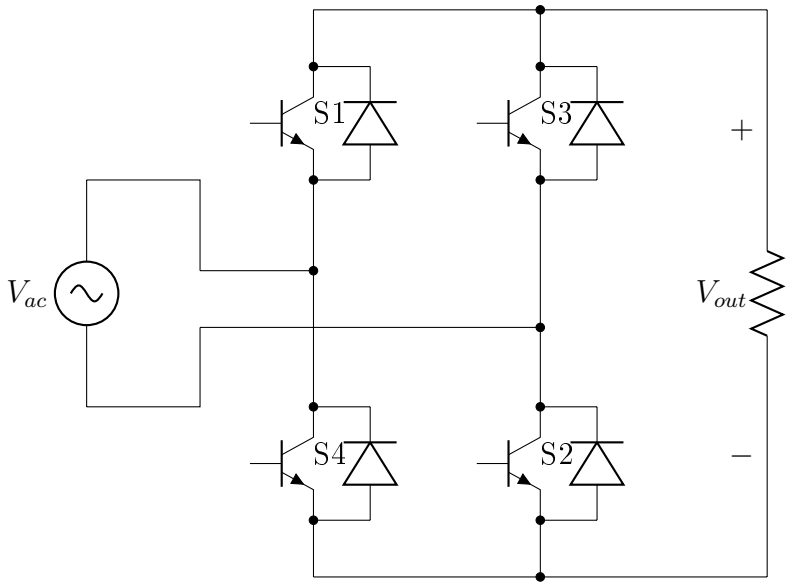

Figure 3.24. H Bridge Rectifier circuit representation.

3.4.4 Bi-directional Buck-Boost Power Factor Correction Space-State Model.

Power Factor Correction circuit of previous section is now modified in order to accommodate bi-directional operations. As explained diode bridge is converted in an H-bridge, a circuit that enables a voltage to be applied across a load in either direc-

tion. It uses 4 BJT or MOSFET devices in a bridge configuration.

As shown in circuit schematic of figure 3.25 the system consists in a single-phase voltage source V_1 with AC side inductor L. The rectifier bridge, explained in previous paragraph consists of four bipolar transistors with anti-parallel diodes. It is controlled by a voltage and current loop and provides a reference PWM signal for the semiconductors. Manual switches in the circuit are intended for the bi-directional use of the converter. They are used here to switch between the AC/DC boost converter with input current shaping and the reverse system of the DC/AC step-down inverter.

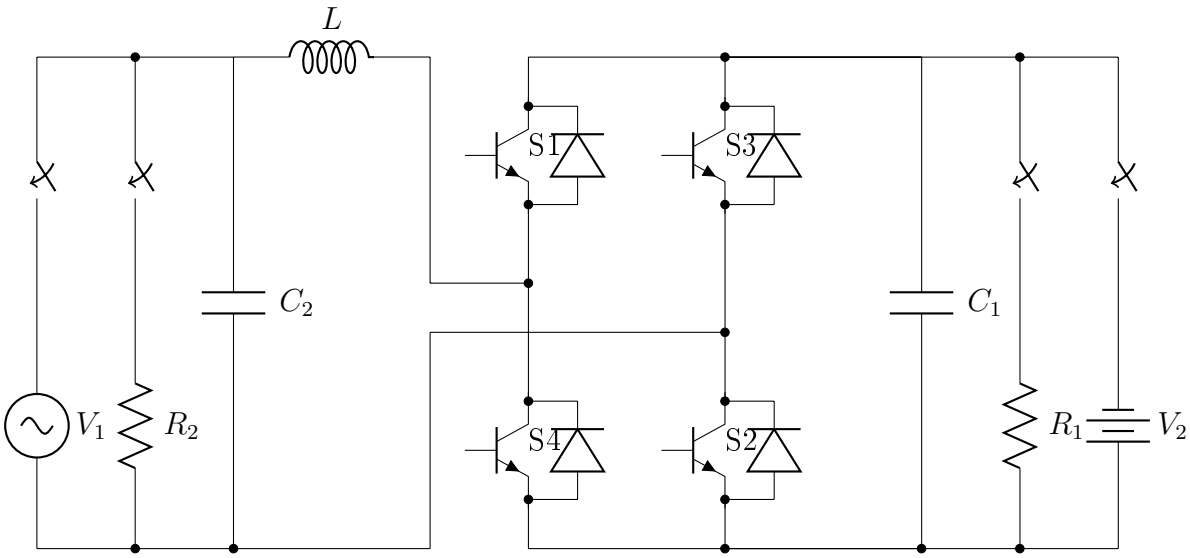

Figure 3.25. Ideal bi-directional PFC circuit representation.

Ideal circuit is here described and the behavior of ideal circuit is examined without considering Equivalent Series Resistors and ON resistors for the switches. Its differential equations are derived with the hypothesis of a large input and output capacitor and a constant output voltage V_{out}.

3.4.4.1 AC/DC mode. Ideal equivalent circuit represented in figure 3.26 shows the AC/DC operating mode. The sinusoidal input voltage is rectified by the H-bridge rectifier and boosted to the desired value V_{out} by the boost step-up converter. Boost rectifier's functioning results to be very similar to simple boost converter. Input voltage is rectified by the use of the absolute value of the input $V_{in} = |v_1| = V_1|sin(\omega t)|$.

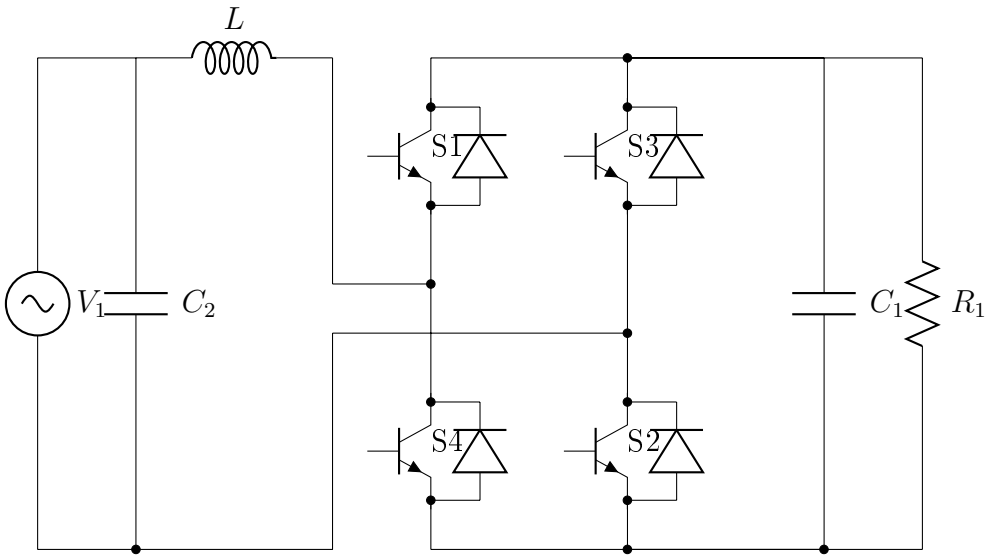

Figure 3.26. Ideal bi-directional PFC circuit representation, in AC/DC operating mode.

Recalling ideal boost model differential equations 3.9 and 3.10, dynamics of the system can be adapted considering the rectified input voltage, as follows:

$$\frac{dv_c}{dt} = -\frac{1}{RC}\, v_c + \frac{i_L}{C}\, u \tag{3.61}$$

$$\frac{di_L}{dt} = \frac{V_{in}}{L} - \frac{v_c}{L}\, u \tag{3.62}$$

3.4.4.2 DC/AC mode. Inverter mode of operation for the bi-directional converter implies the DC/AC mode of operation. The DC input voltage is PWM modulated to obtain a sinusoidal output waveform with the desired amplitude and frequency.

Inverter scheme is represented in figure 3.27 as the ideal equivalent circuit. It works as a step-up converter based on the simple buck converter previously explained, where the output voltage is sinusoidal shaped by the H-bridge converter.

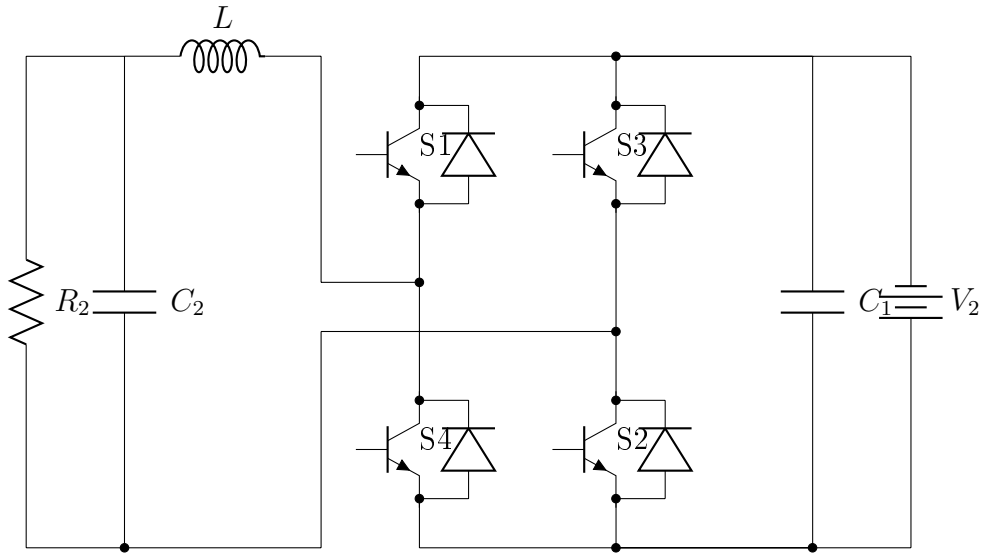

Figure 3.27. Ideal bi-directional PFC circuit representation, in DC/AC operating mode.

Buck equations for the ideal circuit 3.7 and 3.8 are here modified in order to accommodate the PWM generator which creates the output voltage waveform. As before converter output voltage is considered as the rectified version $V_{out} = |v_{C_2}| = V_{C_2}|sin(\omega t)|$.

$$\frac{dv_c}{dt} = \frac{i_L}{C} - \frac{V_{in}}{RC} - \frac{v_c}{RC} \tag{3.63}$$

$$\frac{di_L}{dt} = \frac{V_{in}}{L} - \frac{v_c}{L} \tag{3.64}$$

PWM switching frequency to control the H-bridge switching pattern is calculated comparing a sinusoidal at the desired output frequency and proportional to the output voltage magnitude with a triangular waveform at the switching frequency f_s.

3.4.5 Bi-directional Buck-Boost Power Factor Correction Space-State Model with ESR. Ideal circuit representation of previous section is here modified. Non-ideal elements are introduced to provide a more complete model of the system. Equivalent Series Resistor R_L for inductor and R_{C_1}, R_{C_2} for capacitors, ON resistors R_{on} for BJTs and diodes are added, while diode voltage drop is neglected. This more complex circuit represented in figure 3.28 will be simulated using MATLAB® Simulink in following section.

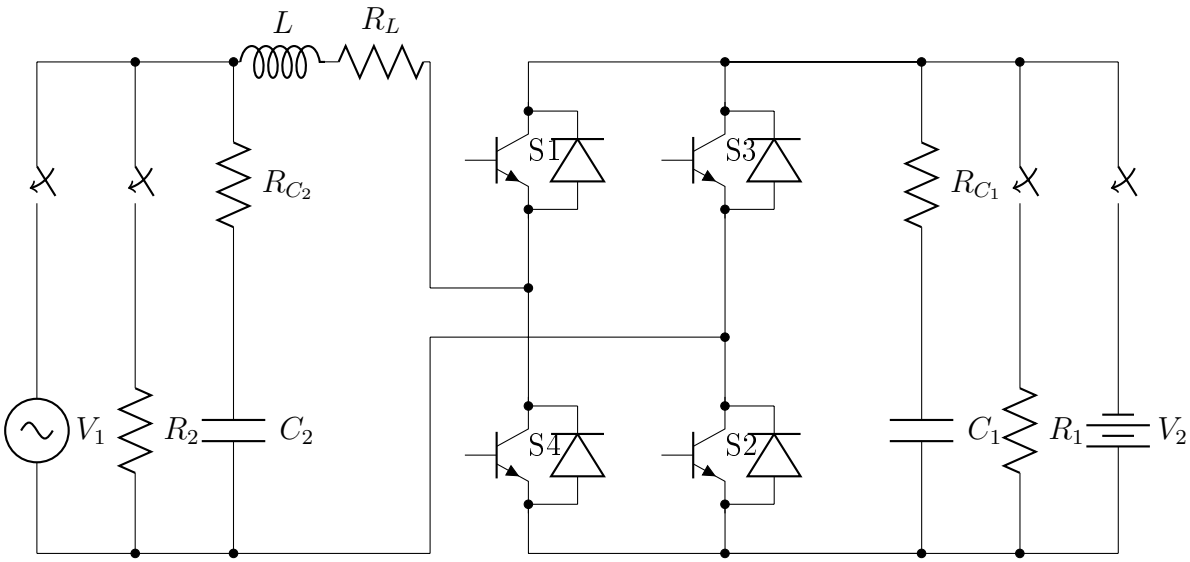

Figure 3.28. Bi-directional PFC circuit representation.

3.4.5.1 AC/DC mode. First mode of operation analyzed is standard boost rectifier PFC circuit. It is obtained considering a switch configuration where the sinusoidal input V_1 on the left side and the battery load R_1 are connected. Power flows from the AC input to the load resulting in a voltage rectification and regulation and in an input current shaping. Circuit schematic is shown in figure 3.29. Usual assumption of neglecting the input capacitor can be made.

For AC/DC boost Power Factor Correction operation mode state space equations can be derived for the two equivalent switches states, S_1, $S_2 = ON$, $S_3, S_4 =$

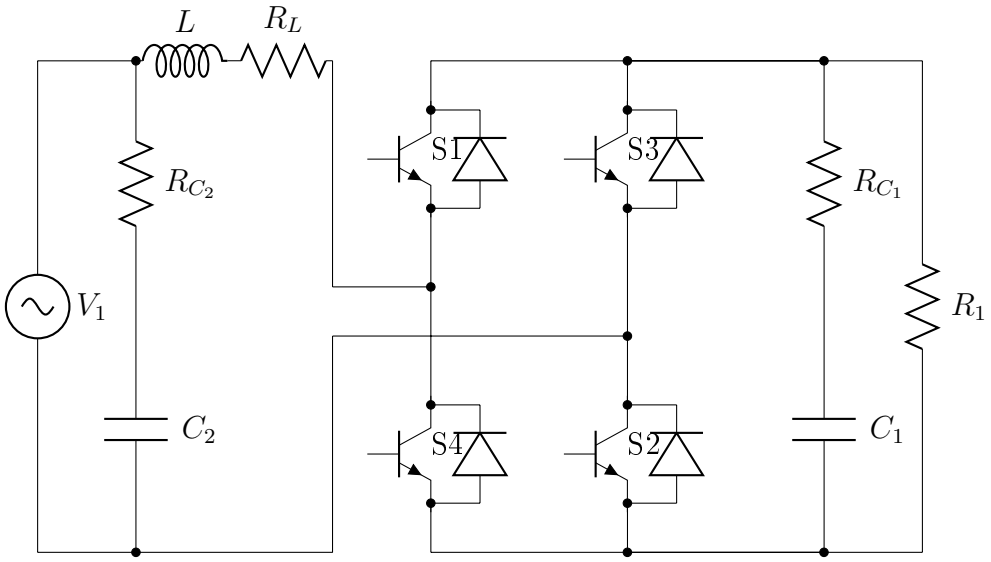

Figure 3.29. Bi-directional PFC circuit representation, in AC/DC operating mode.

OFF and $S_1, S_2 = OFF, S_3, S_4 = ON$ similarly to what has been done in section 3.1. Since the converter is analyzed in continuous conduction mode of operation only 2 switches states are possible. State space equations are derived for each of the possible circuit configurations. Equivalent series resistors are considered for each component and ON resistors are used to model the switch and diode ON state.

Mode 1: $\mathbf{S_1}$, $\mathbf{S_2}$ = ON, $\mathbf{S_3}$, $\mathbf{S_4}$ = OFF

When switches S_1 and S_2 are in the ON state the respective anti-parallel diodes are OFF and switches S_3, S_4 are OFF, whereas diodes D_3, $D_4 = ON$. Following state space equations, referring to state $\mathbf{x} = [v_{R_1} \;\; i_L]'$ are given:

$$\frac{dv_{R_1}}{dt} = -\frac{1}{C_1(R + R_{C_1})}\, v_{R_1} \tag{3.65}$$

$$\frac{di_L}{dt} = -\frac{R_L + R_s}{L}\, i_L \tag{3.66}$$

Mode 2: $\mathbf{S_1}$, $\mathbf{S_2}$ = OFF, $\mathbf{S_3}$, $\mathbf{S_4}$ = ON

Similar analysis has been done for the alternate switches states. Switches S_1 and S_2 are off whereas their anti-parallel diodes D_1, D_2 and switches S_3 and S_4 are ON.

$$\frac{dv_{R_1}}{dt} = -\frac{1}{C_1(R+R_{C_1})}\, v_{R_1} + \frac{R}{C_1(R+R_{C_1})}\, i_L \tag{3.67}$$

$$\frac{di_L}{dt} = -\frac{R}{L(R+R_{C_1})}\, v_{R_1} - \left[\frac{RR_{C_1}}{L(R+R_{C_1})} + \frac{R_L+R_D}{L}\right] i_L \tag{3.68}$$

Combined model can be obtained considering above state space equations in conjunction. Following typical space state system representation is derived:

$$\frac{dv_{R_1}}{dt} = -\frac{1}{C_1(R+R_{C_1})}\, v_{R_1} + \left[\frac{R}{C_1(R+R_{C_1})}\, i_L\right] u$$

$$\frac{di_L}{dt} = -\frac{R_L+R_s}{L}\, i_L - \left[\left(\frac{RR_{C_1}}{L(R+R_{C_1})} + \frac{R_L+R_D}{L}\right) i_L + \frac{R}{L(R+R_{C_1})}\, v_{C_1}\right] u$$

3.4.5.2 DC/AC mode. When manual switches are positioned to work as a DC/AC inverter battery is used as a DC voltage source V_2 to allow power flow to AC side equivalent resistor R_2. Low voltage coming from the battery source is boosted and converted to an AC voltage thanks to a proper switching scheme of the H-bridge. In this operating situation no equations or simulations are derived but equivalent circuit schematic is represented in figure 3.30.

3.4.6 Design Considerations. This section discusses the choice of the most important components, considering the converter to be working mainly as an AC/DC rectifier as a battery charger. Theoretical constraints and practical issues are derived, based on the considerations explained in [3], where the choice of components for a unity power factor correction circuit is derived, providing a rigorous method.

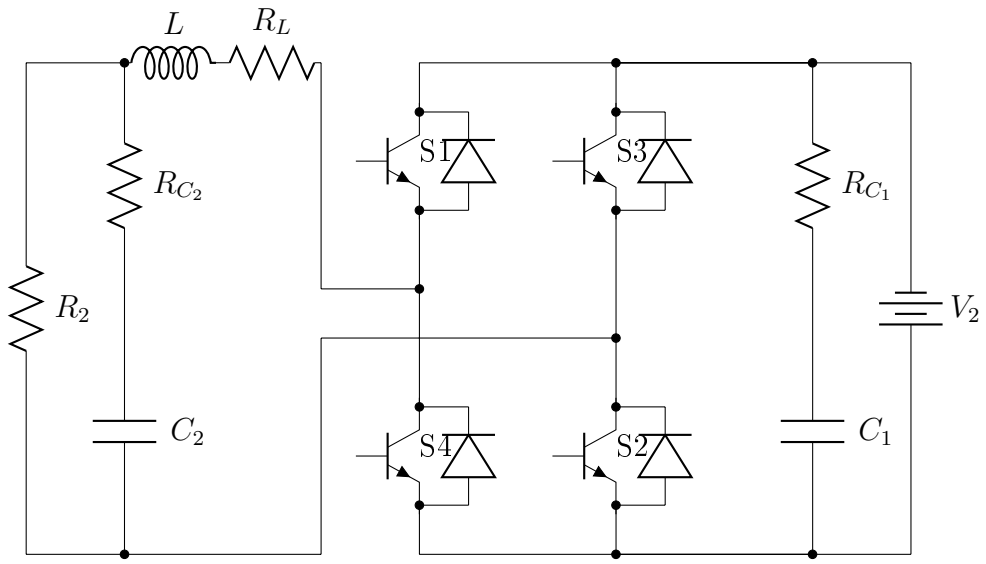

Figure 3.30. Bi-directional PFC circuit representation, in DC/AC operating mode.

As the main purpose of the power factor correction circuit is that to improve the PF value, shaping input current to be perfectly in phase with the input voltage, and being a scaled waveform of it, one of the most critical components is the AC side inductor. In particular, its ripple is considered for continuous conduction mode of operation, and is given by following equation:

$$\Delta I_L = \frac{V_1 d_{AC}}{f_s L} \tag{3.69}$$

whereas before, f_s indicates the switching frequency, and d_{AC} the instantaneous value of the duty cycle.

Ripple in input inductor current, as shown in equation 3.69, is proportional to input voltage amplitude, thus providing a design constraint, which has to be optimized for the maximum input voltage case. On the other hand, a large value of the inductor L will result in a lower current ripple, providing a closer reference tracking, and a lower Total Harmonic Distortion (THD). One major design issue, in the rating of the input inductor, is given by the tradeoff between the ripple amplitude above explained

and the drawn current rating capabilities of the component. In fact, for a low input voltage, the ripple is low while a higher current is drawn from the grid. Thus the inductor has to be sized consequently. Regulation of the input inductor current, which is forced to track a line frequency sine wave, is done through a very fast switching sequence. While it increases the switching losses and significantly decreases efficiency of the converter, it can be used as a design parameter to reduce the amplitude of the current ripple.

Another important component in PFC circuit is given by the DC bus capacitor, responsible for the rectified DC bus voltage ripple, oscillating at twice the line frequency as a perfect sine wave. Considering a constant DC load power, the DC bus capacitor voltage increases when input power is higher than the load power, storing the extra energy provided. On the other hand, when the input power is lower than the load power, the effect is opposite, thus showing the regular oscillating wave in the voltage waveform. As calculated in [3], DC bus voltage V_{bus} can be expressed as:

$$V_{bus} \approx \frac{P_{in}}{2\omega C_1 V_{bus}} sin(2\omega t) \tag{3.70}$$

where P_{in} indicates the input rated power and ω is the angular frequency of input voltage.

As before, a second ripple in the DC bus voltage is given by following relation, function of the duty cycle d_{AC} and also of the equivalent load, or depending on the following DC/DC converter stage d_{DC} in cascaded system.

$$\Delta V_{bus} = \frac{I_{L_{DC}} d_{DC} d_{AC}}{f_s C_1} \tag{3.71}$$

Ripple amplitude is much smaller than the previous case, and has a higher frequency. It is highly dependent on the value of the DC bus capacitor C_1. It is rated such that it minimizes the two identified ripples, as an important issue for the stability performance. Lowest input voltage and rated power conditions have to been used as

the critical case in the sizing of the component, as will be shown later in chapter 5 which deals with the stability analysis.

3.4.7 Simulink Model and Simulations. The bi-directional Power Factor Correction rectifier circuit presented in the previous sections is now modeled using MATLAB® SimPower Systems toolbox in Simulink.

All passive elements, including the AC side inductor, input and output capacitors, are modeled as linear elements with a small valued Equivalent Series Resistor (ESR). Semiconductor devices are modeled using MATLAB® MOSFET blocks, considering the internal resistance R_{on} for the FET and internal resistance of the anti-parallel diode R_d. Switches behavior is considered ideal, as pure ON-OFF switches, where snubber resistance, snubber capacitance and other non-idealities are not considered. Output load of the circuit is modeled as a pure resistive one, whereas when switching to inverter mode, input DC voltage is considered constant and modeled as an ideal voltage source.

Switching between the two systems, corresponding to the AC/DC rectifier or DC/AC inverter circuits, is done using a series of manual switches that connect or disconnect respectively either load or voltage source.

PFC converters, like most power electronics circuits, cannot function without feedback control. As shown in figure 3.31 and 3.32, which represent unregulated PFC operation, without a proper control scheme, output voltage and AC side inductor current shape does not meet the requirements of unity power factor. Output DC voltage presents typical ripple oscillations while inductor current shows alternating spikes with high harmonics content.

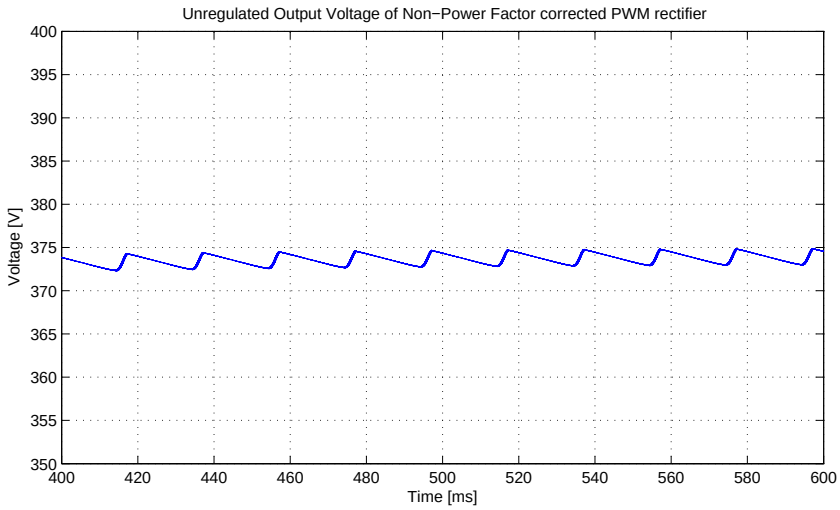

Figure 3.31. Output voltage ripple of a Non-Power Factor regulated Boost Converter.

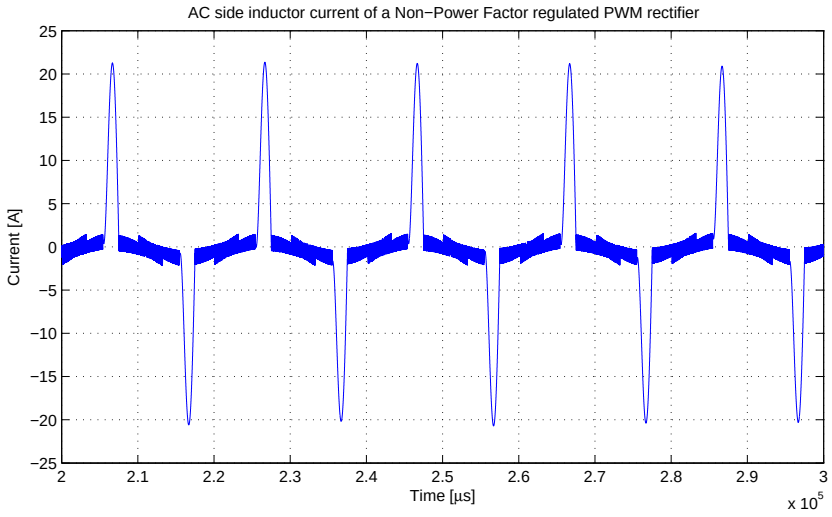

Figure 3.32. Inductor current waveform of a Non-Power Factor regulated Boost Converter.

3.4.7.1 DC Voltage Controller. The outer loop in the control scheme is the voltage feedback. The input to the voltage regulator is the reference DC voltage v_{dc}^{*} and the actual sensed output DC voltage v_{DC}. The voltage error compensator is designed to produce a control signal such as the DC bus voltage remains constant at the desired level, regardless variations of the input or in the load current. Output of this outer loop is then used to determine the inductor current reference signal, thanks to the current controller for the inner loop.

A simple proportional integral (PI) controller is selected for DC voltage regulation, through error feedback of the sensed output voltage compared with reference voltage. Voltage error v_e, is calculated as

$$v_e = v_{dc}^{*} - v_{DC} \tag{3.72}$$

and processed by the PI voltage regulator, which output is given by

$$v_{PI} = K_P \cdot v_e + K_I \cdot \int v_e. \tag{3.73}$$

Controller parameters, given by gains K_P and K_I represent respectively proportional and integral constants.

3.4.7.2 Average Current Control Loop. Average mode current control operates by directly comparing the actual inductor current waveform to the reference signal, obtained as the voltage controller output. This high gain current error amplifier tracks the current sinusoidal reference with a high degree of accuracy, enabling high power factor and providing excellent noise immunity. Output current signal should match as closely as possible the AC input voltage to have high power factor.

Output voltage, from the voltage control loop, is used to control the average value of the current amplitude signal, while a sinusoidal reference signal, in phase with AC input voltage, provides the shape. Current reference signal is calculated by

calculating the product between the scaled input voltage v_{AC}, the voltage controlled error v_{PI} and the output of voltage feed-forward compensator. When input voltage increases, the product of v_{AC} and v_{PI} increases, and thereby increasing the reference i^*_{AC}. When the signal is divided by the square of the average voltage signal, it results in the current reference signal being reduced proportionally. The outcome is that also the current is reduced proportionally to the increase in voltage, thus keeping the input power constant.

If the voltage decreases, the product $v_{AC} \cdot v_{PI}$, which determines current reference, also proportionally decreases. However, to maintain a constant output power at reduced input voltage, the term i^*_{AC} should proportionally increase. The voltage feed-forward compensator is essential to maintain a constant output power because it compensates for the variations in input voltage from its nominal value. This compensator is implemented by calculating the RMS value of the input line voltage, squaring this value and using the result as a divider for the input reference current, which is fed to the current error compensator. If v_{AC} is the sinusoidal input voltage to the PFC circuit, the input voltage feed-forward term is calculated as shown in following equation:

$$v_{FF} = 1/(v_{AC} \cdot 2/pi)^2. \tag{3.74}$$

As before, the input current error is given by the difference between the reference current calculated from the outer control loop and the actual current, $i_e = i^*_L - i_L$. It is processed through a high gain PI controller as

$$i_{PI} = K_P \cdot i_e + K_I \cdot \int i_e. \tag{3.75}$$

Output of PI controller is then processed through a PWM comparator in order to obtain switching pattern for semiconductor devices. Output signal is in fact compared with a fixed frequency saw-tooth waveform oscillating at switching

frequency f_s, obtaining a binary valued square wave.

Some simulation results are shown in figures 3.33 and 3.34, including inductor current waveform perfectly in phase with the AC input voltage, and DC bus voltage. Test results show Power Factor improvements and current harmonic reduction, compared with unregulated waveforms in figure 3.31 and 3.32.

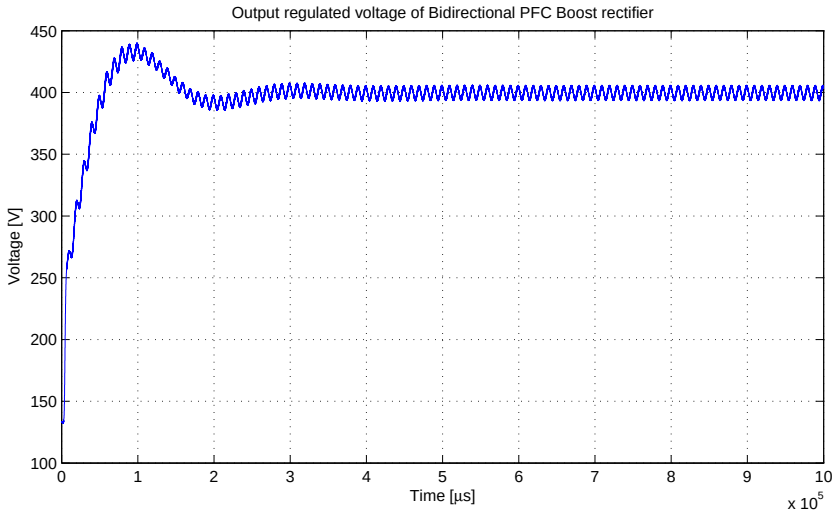

Figure 3.33. Output voltage waveform of a Power Factor regulated Boost rectifier.

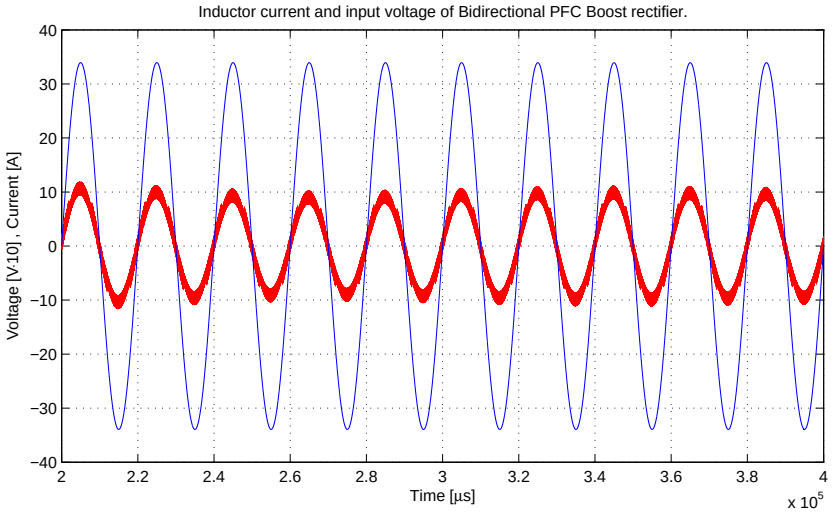

Figure 3.34. Inductor current waveform of a Power Factor regulated Boost rectifier.

DC/AC rectification operation is fairly simple and control structure turns out to be less complex. Reference AC voltage waveform is given by a sinusoidal source, perfectly in phase with desired AC voltage, which amplitude is scaled as to meet the requirements. Sensed output voltage is then compared with the reference, producing the error signal, which is processed through a PI controller and a pulse generator. PWM generator output is a series of pulses with values 0 or 1, for the upper switches and for the lower switches respectively, proportional to its input signal.

Results of the DC/AC inverter operation mode are shown in following figures, including the generation of an AC sinusoidal voltage waveform and the corresponding AC side inductor current.

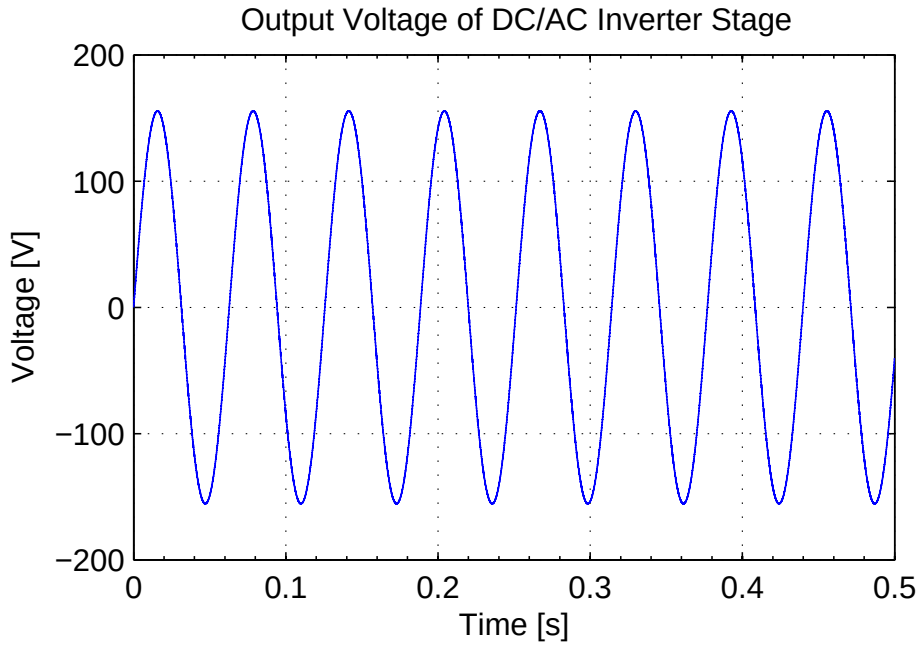

Figure 3.35. Output voltage waveform of a DC/AC PFC inverter.

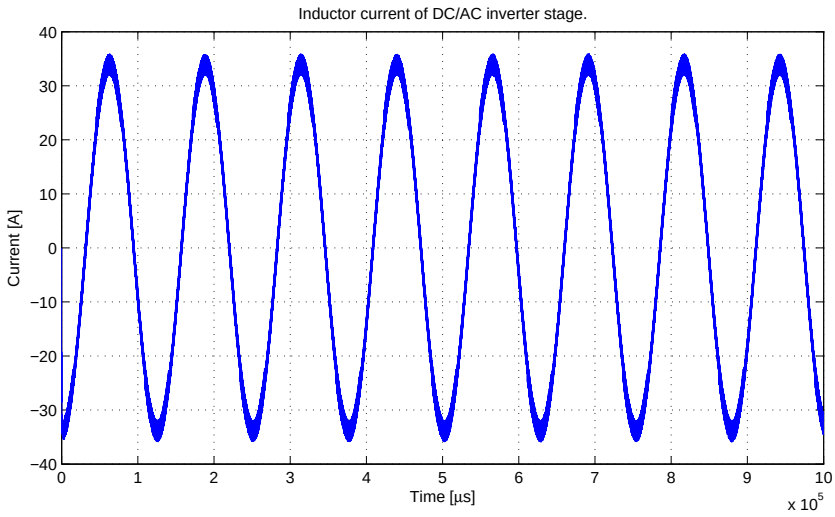

Figure 3.36. Inductor current waveform of a DC/AC PFC inverter.

3.5 Overall Battery Charger Model

The section describes the modeling of the overall converter using a state-space system, which is given as a cascaded configuration of two circuits explained above. Switching between linear circuits, consisting of a series of storage elements, inductances and capacitors, can be obtained by use of transistors, diodes and other switching devices. Under the assumption that circuits are working in Continuous Conduction Mode of operation, in which instantaneous inductor current never drops to zero at any point has been chosen conveniently following usual adoption for electrical networks. They can be represented by a set of linear state space equations, which can be combined together to form global state space model.

Non-linear continuous systems, such as those described, can be written in the typical form of space-state models using following system equations, where an n-dimensional vector state $\mathbf{x}$ and an m-dimensional input u are considered as shown:

$$\dot{\mathbf{x}}(t) = A(\mathbf{x}, t) + B(\mathbf{x}, t)\, u \tag{3.76}$$

$$\mathbf{y}(t) = C(\mathbf{x}, t) + D(\mathbf{x}, t)\, u \tag{3.77}$$

Furthermore, to replace the state space descriptions of equivalent linear circuit given by the different switches values across the whole period T, a single system can be derived. Differential equations for the two configurations are averaged by summing the equations for interval d and $(1-d)$. As before, resulting equations for equivalent circuit during interval d, and its complementary $d' = (1-d)$, can be grouped in a single expression, resulting in the following linear continuous system:

$$\begin{aligned}\dot{\mathbf{x}} &= d(A_1\mathbf{x} + B_1\, u) + d'(A_2\mathbf{x} + B_2\, u) \\ &= (dA_1 + d'A_2)\mathbf{x} + (dB_1 + d'B_2) \\ \mathbf{y} &= dy_1 + d'y_2 = (dC_1 + d'C_2) + (dD_1 + d'D_2)\mathbf{x}\end{aligned}$$

As shown in above equation, system matrix A of the averaged model can be obtained by taking the average of the two switched model matrices A_1 and A_2, which dynamic is given by the average of the two state dynamic matrices weighted with the duty cycle value. In this particular application, whereas state space averaging techniques have been largely adopted in many research papers, it is chosen not to linearize the circuit, thus considering its large-signal model. In particular high-frequency modulation effects cannot be seen using the small-signal model. Furthermore the circuit is now analyzed considering its time-variant state space representation, given by mathematical equations shown in following section.

Similarly, using linear system theory knowledge, input-output and input-state relations can be derived from the dynamic model as vector transfer functions. Complete description of system behavior using t.f., adopted in particular for stability analysis as will be explained later, in the frequency domain, is simply given by the general form:

$$\frac{X(s)}{U(s)} = (sI - A)^{-1}B \tag{3.78}$$

$$\frac{Y(s)}{U(s)} = C(sI - A)^{-1}B + D \tag{3.79}$$

3.5.1 State-Space Model. The illustrated technique that was used for the two separate stages of the converter in previous sections is now applied to overall system. Equivalent circuit of proposed battery charger, composed of the cascaded converters, is now simplified in order to obtain a single input output relation.

Rectification operation, previously obtained using a four switches device, is now schematized with a single switch which provides already rectified input voltage. Sinusoidal inductor current is thus maintained by changing the direction of the current during the negative half cycle of line voltage by changing the pair of switches. Parasitic elements and on-state resistor are considered in the non-ideal model description, where switching devices are represented by $S_{boost} = S_1$ and $S_{buck} = S_2$. Equivalent resistor load for the PFC boost rectifier is now substituted with the DC/DC converter and battery load is considered to be simply resistive. PWM boost rectifier followed by bi-directional buck-boost circuit is thus considered equivalent to circuit in figure 3.37, where $V_S = |V_{AC}|$ is the rectified version of the input voltage.

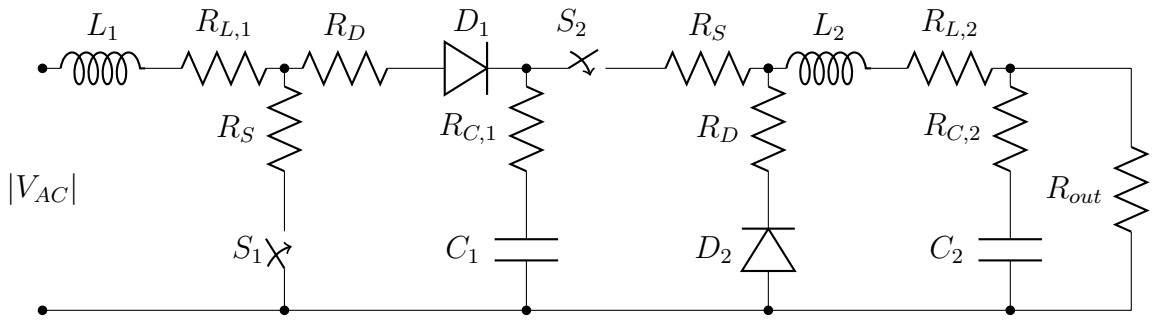

Figure 3.37. Equivalent Non-Ideal circuit representation for charger.

Two above described models can be combined together in order to summarize bi-directional buck-boost non-ideal circuit, writing a new system of four equations considering following states variables $v_{C,1}$, $v_{C,2}$, $i_{L,1}$ and $i_{L,2}$. State vector is given by

$$\mathbf{x} = \begin{bmatrix} v_{C,1} & v_{C,2} & i_{L,1} & i_{L,2} \end{bmatrix}^T,$$

while input is scalar and consisting in rectified version of sinusoidal AC voltage waveform $|V_{AC}|$. Matrices of the system expressed in the form 3.76 and 3.77, where matrix $D(\mathbf{x}, t) = 0$, are the following:

$$A = \begin{bmatrix} 0 & 0 & \frac{1}{C_1}(1-d_{AC}) & -\frac{1}{C_1}d_{DC} \\ 0 & -\frac{1}{C_2(R_{out}+R_{C,2})} & 0 & \frac{R_{out}}{C_2(R_{out}+R_{C,2})} \\ -\frac{1}{L_1}(1-d_{AC}) & 0 & -\frac{R_{L,1}+2R_{S,1}}{L_1} - \frac{R_{C,1}(1-d_{AC})}{L_1} & \frac{R_{C,1}(1-d_{AC})d_{DC}}{L_1} \\ \frac{1}{L_2}d_{DC} & -\frac{R_{out}}{L_2(R_{out}+R_{C,2})} & \frac{R_{C,1}}{L_2}(1-d_{AC})d_{DC} & -\frac{R_{out}R_{C,2}}{L_2(R_{\text{out}}+R_{C,2})} - \frac{R_{L,2}+R_{DS}}{L_2} - \frac{R_{C,1}}{L_2}d_{DC} \end{bmatrix}$$

$$B = \begin{bmatrix} 0 \\ 0 \\ \dfrac{1}{L_1} \\ 0 \end{bmatrix}$$

$$C = \begin{bmatrix} 0 & \dfrac{R_{\text{out}}R_{C,2}}{R_{\text{out}}+R_{C,2}} & 0 & \dfrac{R_{\text{out}}}{R_{\text{out}}+R_{C,2}} \end{bmatrix}$$

As can be easily noticed, the time-variant characteristic of the circuit, is expressed by the duty cycles instantaneous values d_{AC} and d_{DC}, representing the PFC circuit and DC/DC converter switches respectively. In particular, the configuration of the system, highly dependent on the binary values of the switching devices, and not on their averaged value, will be further analyzed in following sections.

3.5.2 Simulink Model and Simulation Results. Simulation results from the overall model of the battery charger, working as a bi-directional converter is implemented here in MATLAB® Simulink, in both the circuital and mathematical model are presented. Mathematical model previously derived, due to some basic assumptions done to simplify the circuit behavior, is working only as a unidirectional converter. In this study only charging simulations will be presented, recalling previous sections for the DC/AC operation mode of the cascaded system.

Important waveforms are shown here, and will be further discussed in following chapters where a detailed comparison with the novel digital approach and stability analysis for the two different strategies is done. Input inductor current, which is shaped by the two-loop controller, is shown in figure 3.38, where, after a small transient, it follows the sinusoidal voltage reference, obtaining in the steady state an

almost perfect sine waveform, as can be seen also from the FFT analysis in figure 3.39.

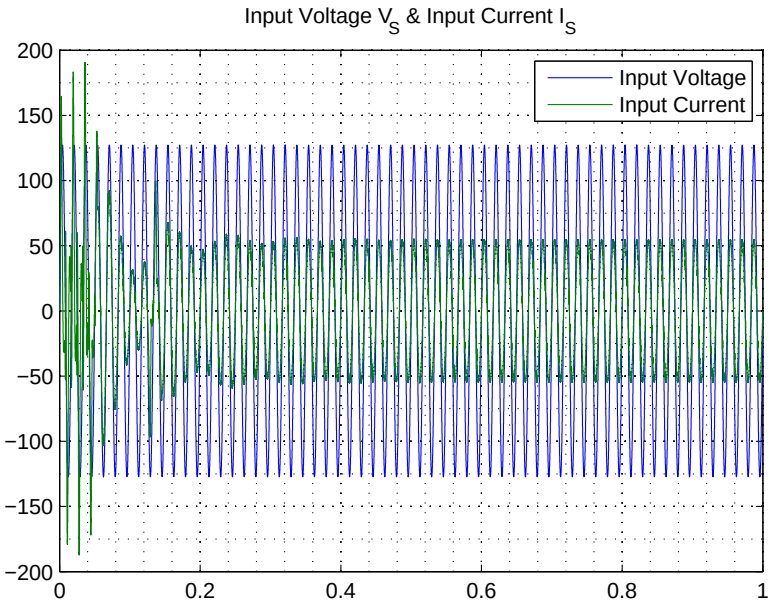

Figure 3.38. Input current and sinusoidal voltage reference plots.

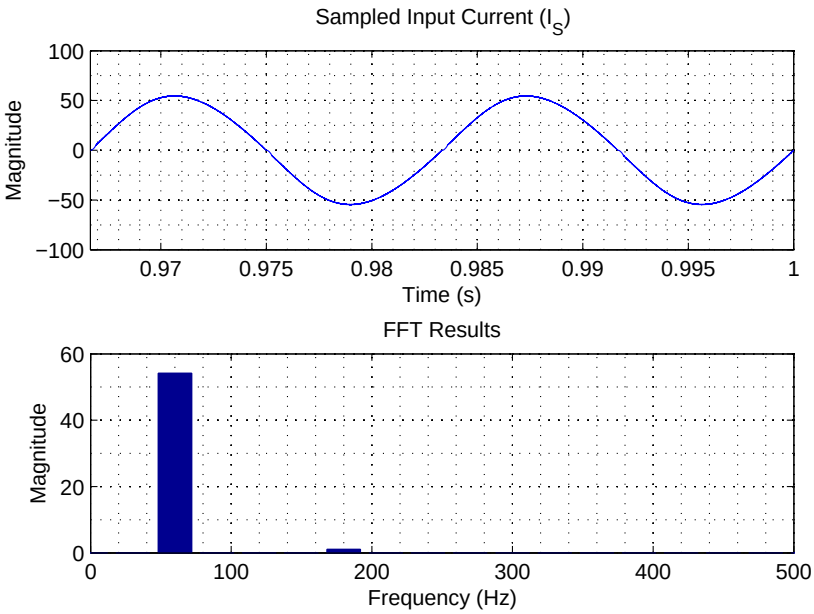

Figure 3.39. FFT analysis and steady state plot of sinusoidal input current.

Second important waveform is the response of the DC bus capacitor voltage, V_{bus}, which is characterized by a ripple at twice the input frequency given, as explained, by the imbalance of the AC input and DC output power. The voltage waveform, shown in figure 3.40 represents a stable operating point, where the transient response is fast and desired output is easily obtained thanks to a precise tuning of controllers' parameters.

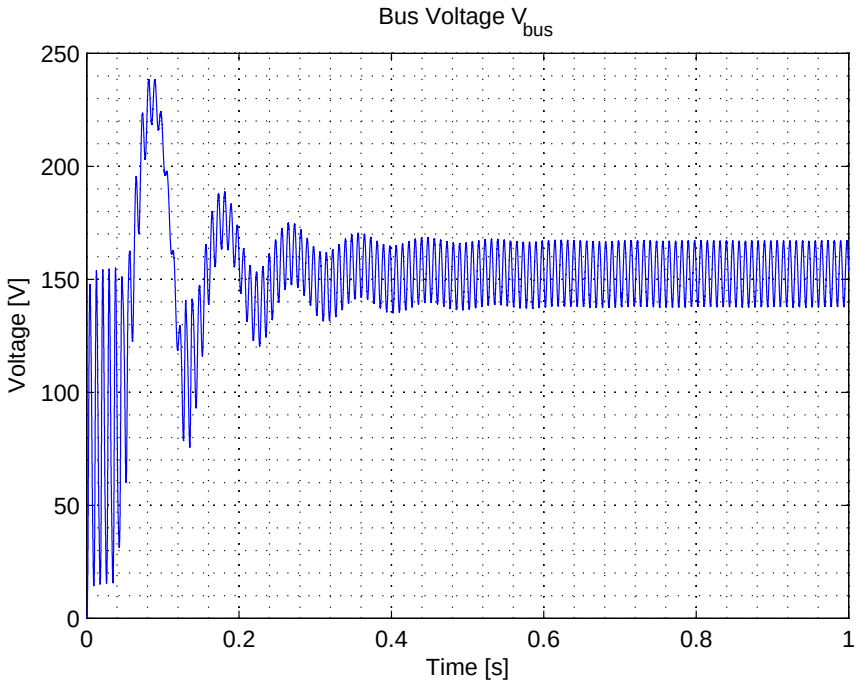

Figure 3.40. DC bus voltage waveform plot.

Output stage, given by the DC/DC converter, working as a buck, provides regulated output current at the battery constant voltage V_b, thanks to the PI control loop. Therefore, the output current settles to reference value after a small transient as shown in figure 3.41.

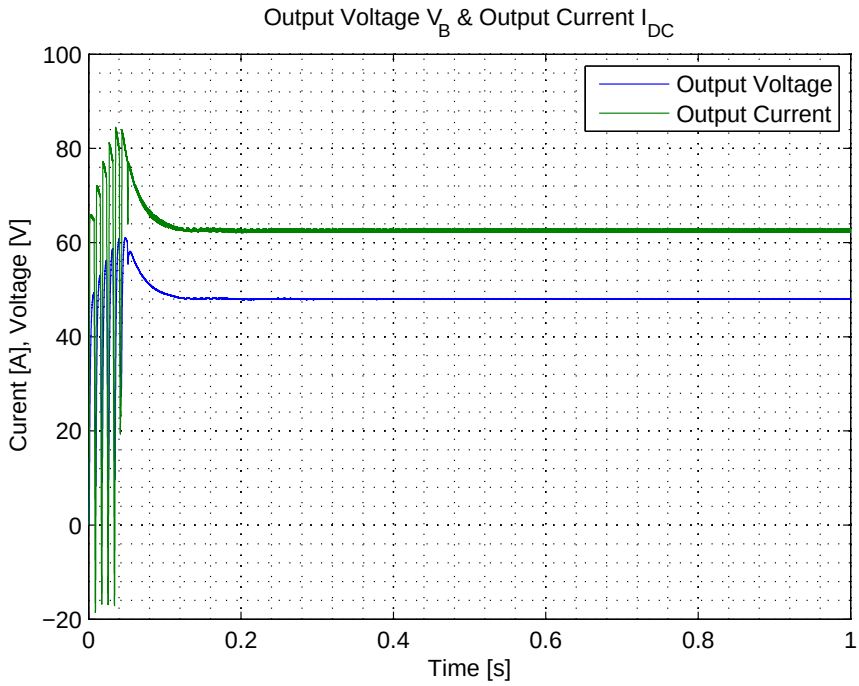

Figure 3.41. DC/DC converter output waveforms plots.

3.5.3 Transfer Functions of the system. The derived space state model is completely described by matrices $\Sigma = (A, B, C, D)$ represents a highly non-linear and time-variant system. System configuration depends on the different states of the switches d_{AC} and d_{DC}. Specifically, since each switch can assume values in the discrete set $d \in \{0, 1\}$, possible states combinations include both switches open, both switches closed, and the alternate case. All possible scenarios for this non-linear system are studied providing the bases for a full analysis performed in next chapter, involving different criteria. State space mathematical model is therefore simplified considering each different configuration separately. Mathematical analysis can be done for each system, using four different matrices sets.

In following pages, a preliminary mathematical representation of the system is provided. Transfer functions, which can be easily used for the stability analysis and to analyze poles plots, are calculated. A more precise and analytical approach can be pursued in order to confirm practical results obtained in this work.

In particular, a general vectorial input-state transfer function $W_{IS}(s)$ for global system is derived as follows:

$$W_{IS}(s) = \frac{X(s)}{U(s)} = (sI - A)^{-1}B \tag{3.80}$$

where A and B matrices are given in previous section.

Using equation 3.80 four different transfer functions are derived for each state $\mathbf{x}$ as follows.

3.5.3.1 S_1 ON, S_2 ON. When both switches are in the ON state, duty cycle d_{AC} and d_{DC} assume unit value, and equivalent matrix A is obtained:

$$A_{1,1} = \begin{bmatrix} 0 & 0 & 0 & -\frac{1}{C_1} \\ 0 & -\frac{1}{C_2(R_{out}+R_{C,2})} & 0 & \frac{R_{out}}{C_2(R_{out}+R_{C,2})} \\ 0 & 0 & -\frac{R_{L,1}+2R_{S,1}}{L_1} & 0 \\ \frac{1}{L_2} & -\frac{R_{out}}{L_2(R_{out}+R_{C,2})} & 0 & -\frac{R_{out}R_{C,2}}{L_2(R_{out}+R_{C,2})} - \frac{R_{L,2}+R_{DS}}{L_2} - \frac{R_{C,1}}{L_2} \end{bmatrix}$$

Calculating transfer function W_1 we get following third grade rational expression, for given components values:

$$W_1(s) = \frac{X_1(s)}{U(s)} = (sI - A_{1,1})^{-1}B \equiv 0 \tag{3.81}$$

Similarly, transfer functions W_2, W_3 and W_4 are calculated, and their bode plots and root locus diagrams are shown.

$$W_2(s) = \frac{X_2(s)}{U(s)} \equiv 0 \tag{3.82}$$

$$W_3(s) = \frac{X_3(s)}{U(s)} = \frac{10^4 L_1}{3(R_{L,1} + 2R_{S,1} + L_1 s)} = \frac{3333}{s + 133.3} \tag{3.83}$$

$$W_4(s) = \frac{X_4(s)}{U(s)} \equiv 0 \tag{3.84}$$

As can be easily noticed, all scalar transfer functions are characterized by same poles position. Denominator analytical expression comes from the determinant of matrix $(sI - A_{i,i})$ and depends on parameters defined in Appendix. Bode plots for derived functions are given, together with root locus graphs.

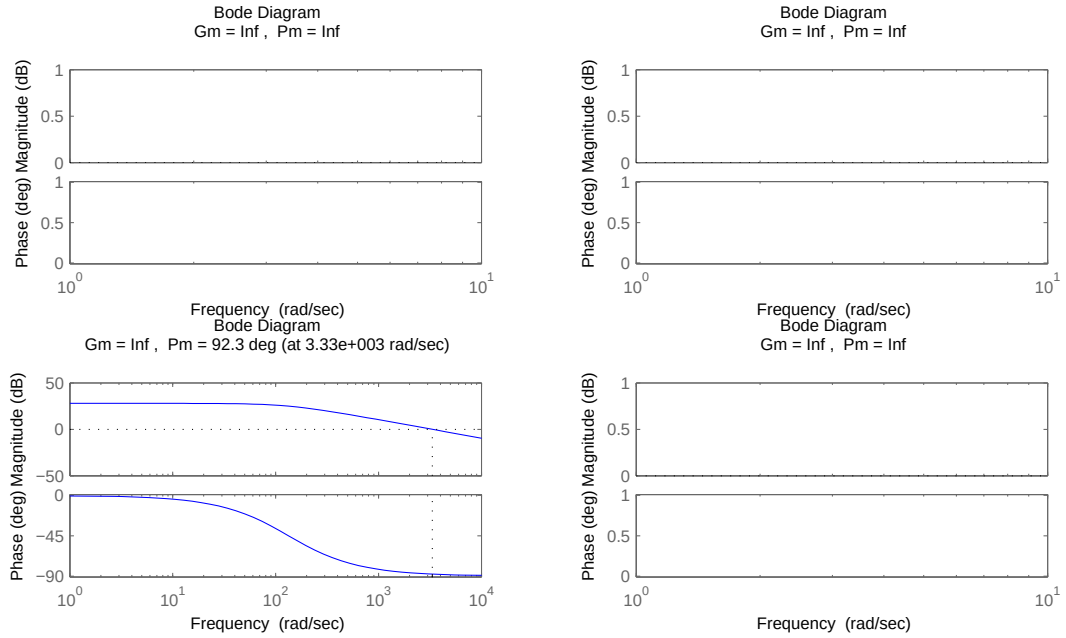

Figure 3.42. Bode plots for the four transfer functions corresponding to $d_{AC} = 1$ and $d_{DC} = 1$.

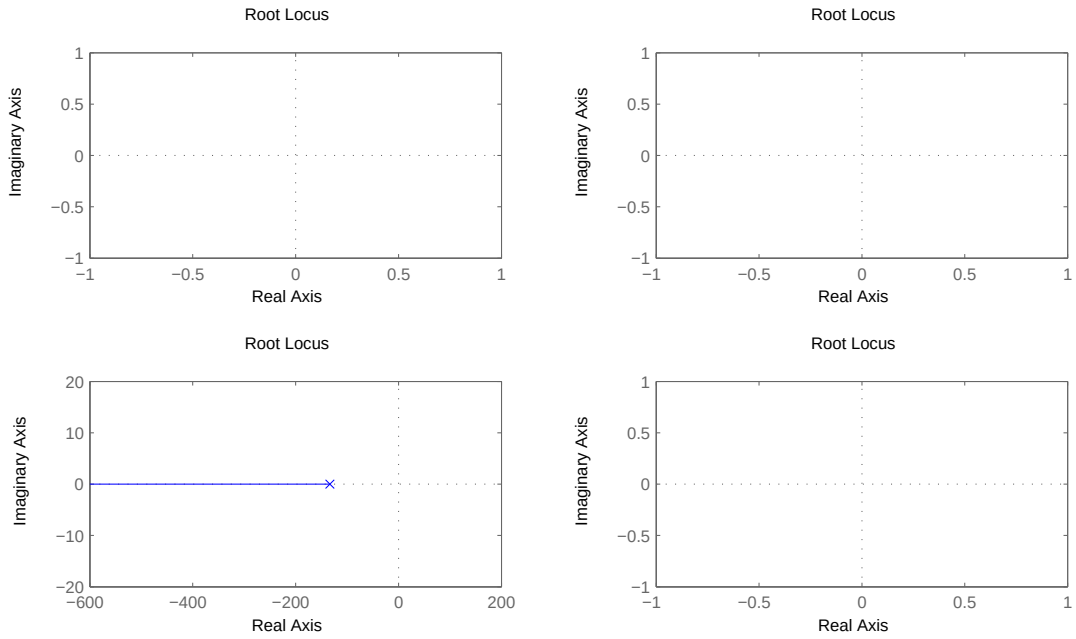

Figure 3.43. Root locus diagram for the four transfer functions corresponding to $d_{AC} = 1$ and $d_{DC} = 1$.

3.5.3.2 S_1 **OFF,** S_2 **ON.** When switches configurations corresponds to instantaneous duty cycle values of $d_{AC} = 0$ and $d_{DC} = 1$, equivalent matrix A is obtained:

$$A_{0,1} = \begin{bmatrix} 0 & 0 & \frac{1}{C_1} & -\frac{1}{C_1} \\ 0 & -\frac{1}{C_2(R_{out}+R_{C,2})} & 0 & \frac{R_{out}}{C_2(R_{out}+R_{C,2})} \\ -\frac{1}{L_1} & 0 & -\frac{R_{L,1}+2R_{S,1}}{L_1} - \frac{R_{C,1}}{L_1} & \frac{R_{C,1}}{L_1} \\ \frac{1}{L_2} & -\frac{R_{out}}{L_2(R_{out}+R_{C,2})} & \frac{R_{C,1}}{L_2} & -\frac{R_{out}R_{C,2}}{L_2(R_{out}+R_{C,2})} - \frac{R_{L,2}+R_{DS}}{L_2} - \frac{R_{C,1}}{L_2} \end{bmatrix}$$

Exactly as before the four scalar transfer functions are calculated using formula 3.80.

$$W_1(s) = \frac{X_1(s)}{U(s)} = \frac{2.778 \cdot 10^6 s^2 + 3.182 \cdot 10^9 s + 3.817 \cdot 10^{12}}{s^4 + 1279 s^3 + 5.863 \cdot 10^6 s^2 + 1.373 \cdot 10^8 s + 2.095 \cdot 10^{12}} \tag{3.85}$$

$$W_1(s) = \frac{[10^4 L_1(R_{DS} + R_{L_2} + R_{out} + L_2 s + C_2 L_2 R_{C_2} s^2 + C_2 L_2 R_{out} s^2 + \dots}{D(s)} \tag{3.86}$$

$$\dots \frac{+C_2 R_{C_2} R_{DS} s + C_2 R_{C_2} R_{L_2} s + C_2 R_{C_2} R_{out} s + C_2 R_{DS} R_{out} s + C_2 R_{L_2} R_{out} s)]}{D(s)}$$

$$W_2(s) = \frac{X_2(s)}{U(s)} = \frac{8.815 \cdot 10^8 s + 3.673 \cdot 10^{12}}{s^4 + 1279 s^3 + 5.863 \cdot 10^6 s^2 + 1.373 \cdot 10^8 s + 2.095 \cdot 10^{12}} \tag{3.87}$$

$$W_2(s) = \frac{10^4 L_1 R_{out}(C_1 R_{C_1} s + 1)}{D(s)} \tag{3.88}$$

$$W_3(s) = \frac{X_3(s)}{U(s)} = \frac{3333 s^3 + 6.04 \cdot 10^6 s^2 + 1.499 \cdot 10^{10} s + 4.783 \cdot 10^{12}}{s^4 + 1279 s^3 + 5.863 \cdot 10^6 s^2 + 1.373 \cdot 10^8 s + 2.095 \cdot 10^{12}} \tag{3.89}$$

$$W_3(s) = \frac{10^4 L_1 [C_1 R_{C_1} s + C_2 R_{C_2} s + C_1 R_{DS} s + C_1 R_{L_2} s + C_1 R_{out} s + C_2 R_{out} s + \dots}{D(s)} \tag{3.90}$$

$$\cdots \frac{+C_1L_2s^2 + C_1C_2L_2R_{C_2}s^3 + C_1C_2L_2R_{out}s^3 + C_1C_2R_{C_1}R_{C_2}s^2 + C_1C_2R_{C_2}R_{DS}s^2 + }{D(s)} \cdots$$
$$\cdots \frac{+C_1C_2R_{C_2}R_{L_2}s^2 + C_1C_2R_{C_1}R_{out}s^2 + C_1C_2R_{C_2}R_{out}s^2 + C_1C_2R_{DS}R_{out}s^2 + }{D(s)} \cdots$$
$$\cdots \frac{+C_1C_2R_{L_2}R_{out}s^2 + 1]}{D(s)}$$

$$W_4(s) = \frac{X_4(s)}{U(s)} = \frac{2.222 \cdot 10^6 s^2 + 1.041 \cdot 10^{10} s + 4.783 \cdot 10^{12}}{s^4 + 1279s^3 + 5.863 \cdot 10^6 s^2 + 1.373 \cdot 10^8 s + 2.095 \cdot 10^{12}} \tag{3.91}$$

$$W_4(s) = \frac{10^4 L_1(C_1R_{C_1}s + 1)(C_2R_{C_2}s + C_2R_{out}s + 1)}{D(s)} \tag{3.92}$$

$$D(s) = 3[R_{DS} - 2R_{C_1} + R_{L_1} + R_{L_2} + 2R_{S1} + R_{out} + L_1s + L_2s - 2C_1R_{C_1}^2 s + \cdots \tag{3.93}$$

$$\cdots + C_1L_1L_2s^3 + C_1L_1R_{C_1}s^2 - C_1L_2R_{C_1}s^2 + C_2L_1R_{C_2}s^2 + C_1L_1R_{DS}s^2 + C_2L_2R_{C_2}s^2 + \cdots$$

$$\cdots + C_1L_1R_{L_2}s^2 + C_1L_2R_{L_1}s^2 + 2C_1L_2R_{S1}s^2 + C_1L_1R_{out}s^2 + C_2L_1R_{out}s^2 + C_2L_2R_{out}s^2 + \cdots$$

$$\cdots - 2C_2R_{C_1}R_{C_2}s - C_1R_{C_1}R_{DS}s + C_2R_{C_2}R_{DS}s + C_1R_{C_1}R_{L_1}s + C_2R_{C_2}R_{L_1}s + \cdots$$

$$\cdots + C_2R_{C_2}R_{L_2}s + C_1R_{DS}R_{L_1}s + 2C_1R_{C_1}R_{S1}s + 2C_2R_{C_2}R_{S1}s + 2C_1R_{DS}R_{S1}s + \cdots$$

$$\cdots + C_1R_{L_1}R_{L_2}s + 2C_1R_{L_2}R_{S1}s - C_1R_{C_1}R_{out}s - 2C_2R_{C_1}R_{out}s + C_2R_{C_2}R_{out}s + \cdots$$

$$\cdots + C_2R_{DS}R_{out}s + C_1R_{L_1}R_{out}s + C_2R_{L_1}R_{out}s + C_2R_{L_2}R_{out}s + 2C_1R_{S1}R_{out}s + \cdots$$

$$\cdots - C_1R_{C_1}R_{L_2}s + C_1C_2L_1L_2R_{C_2}s^4 + C_1C_2L_1L_2R_{out}s^4 + C_1C_2L_1R_{C_1}R_{C_2}s^3 + \cdots$$

$$\cdots + 2C_2R_{S1}R_{out}s - 2C_1C_2R_{C_1}^2R_{C_2}s^2 - 2C_1C_2R_{C_1}^2R_{out}s^2 - C_1C_2L_2R_{C_1}R_{C_2}s^3 + \cdots$$

$$\cdots + C_1C_2L_1R_{C_2}R_{DS}s^3 + C_1C_2L_1R_{C_2}R_{L_2}s^3 + C_1C_2L_2R_{C_2}R_{L_1}s^3 + 2C_1C_2L_2R_{C_2}R_{S1}s^3 + \cdots$$

$$\cdots + C_1C_2L_1R_{C_1}R_{out}s^3 + C_1C_2L_1R_{C_2}R_{out}s^3 - C_1C_2L_2R_{C_1}R_{out}s^3 + C_1C_2L_1R_{DS}R_{out}s^3 + \cdots$$

$$\cdots + C_1C_2L_1R_{L_2}R_{out}s^3 + C_1C_2L_2R_{L_1}R_{out}s^3 + 2C_1C_2L_2R_{S1}R_{out}s^3 - C_1C_2R_{C_1}R_{C_2}R_{DS}s^2 + \cdots$$

$$\cdots + C_1C_2R_{C_1}R_{C_2}R_{L_1}s^2 - C_1C_2R_{C_1}R_{C_2}R_{L_2}s^2 + C_1C_2R_{C_2}R_{DS}R_{L_1}s^2 + \cdots$$

$$\cdots + 2C_1C_2R_{C_1}R_{C_2}R_{S1}s^2 + 2C_1C_2R_{C_2}R_{DS}R_{S1}s^2 + C_1C_2R_{C_2}R_{L_1}R_{L_2}s^2 + \cdots$$

$$\cdots + 2C_1C_2R_{C_2}R_{L_2}R_{S1}s^2 - C_1C_2R_{C_1}R_{C_2}R_{out}s^2 - C_1C_2R_{C_1}R_{DS}R_{out}s^2 + \cdots$$

$$\cdots + C_1C_2R_{C_1}R_{L_1}R_{out}s^2 - C_1C_2R_{C_1}R_{L_2}R_{out}s^2 + C_1C_2R_{C_2}R_{L_1}R_{out}s^2 + \cdots$$

$$\cdots + C_1C_2R_{DS}R_{L_1}R_{out}s^2 + 2C_1C_2R_{C_1}R_{S1}R_{out}s^2 + 2C_1C_2R_{C_2}R_{S1}R_{out}s^2 + \cdots$$

$$\cdots + 2C_1C_2R_{DS}R_{S1}R_{out}s^2 + C_1C_2R_{L_1}R_{L_2}R_{out}s^2 + 2C_1C_2R_{L_2}R_{S1}R_{out}s^2]$$

Bode plots and root locus are shown for the case S_1 OFF, S_2 ON.

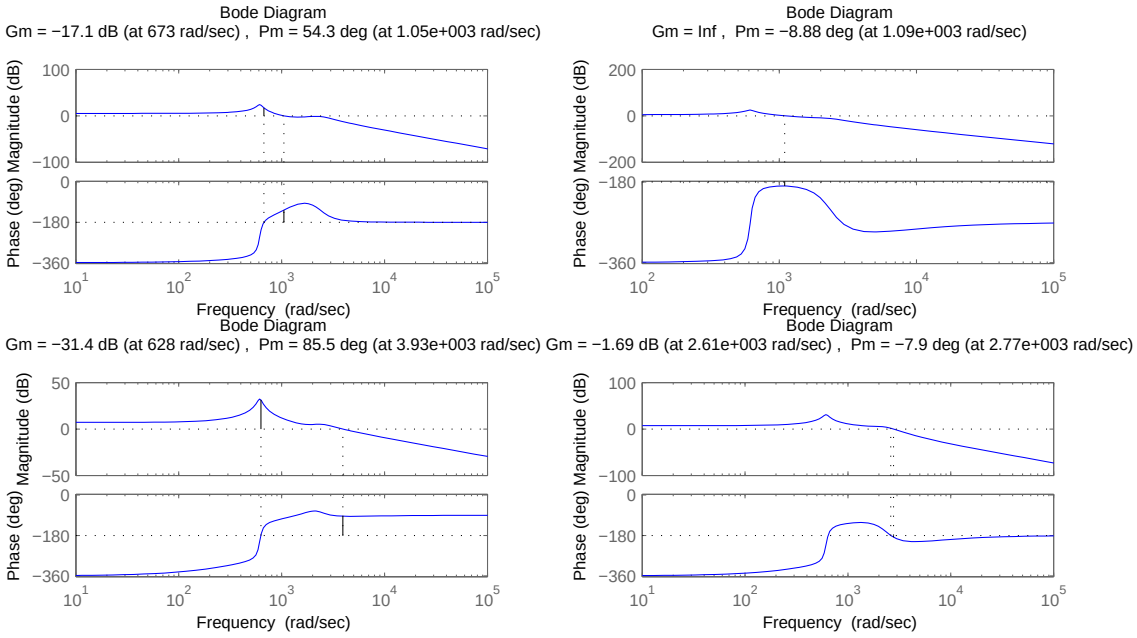

Figure 3.44. Bode plots for the four transfer functions corresponding to $d_{AC} = 0$ and $d_{DC} = 1$.

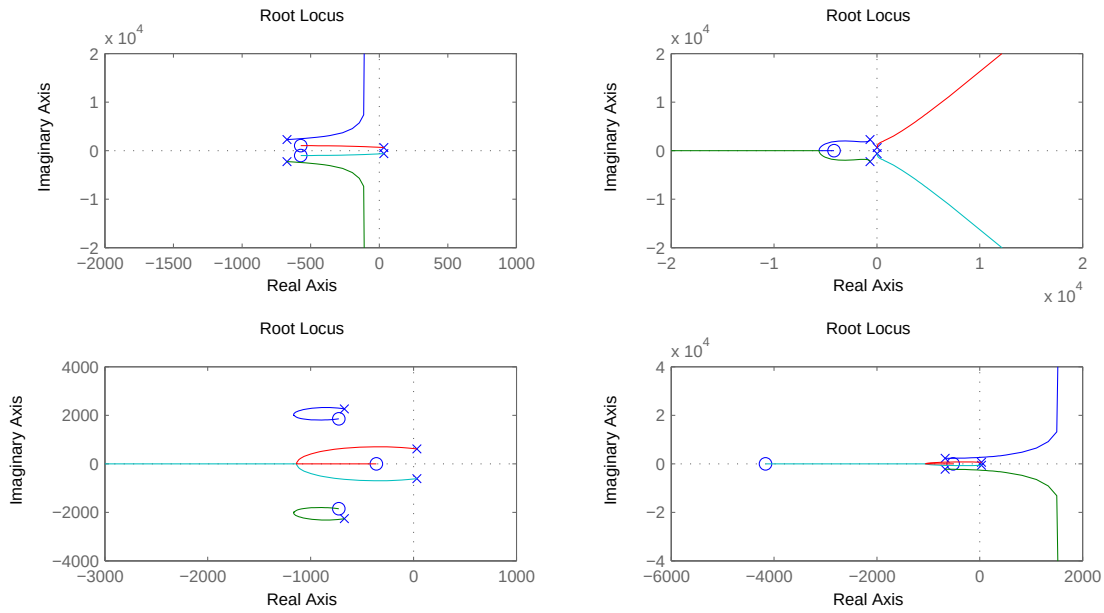

Figure 3.45. Root locus diagram for the four transfer functions corresponding to $d_{AC} = 0$ and $d_{DC} = 1$.

3.5.3.3 S_1 **ON,** S_2 **OFF.** Alternate configuration of the switches is here studied. AC side switch is considered to be in the ON state, whereas DC side switch is OFF. System A matrix modify as follows:

$$A_{1,0} = \begin{bmatrix} 0 & 0 & 0 & 0 \\ 0 & -\frac{1}{C_2(R_{out}+R_{C,2})} & 0 & \frac{R_{out}}{C_2(R_{out}+R_{C,2})} \\ 0 & 0 & -\frac{R_{L,1}+2R_{S,1}}{L_1} & 0 \\ 0 & -\frac{R_{out}}{L_2(R_{out}+R_{C,2})} & 0 & -\frac{R_{out}R_{C,2}}{L_2(R_{\mathrm{out}}+R_{C,2})} - \frac{R_{L,2}+R_{DS}}{L_2} \end{bmatrix}$$

$$W_1(s) = \frac{X_1(s)}{U(s)} \equiv 0 \tag{3.94}$$

$$W_2(s) = \frac{X_2(s)}{U(s)} \equiv 0 \tag{3.95}$$

$$W_3(s) = \frac{X_3(s)}{U(s)} = \frac{10^4 L_1}{3(R_{L,1} + 2R_{S,1} + L_1 s)} = \frac{3333}{s + 133.3} \tag{3.96}$$

$$W_4(s) = \frac{X_4(s)}{U(s)} \equiv 0 \tag{3.97}$$

Transfer functions corresponding to $d_{AC} = d_{DC} = 1$ and $d_{AC} = 1$, $d_{DC} = 0$, even if matrices $A_{1,1}$ and $A_{1,0}$ are different, due to some cancelations, result identical, thus also zeros and poles positions correspond. Therefore, bode plots and root loci represented in following figures are identical to figures 3.42 and 3.43.

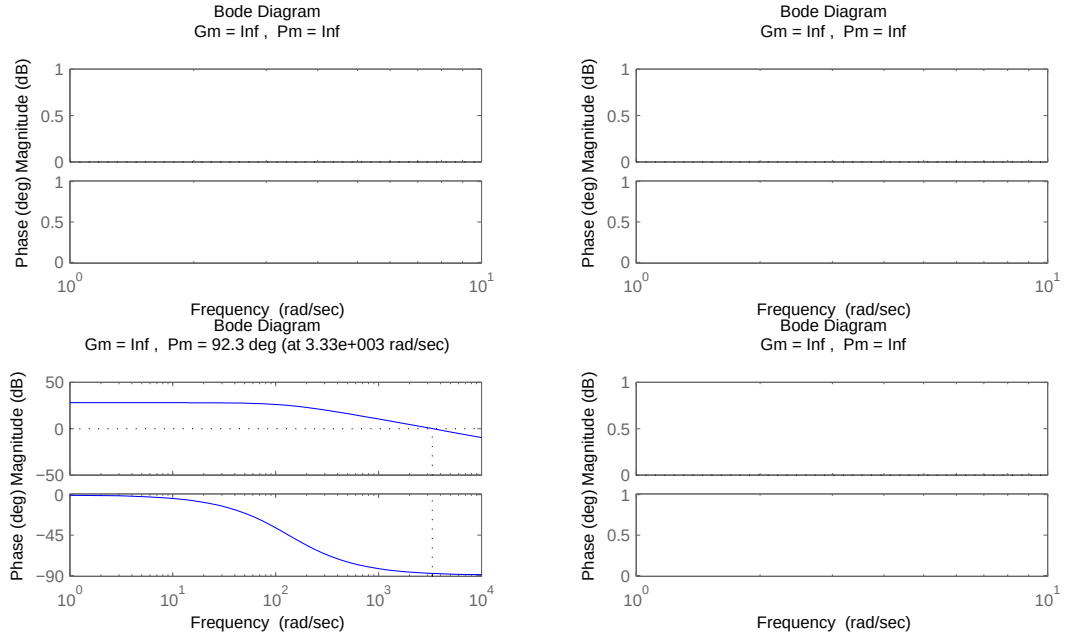

Figure 3.46. Bode plots for the four transfer functions corresponding to $d_{AC} = 1$ and $d_{DC} = 0$.

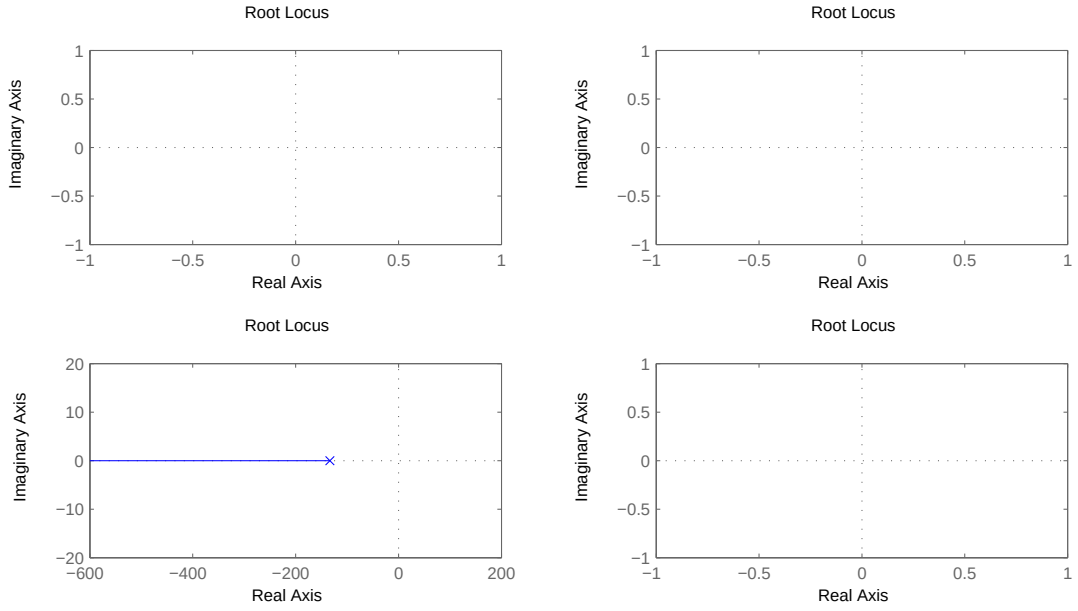

Figure 3.47. Root locus diagram for the four transfer functions corresponding to $d_{AC} = 1$ and $d_{DC} = 0$.

3.5.3.4 S_1 OFF, S_2 OFF.

$$A_{0,0} = \begin{bmatrix} 0 & 0 & \frac{1}{C_1} & 0 \\ 0 & -\frac{1}{C_2(R_{out}+R_{C,2})} & 0 & \frac{R_{out}}{C_2(R_{out}+R_{C,2})} \\ -\frac{1}{L_1} & 0 & -\frac{R_{L,1}+2R_{S,1}}{L_1} - \frac{R_{C,1}}{L_1} & 0 \\ 0 & -\frac{R_{out}}{L_2(R_{out}+R_{C,2})} & 0 & -\frac{R_{out}R_{C,2}}{L_2(R_{\text{out}}+R_{C,2})} - \frac{R_{L,2}+R_{DS}}{L_2} \end{bmatrix}$$

$$W_1(s) = \frac{X_1(s)}{U(s)} = \frac{(C_2L_2R_{C_2} + C_2L_2R_{out}) \cdot s^2 + (L_2 + C_2R_{C_2}R_{DS} + C_2R_{C_2}R_{L_2} + \dots}{D(s)} \tag{3.98}$$

$$\dots \frac{+C_2R_{C_2}R_{out} + C_2R_{DS}R_{out} + C_2R_{L_2}R_{out}) \cdot s + (R_{DS} + +R_{L_2} + R_{out})}{D(s)} =$$

$$= \frac{5.808 \cdot 10^{-7}s^2 + 0.0006653s + 0.798}{2.091 \cdot 10^{-13}s^4 + 1.28 \cdot 10^{-10}s^3 + 7.403 \cdot 10^{-7}s^2 + 0.0005121s + 0.798}$$

$$W_2(s) = \frac{X_2(s)}{U(s)} \equiv 0 \tag{3.99}$$

$$W_3(s) = \frac{X_3(s)}{U(s)} = \frac{(C_1C_2L_2R_{C_2} + C_1C_2L_2R_{out}) \cdot s^3 + (C_1L_2 + C_1C_2R_{C_2}R_{DS} + \dots}{D(s)} \tag{3.100}$$

$$\dots \frac{+C_1C_2R_{C_2}R_{L_2} + C_1C_2R_{C_2}R_{out} + C_1C_2R_{DS}R_{out} + C_1C_2R_{L_2}R_{out}) \cdot s^2 + \dots}{D(s)}$$

$$\dots \frac{+(C_1R_{DS} + C_1R_{L_2} + C_1R_{out}) \cdot s}{D(s)} =$$

$$= \frac{6.97 \cdot 10^{-10}s^3 + 7.983 \cdot 10^{-7}s^2 + 0.0009576s}{2.091 \cdot 10^{-13}s^4 + 1.28 \cdot 10^{-10}s^3 + 7.403 \cdot 10^{-7}s^2 + 0.0005121s + 0.798}$$

$$W_4(s) = \frac{X_4(s)}{U(s)} \equiv 0 \tag{3.101}$$

$$D(s) = (C_1C_2L_1L_2R_{C_2} + C_1C_2L_1L_2R_{out})(C_1L_1L_2 - C_1C_2L_2R_{C_1}R_{C_2} + \cdots \quad (3.102)$$

$$\cdots + C_1C_2L_1R_{C_2}R_{DS} + C_1C_2L_1R_{C_2}R_{L_2} + C_1C_2L_2R_{C_2}R_{L_1} + 2C_1C_2L_2R_{C_2}R_{S_1} + \cdots$$

$$\cdots + C_1C_2L_1R_{C_2}R_{out} - C_1C_2L_2R_{C_1}R_{out} + C_1C_2L_1R_{DS}R_{out} + C_1C_2L_1R_{L_2}R_{out} + \cdots$$

$$\cdots + C_1C_2L_2R_{L_1}R_{out} + 2C_1C_2L_2R_{S_1}R_{out})(-C_1L_2R_{C_1} + C_1L_1R_{DS} + C_2L_2R_{C_2} + \cdots$$

$$\cdots + C_1L_1R_{L_2} + C_1L_2R_{L_1} + 2C_1L_2R_{S_1} + C_1L_1R_{out} + C_2L_2R_{out} - C_1C_2R_{C_1}R_{C_2}R_{DS} + \cdots$$

$$\cdots - C_1C_2R_{C_1}R_{C_2}R_{L_2} + C_1C_2R_{C_2}R_{DS}R_{L_1} + 2C_1C_2R_{C_2}R_{DS}R_{S_1} + C_1C_2R_{C_2}R_{L_1}R_{L_2} + \cdots$$

$$\cdots + 2C_1C_2R_{C_2}R_{L_2}R_{S_1} - C_1C_2R_{C_1}R_{C_2}R_{out} - C_1C_2R_{C_1}R_{DS}R_{out} - C_1C_2R_{C_1}R_{L_2}R_{out} + \cdots$$

$$\cdots + C_1C_2R_{C_2}R_{L_1}R_{out} + C_1C_2R_{DS}R_{L_1}R_{out} + 2C_1C_2R_{C_2}R_{S_1}R_{out} + 2C_1C_2R_{DS}R_{S_1}R_{out} + \cdots$$

$$\cdots + C_1C_2R_{L_1}R_{L_2}R_{out} + 2C_1C_2R_{L_2}R_{S_1}R_{out})(L_2 - C_1R_{C_1}R_{DS} + C_2R_{C_2}R_{DS} - \cdots$$

$$\cdots - C_1R_{C_1}R_{L_2} + C_2R_{C_2}R_{L_2} + C_1R_{DS}R_{L_1} + 2C_1R_{DS}R_{S_1} + C_1R_{L_1}R_{L_2} + 2C_1R_{L_2}R_{S_1} \cdots$$

$$\cdots - C_1R_{C_1}R_{out} + C_2R_{C_2}R_{out} + C_2R_{DS}R_{out} + C_1R_{L_1}R_{out} + C_2R_{L_2}R_{out} + 2C_1R_{S_1}R_{out}) \cdots$$

$$\cdots (R_{DS} + R_{L_2} + R_{out})$$

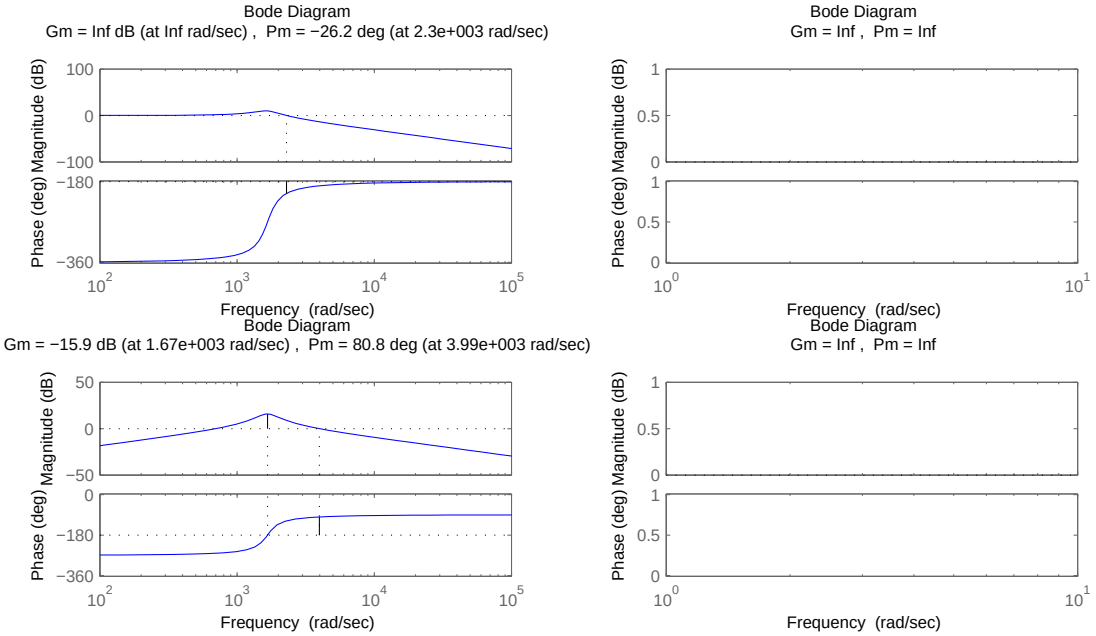

Figure 3.48. Bode plots for the four transfer functions corresponding to $d_{AC} = 0$ and $d_{DC} = 0$.

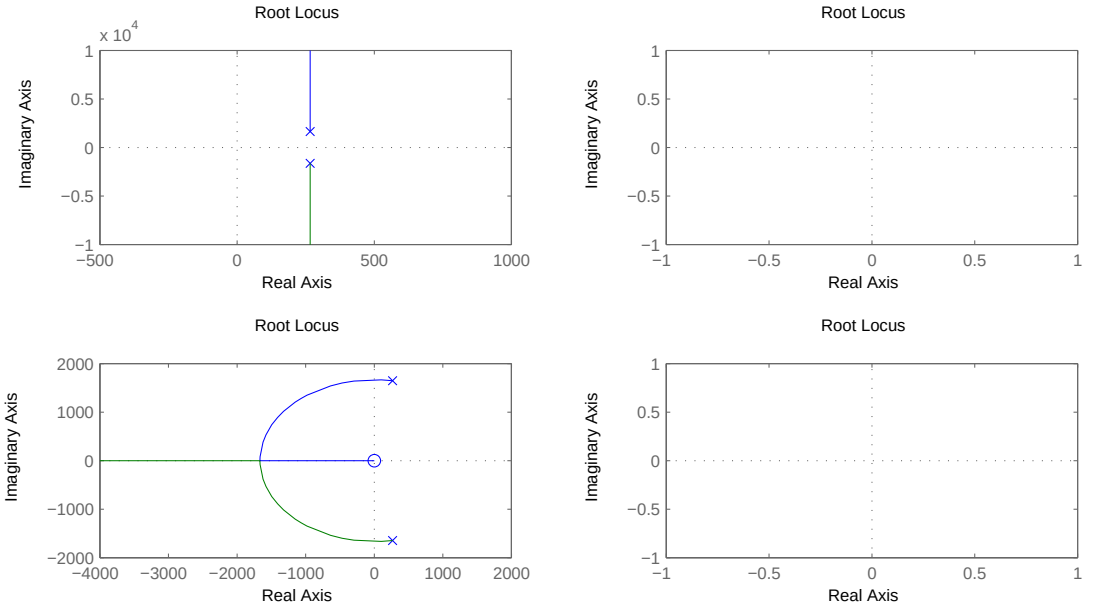

Figure 3.49. Root locus diagram for the four transfer functions corresponding to $d_{AC} = 0$ and $d_{DC} = 0$.

3.5.4 Considerations on Transfer Function Structure. The transfer functions derived fully describe the dynamic behavior of the system. Equation for every configuration explains the relations between the input signal and the state variables. This relation can lead to a different implementation of the equivalent state space system in Simulink. Transfer function structure is here analyzed and their implementation is explained in terms of system dynamics analysis. Simple considerations are also made in terms of stability and relations between system variables.

As can be seen from previous sections, structure of the tf follows a straightforward scheme. Independence of the state variable with respect to the input is expressed by an identically zero relation. In particular, output voltage and output current are only controllable with the switches in position S_1 OFF and S_2 ON. Similarly, DC bus capacitor results to be independent from the input in the configuration $d_{AC} = d_{DC} = 1$.

Stability margins can be read in the bode plot or through the crossing point of the imaginary axis in the root locus. Open loop system, separated into four equivalent states, does not meet stability requirements. This can be easily seen from the simulation results provided in previous sections. For a PFC circuit an active control is required thus open loop responses result to be unstable.

Through the use of derived transfer functions, an alternative implementation is built in MATLAB® Simulink. Exploiting the non-linear nature of the system, a switching scheme is studied to resemble the alternation between the four equivalent configurations [18]. Control input selects which system to switch to. Also initial conditions, depending on previous step, are implemented in the model. Therefore, based on the instantaneous duty cycles' values and on initial conditions, the system *moves* towards the next state.

Logical decision block is built for the automatical switching based on the duty cycle values at each step of iteration. Corresponding system matrices are selected and employed for the calculation of the dynamics through the state-space implementation. Obtained waveforms and control design matches those of the space state implementation described in previous section.

3.5.5 Differential Equations Model Implementation. An alternative way to implement the system in the MATLAB® Simulink environment is chosen to use the solving of differential equations given by the state space system, at each sampling instant. Results of calculations are used to feedback the initial conditions for the following sampling instant. The switching between the four different systems configurations are managed with the selection of one of the four different equations sets.

Simulink model uses atomic sub-systems to synchronize the operation at each step. It considers four different switches combinations for the solving of four different differential equation sets, in the form of state-space blocks. Output of the block function gives the values of the four states at each step, which is also used for the implementation of the *initial condition* calculation algorithm. Controllers uses the output value of the states to elaborate the error signal and to command the switching for the following step.

The main issue here is similar to the transfer function model, which is the dependence of the system by the previous state. In particular, the transition of the circuit from a state to another, is based on complex interactions between the controller and the previous instant state. Switching patterns therefore strictly depends on

Stability analysis and analytical consideration can therefore be made separately for each different switch configuration. As it has been proven in literature [42], mathematical equations and resulting model are simpler to be treated.

CHAPTER 4
DIGITAL CONTROL

An alternative approach for the average current mode control, with respect to the classical analog control, uses a state of the art technique [24]. Digital control strategy can be used in the power electronic converter for power factor regulation and control of the output voltage level [23].

Digital controllers offer several advantages compared to conventional analog regulators, owing to their simple control structure and capability to implement several algorithms [33]. They offer the flexibility to design complex and non-linear control techniques [17]. Moreover the control section can be easily integrated in a larger system with diagnostic capabilities and they are especially suitable for switching-mode power electronic converters. This simple structure reduces both the number of components and provides high reliability and low sensitivity to components' aging or other variations. On the other hand, typical drawbacks are the limitation of the control bandwidth due to the sampling issues. This can now be overcome to some degree by utilizing modern micro controllers, which are now available at a relatively low cost.

Previous approaches, based on analog circuit design, used hysteresis control or used analog components such as comparators, multipliers and op amps. Standard PID controllers can be also applied as shown for the PFC circuit voltage and current loops, as well as for the output current control [35]. Their standard control structure has been largely used in a variety of applications. Good results, as those shown above, can be obtained with a precise tuning of the parameters and gains. On the other hand, analog control gives a minor flexibility to the system, which might need to be re-tuned for particular cases. Reliability and robustness of the system are not considered among primary advantages of this technique.

Significant research has been done in the use of the well known $UC1854$ or $UC3854A$ enhanced high power factor pre regulator integrated circuit, distributed by *Unitrode* in [7] and [64]. This integrated circuit has been widely used over the last few years in dual stage cascaded switching converter applications [39]. The IC uses average current mode control, maintaining a stable low-distorted sinusoidal input current, without the need for slope compensation. Line voltage feed-forward is also implemented using this component along with a PWM switching regulator for the converter.

Other common techniques involve the discretization of continuous controllers, producing a digital implementation. This is not considered as pure digital control and usually adds complexity to the overall design. Moreover, the operation in the discrete domain introduces design and stability issues to the original analog regulator system. Among these, the most important are the correspondence between stable areas in the s-domain and the z-domain, and sampling time definition.

Classic control and linear system theory are well known and have widely been investigated, but their high complexity requires a deep control theory background. A sophisticated controller has to be designed ad-hoc for each application, in order to obtain good performances. Digital control theory, on the other hand, allows the controller to be designed as a more flexible and cost-effective solution. Also its implementation in micro-controllers or DSPs makes this approach preferable.

Lately, digital control techniques have been developed and used in many research areas, such as power electronics or electrical drives. Digital Pulse Width Modulation (PWM) control in particular exploits the binary nature of pure digital control. Several techniques can be adopted considering the digital control strategy and some of them will be analyzed in the following pages.

4.1 Digital Control for Switching Converters

As briefly discussed, digital control approach for power electronics switching converters is a growing area, which is gaining growing interest owing to the advantages previously listed. Moreover, highly non-linear structure of SMPS, and their not very demanding dynamic performances, make digital control the perfect application for these systems [69].

The control strategy is usually based on conventional analog controllers, and widely discussed in literature. Basic structure consists of a multi loop control for the PFC circuit and a simple single controller for the cascaded DC/DC converter. Control algorithm is essentially based on an outer voltage loop, determining the reference signal for the inner current controller by multiplying a signal proportional to the input sinusoidal voltage waveform.

Digital control techniques can be used to exploit all advantages coming from this implementation. For instance different control strategies are generally possible to improve the system dynamics. Digital filtering or other techniques can be used for example to remove the DC bus voltage ripple at twice the line frequency. Similarly algorithms capabilities can be used for filtering applications, also using auto-tuning digital filters, or to avoid input voltage sensing with estimators.

Digital control proposed here uses a completely different approach, in which a novel design is considered, using a very simple hardware structure and obtaining very impressive results. Digital control structure is described in following pages, providing a simple mathematical analysis along with some practical considerations in the converters.

4.2 Sliding Mode Control

One of the most used control techniques for non-linear systems, and especially for switched-controlled circuits, is Sliding Mode [32]. Essentially, the sliding-mode control utilizes a high-speed switching controlled law to drive and maintain the non-linear state trajectory onto a specified sliding surface in the state space.

The main benefit of the sliding mode is the robustness of the system against disturbances in the load and in the input voltage. This makes Sliding Mode control a good option for circuits controlled by switching devices where the control variable can assume only a binary or discrete set of values. Power converters such as those implemented in this design, inherently include switching devices and hence it is straightforward to design sliding mode discontinuous control law.

The fundamental idea of the design is to calculate a switching sequence that will drive and maintain the system state to the switching surface. Lyapunov method, which is usually used to determine the stability properties of an equilibrium point, considers a scalar function $V(x)$, called Lyapunov function without solving the state equations. Let $V(x)$ be a continuously differentiable scalar function defined in a domain D that contains the origin into real values $\mathbb{R}$. Lyapunov function $V(x)$ is said to be positive definite if $V(0) = 0$ and $V(x) > 0 \, \forall x$. It is said to be negative definite if $V(0) = 0$ and $V(x) > 0$ for all x. Lyapunov method assures the system to be stable if the function is positive definite and its differential is negative. A generalized Lyapunov function is defined in terms of the surfaces and characterizes the motion of the state trajectory onto the sliding surface. Switching control strategy chooses the control sequence such as the derivative of the Lyapunov function is negative definite and the motion follows the surface. First step in the controller design is the definition of the sliding surface, which has to be constructed to lead to an equilibrium point and which defines the rules for proper switching.

Thus, considering a non-linear model such as the one analyzed, represented by state space equation in 4.1, where time dependence of switching scheme is included in matrix $f(\mathbf{x}, t)$ and input vector is given by $\mathbf{u}(t) \in \mathbb{R}^m$.

$$\dot{\mathbf{x}}(t) = f(\mathbf{x}, t) + B(\mathbf{x}, t)\mathbf{u}(t) \tag{4.1}$$

In sliding-mode control, system trajectories expressed by 4.1, are forced to remain into a subspace of the states, and then hold so that they slide along it providing a stable constraint [69]. This reduced-order subspace is referred to as a sliding surface. When closed-loop state feedback forces trajectories to slide along it, it is referred to as a sliding mode of the closed-loop system. Trajectories along this subspace can be likened to trajectories along eigenvectors and modes of LTI systems. However, the sliding mode is enforced by increasing the vector field with high-gain feedback.

In order to attract systems' trajectories to the hyper surface, a switching function $\sigma : \mathbb{R}^n \rightarrow \mathbb{R}^m$ is defined, to represent the switching criteria. A state outside the sliding surface is characterized by having $\sigma(\mathbf{x}) \neq 0$, whereas a state lying in the surface has $\sigma(\mathbf{x}) = 0$. The sliding mode control law switches from one state to another based on the sign of this distance, in a discrete fashion, thus the trajectory approaches the surface in a finite time. Once the trajectory has reached the surface, it slides along it and may, for example, move toward the equilibrium point.

Mathematically, above relations can be easily expressed considering the definition of the Lyapunov function candidate as

$$V(\sigma(\mathbf{x})) = \frac{1}{2}||\sigma(\mathbf{x})||_2^2 \tag{4.2}$$

$V(\cdot)$ is a quadratic function of the sliding surface $\sigma(\cdot)$, where $||\cdot||$ indicates the Euclidean norm, which consists in the distance from the sliding surface corresponding to $\sigma(\mathbf{x}) = 0$. As explained, the attraction of system trajectories to the surface is

possible when the derivative of the Lyapunov function is negative definite, that is

$$\frac{dV}{dt} = \frac{\partial V}{\partial \sigma}\frac{d\sigma}{dt} < 0 \tag{4.3}$$

In the simple scalar case, when $m = 1$, this corresponds to a control input $u(\mathbf{x})$ that is chosen such as to achieve $\sigma\dot{\sigma} < 0$. According to Lyapunov theory the system is always moving towards the surface. In particular, when $\sigma(\mathbf{x})$ is positive, $u(\mathbf{x})$ makes $\dot{\sigma}(\mathbf{x})$ negative and when $\sigma(\mathbf{x})$ is negative, the input produces a positive $\dot{\sigma}(\mathbf{x})$. Moreover, if the condition to be reachable, given by

$$\frac{dV}{dt} \leq -\mu(\sqrt{V})^{\alpha} \tag{4.4}$$

where $\mu > 0$ and $0 < \alpha \leq 1$ are constants, is satisfied, the sliding mode surface will be attained in finite time.

From the hardware point of view, whereas the simple SMC structure can be easily implemented in a DSP through a series of *if-then* loops and with very few lines of code, an alternative classical system can be also used. In particular, basic structure of the sliding mode controller involves simple elements which can be also designed using analog components such as comparators and multipliers. Main disadvantages result in a more complicate structure and less flexibility for future improvements or modifications.

On the contrary, sliding mode control approach considers a mathematical knowledge of the system and of its trajectories. Definition of the sliding surface also needs a quite complex analysis of the system and some peculiar assumption to simplify its design. Also the stability of the ideal switching-motion stability and of the designed controller has to be proven. For the sake of simplicity, both from the theoretical design and hardware implementation point of view, a different technique is here explained.

4.3 True Digital Control

A novel approach in digital control is presented here, for the specific case of switching mode power electronic converters, which are well suited for this technique. This new solution treats the system to be controlled as a digital system, in which the states are alternating in a binary fashion. In particular, given its switching nature, it only operates in two different predefined states for each switch. Furthermore the control only manages the switching between the different configurations of the system [24].

Controller action is aimed to decrease the error function, given as the difference between desired signal and the actual one. Its operating principle commands the system to switch to either a state that will increase the value of the measured signal or reduce it. One configuration, corresponding to a positive error, will increase actual signal thus decreasing and bringing to zero the error. On the other hand, in correspondence to a negative sign of the error signal, the control switches the system to a so-called low-energy state. In this situation it will produce a decrease in the feedback signal.

Control scheme, described above, can be easily schematized, and therefore digitally implemented, as follows:

$$s_{ref}(\cdot) - s_{mes}(\cdot) = e(\cdot) \;\rightarrow\; \begin{cases} e > 0 \;\Rightarrow\; \textit{low energy state} \\ e < 0 \;\Rightarrow\; \textit{high energy state} \end{cases} \tag{4.5}$$

Therefore, thanks to the application of this switching fashion, the system is controlled to zero error, through a variable switching frequency. Following simple *if-then* statements, which can be easily implemented in a digital integrated circuit, summarizes control operation:

- If actual measured signal is greater than the reference signal, then switch or stay at low-energy state;
- If actual measured signal is less than the reference signal, then switch or stay at high-energy state.

Given the complexity of the described battery charger system to which pure digital control is applied, regulator structure is presented only for the general case. In following sections, it is described for each converter circuit. A particularly simple, thus effective representation of the principle of true digital control hereby described, is provided through following block scheme (figure 4.1). System structure consists also in a possible implementation of the real controller in terms of analog circuit design or Simulink modeling.

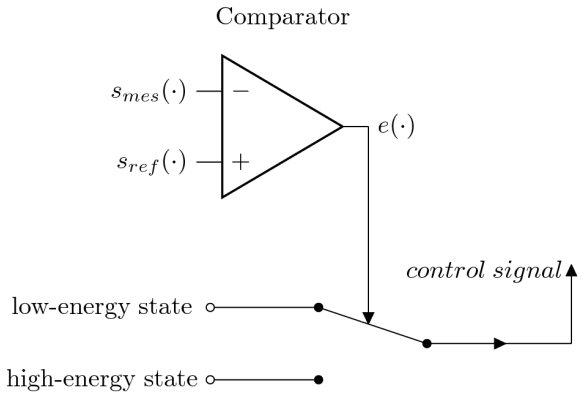

Figure 4.1. Schematic circuit of proposed true digital control.

The proposed scheme, which consists in a very simple structure, takes advantage of the switching feature of the converters. Its working principle is based on the generation of a binary output PWM pattern of zeros and ones for the switches, based on the sign of the input signal. Mathematically, control sequence is calculated from the error between the reference signal and actual measured values. Control signal is elaborated through a sign function, given output values $\{-1, 0, 1\}$, based on the sign of the error. Controller output is given by a sequence of binary values $\{0, 1\}$ forced

by a saturator block, in order to obtain direct switching patterns.

Hardware structure is either simple and of easy implementation in any of common commercial micro controllers, in which a sign function is implemented. Its Simulink realization, obtained cascading a sign block followed by a saturator is represented in figure 4.2.

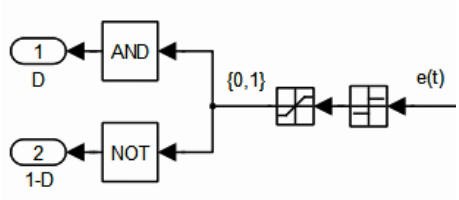

Figure 4.2. Simulink block scheme of True Digital Control.

4.4 True Digital Control for Switching Converters

Conventionally switching mode power supplies and power electronics converters have been controlled using analog integrated circuit technology and linear system design techniques [50]. Analog control techniques have been so far predominant due to their simplicity as well as their low implementation cost. However, they are sensitive to environmental disturbances such as noise, temperature and components' aging. Besides, implementation of sophisticated advanced control techniques is inherently difficult employing analog circuits.

A novel approach in control design is here discussed, introducing advanced digital control techniques, such as True Digital Control, which provide numerous advantages over classical analog methods and is becoming the new standard for switching converters.

Even if digital control compensation development and design tends to be less intuitive than analog methodologies, however, with the decreasing cost and size of digital circuits exponentially shrinking, digital control is beginning to replace analog controllers. Thus, recent research has been conducted on digital controllers, which perform functions that are not realizable in the analog domain [12]. Most important features are communication and system-level integration, controller auto tuning, on-the-fly efficiency monitoring and optimization, and complex nonlinear control for improved dynamic performance.

Advantages of digital design techniques are numerous, dealing with implementation simplicity, hardware flexibility and robustness of the scheme. Digital control assures a simpler and more effective structure with respect to classic analog control approach. In particular modern integrated circuits offer low implementation cost and a simple design with theoretically infinite resolution. Moreover components' drift and

noise are one of the primary disadvantages for analog circuits. Nevertheless in order to obtain high performances, complex circuits are needed and analog implementation for advanced control schemes results difficult and expensive.

On the other hand, true digital control offers a series of fundamental advantages which make it a desired choice for power electronic systems' control. Especially it is very well suited for switching mode converters, due to their intrinsic non-linearities. High noise immunity, along with a less susceptibility to parameter variations make digital controllers desirable for electronic circuits. Digital control scheme results also in a simpler approach, dealing with very few hardware changing. This important advantage is mainly due to an easy implementation of the algorithm on a simple micro controller. In fact, a changing in the controller scheme does not usually require an hardware modification. Also the ability to interface with an external host computer or a user friendly display has led to a wide spread of digital controllers. On the other hand, a limited resolution due to analog-to-digital conversion, and an inherent time delay for computational tasks are the main disadvantages of this technique.

4.4.1 True Digital Control for PFC Circuit. First application of True Digital Control, in this thesis is provided by the two regulation loops for the first power electronic converter, the PFC boost rectifier. As explained above, instead of the canonical analog control design, a digital approach is here discussed, whereas in this paragraph, the inner PID control loop is maintained.

Control structure is based on previously explained principle of digital average current control, now applied to switching mode converters. In the first implementation the basic structure of the classical controller consists in a double feedback loop, in which two regulators are operating at the same time. External loop is characterized by a large bandwidth and therefore by a high operating frequency. Its purpose is to

track the sinusoidal current reference signal, which is provided by the inner control loop. On the other hand, inner loop requires much slower operation. It only has to provide the correct amplitude of the sinusoidal signal, scaled accordingly to the error in the voltage. Therefore, for the voltage control loop the highly reactive digital control is not suitable. In following sections several alternatives are presented in order to completely digitalize and thus simplify the feedback control structure.

A classical PID controller is implemented in this study. Feed-forward component, while it is necessary for the analog control technique [72] due to instability problems especially at low input voltages, can be neglected here. This simpler design allows a simplified hardware structure, which will reduce both costs and the need for maintenance.

DC bus voltage measured at the PFC circuit output is shown in figure 4.3 and is compared to the desired voltage level. Through a simple calculation the error signal to the PID controller is provided. Here only the proportional gain is considered. Controller output is proportional to the error with the coefficient K_p, and represents the inductor current reference signal, as follows:

$$i_{ref}(\cdot) = K_p \cdot [v_{ref}(\cdot) - v_{mes}(\cdot)] = K_p \cdot e_v(\cdot) \tag{4.6}$$

On the other hand, features of the true digital control perfectly fit the needs of fast reacting and robust regulation for the current control loop [37]. Thus previously explained structure of the true digital control is adopted here for the outer feedback loop.

In particular, switching pattern for the digital controller is provided by sensing the sign of the error in the current waveform. The difference of desired reference and measured inductor current produces control signal as follows:

$$e_{i_L}(\cdot) = i_{ref}(\cdot) - i_{mes}(\cdot) \tag{4.7}$$

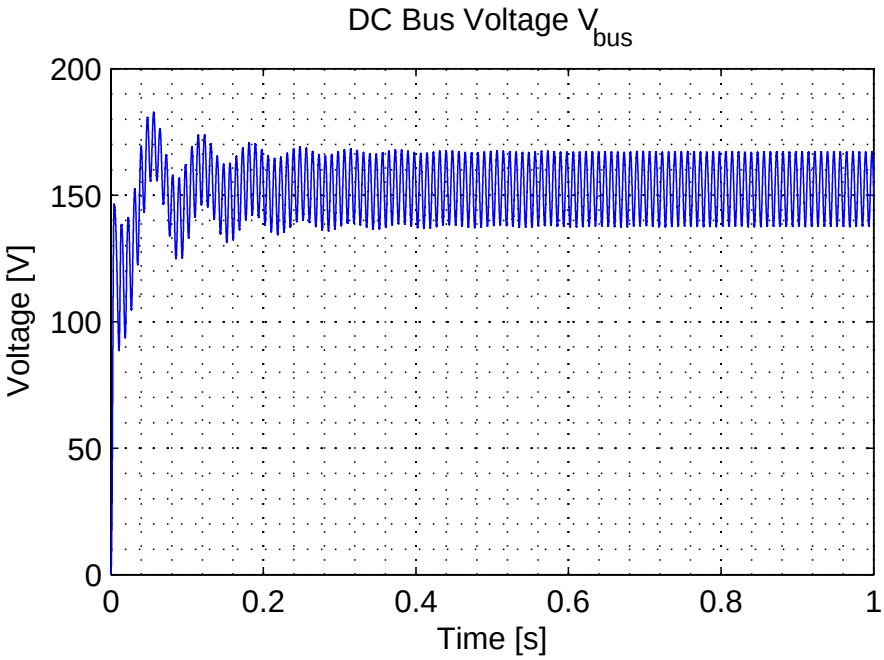

Figure 4.3. Regulated DC bus voltage waveform with typical oscillations at twice the line frequency.

where i_{ref} is the output of the inner control loop of equation 4.6. Then, digital control operates following the decision rule explained in previous section, analyzing the error sign and producing the output signal accordingly. Thus, recalling equation 4.5, the system is switched to either a low state, corresponding to 1 control output, or a high state with 0 as PWM value.

Different high and low duty cycles values have been tested, based on recent research papers. Usually the switching of the system is done between two constant modulated signals at a fixed frequency. High and low duty cycles are then used to correct the error of controlled signal. The two duty cycles values can be adjusted by the designer in order to obtain the best performance for the circuit. In the case of this peculiar application, the complex interaction between the two control loops makes the design choice of the duty cycles easier. In particular, stability of the system can be obtained only with a faster operating current controller. Therefore the choice of D_H and D_L is given to be the two constant values 0 and 1.

This switching fashion produces a signal which compensates the error sign, allowing the controller to track desired sinusoidal waveform (figure 4.4). In particular, when the error signal is positive, the reference is bigger than actual current and the control produces an output which will correspond to a low energy state. An *high* switching command for the direct switch signal and a *zero* for the complementary switch are provided. Those PWM signals will be applied to the gates of the semiconductor devices in the original circuit and will consequently produce an output to compensate the error.

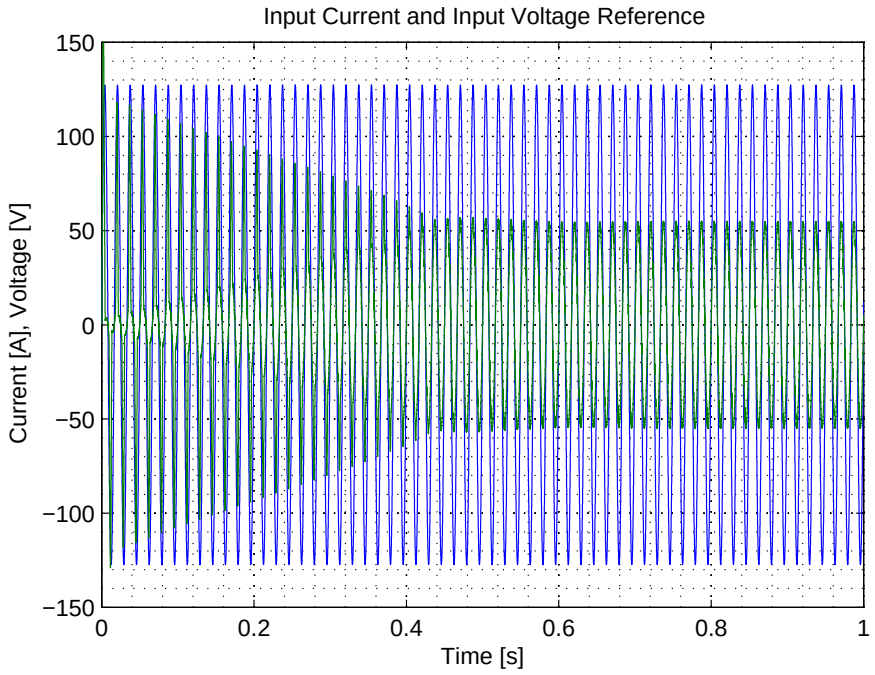

Figure 4.4. Power factor corrected sinusoidal input current.

In correspondence with a negative error signal the system will be switched to a high energy state, again to eliminate the difference between desired and sensed current.

Inverse mode of operation considers the PFC circuit as an inverter. Previously implemented control circuit result to be simple and effective. True digital control

may also be used to further simplify it. However, in this thesis its design it is not considered. Therefore, all simulation results for following sections include only the charging mode of operation. AC/DC behavior of the circuit is investigated.

4.4.2 True digital control for DC/DC converters. True digital control in DC/DC converter is easily applied without any drawback with respect to presented PID classical solution [23]. Adopted strategy considers the basic structure explained above. Its working principle is again based on the simple decision rule given by the sign of the error signal.

Several digital implementations consider the switching between two different states, based on the sign of the error. Those states are usually a high and low duty cycle PWM sequences as in [52]. The alternation between two constant-modulated patterns will control the system as explained. Moreover, switching frequency of the controller will result to be at the fixed value given by the modulation, thus eliminating high and variable frequency issues.

A different approach is here used to get a faster response for the system. High and low duty cycles values are substituted as before with constant values. Stability and performances of the system result to be optimized for chosen constant values and waveform results will be shown later.

Future work on the controller design might add a varying high and low duty cycles values. It will be able to optimize its behavior for different voltage levels at the input or in the DC bus. Efficiency of the controller, as well as its response can be designed specifically for the different conditions. Considered design, however, shows good results for the full range required by this application.

As before MATLAB® Simulink implementation is given by the cascade of the signum function block and a saturator in figure 4.2. Its input is the error between

the desired signal and the actual measure which will produce either a positive or a negative value. This signal is then saturated in order to obtain a suitable range for switching states. In particular, switching rule evaluates the difference between desired current reference and measured output as follows

$$e_{i_L}(\cdot) = i_L ref(\cdot) - i_L mes(\cdot) \tag{4.8}$$

Sign of the error signal is then calculated by the sign function. Saturation block saturates the signal as to assume only the binary set of values $\{0, 1\}$, which are used to control the gates of the switching devices. In correspondence of a negative error the actual measured current value is greater than the reference signal. This means that the controller will provide a zero valued signal to the MOSFET corresponding to an OFF switch. On the other hand, a positive error applied to the controller will provide and high output signal to make the semiconductor device conduct, acting as a small valued resistor. With such a switching fashion output current of the DC/DC converter will be adjusted to balance the error and minimize the difference between the desired and the actual signal.

Global control structure also includes the slow PID control loop for the voltage regulation. In particular, while the structure from the previously mentioned approach is maintained, its gains have to be modified. Tuning of the PID parameters is done accordingly to practical simulation results that consider the settling time as well as stability issues. Several simulations were carried out to optimize the choice of K_p and K_i. Unstable phenomena have been recorded for higher values of proportional gain, whereas low values will cause a slower settling time. Similarly, a reduction in the integral gain will produce unstable behavior for the circuit. Total Harmonic Distortion will drastically increase. A higher K_i will cause a faster response but higher frequency components in the sinusoidal input current.

Digital controller here implemented works very well in the bi-directional buck-boost circuit described, showing a fast response and optimal performances. Better waveforms are obtained here, with respect to the classical analog control strategy, as can be seen from the output current and voltage plots in figure 4.5.

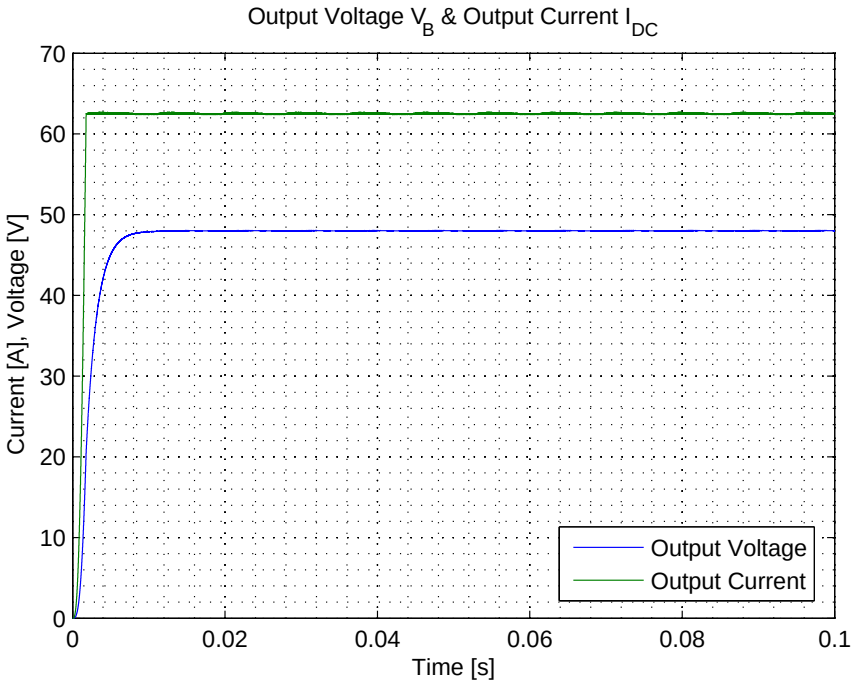

Figure 4.5. Regulated output current and voltage waveforms.

Digital control technique can here be used also for inverted operation of the converter. DC/DC bi-directional buck-boost can be easily controlled by the circuit of figure 4.2 when it is operating in boost mode. Effectiveness of the controller can be easily verified with some simulation results that are not shown in this thesis.

4.4.3 Switching Frequency Issues. In this section an important issue relating to the switching frequency of the converters is discussed. Novel digital control technique introduces a different switching strategy with respect to classical PWM control. Conventional Pulse Width Modulation control takes advantage of the fixed frequency f_s used for the modulation of the signal. Thus the control structure and

system behavior are simpler but maximum bandwidth and reactivity of the system are limited.

On the other hand, digital control approach is based on the evaluation of the sign of the error signal. Switching frequency and command signals for the devices are given only by the output of the digital regulator, without any modulation. Therefore switching frequency of the generated sequence results to be highly variable in time. Theoretical maximum pulse period is given by the inverse of the sampling time of the model $T_s = 1/f_s$, whereas in simulated application is much slower. However, in order to limit maximum switching frequency and allow a proper response for the actual circuit components, some expedients need to be employed. Considering the ease of implementation on the DSP used in the circuit, a fixed frequency approach is here preferred. In particular, a simple modulation is added at the output of the digital controller. This will cause the switching signal to be modulated at desired rate without affecting visibly system performances.

Simulations driven in MATLAB® Simulink have shown a high maximum value of the f_s produced by the digital controller, of around $f_s \simeq 5 \cdot 10^5\ Hz$. In practice, even if some high frequency peaks are present, the average is much lower. Also only in particular time instants the digital control needs to be reactive and requiring in terms of bandwidth.

Reducing the sampling time of the system, or of the digital controller, does not provide desired solution. The main drawback was found to be a noticeable increase in the ripple in input and output current waveform. Bandwidth of the system is then reduced, for safety issues and to assure a good performance to the actual circuit. As can be seen in the model of figure 4.6, switching frequency of the digital controller is here modulated at the fixed frequency of $f_s = 60\ kHz$. Even if this reduces the reactivity of the controller slowing down transient responses, final performances are

satisfactory. Minor differences can be seen from previous modeled regulator, as shown in the comparisons of figure 4.7 and 4.8.

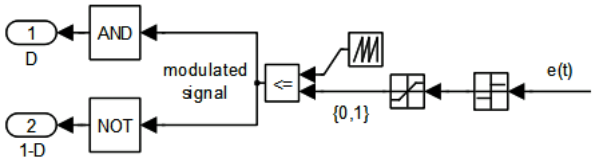

Figure 4.6. Simulink model of fixed frequency True Digital Controller.

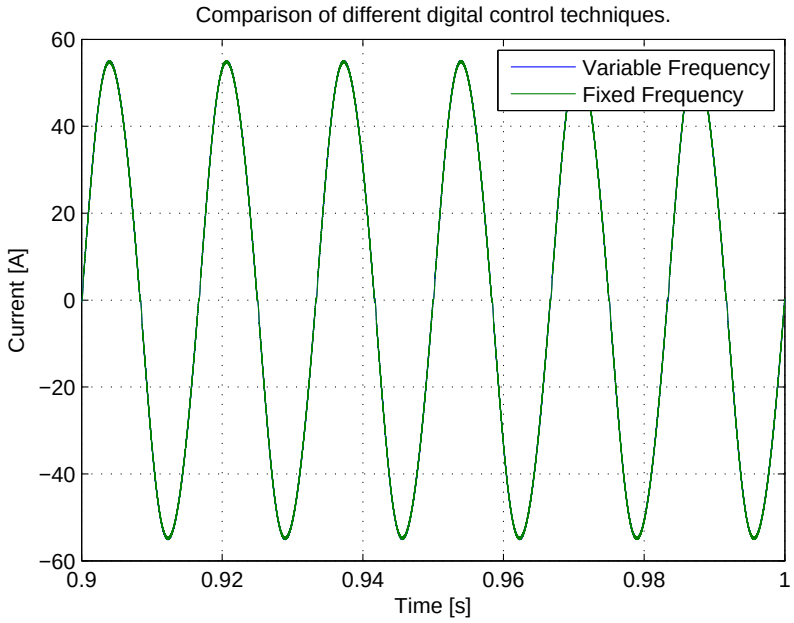

Figure 4.7. Comparison of input currents for fixed and variable frequency PWM.

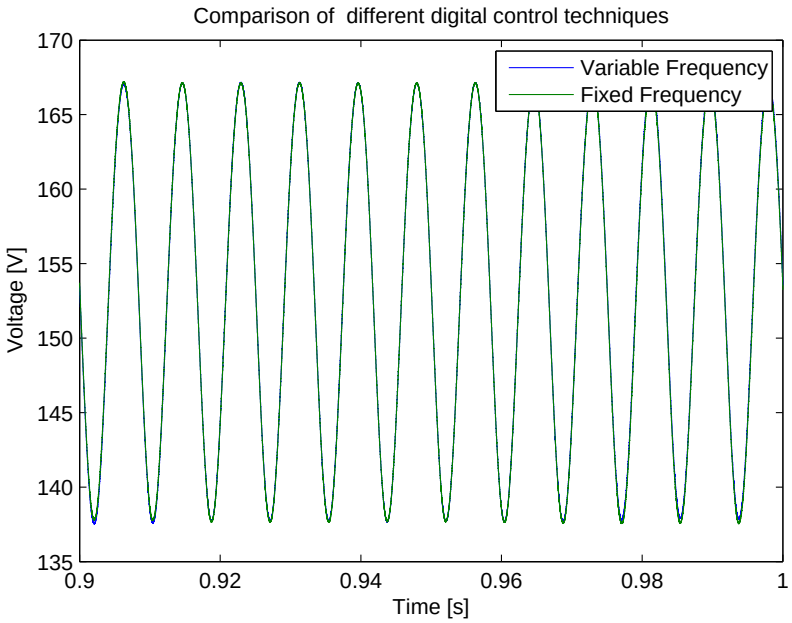

Figure 4.8. Comparison of DC bus voltage for fixed and variable frequency PWM.

4.5 Comparison With Conventional Analog Controller

In this section a detailed comparison between the two control approaches is provided. Major advantages of the true digital control over the conventional PID controller are also explained. Both theoretical and practical considerations are presented to show the improvements in terms of stability and performance. Reliability of the system and the hardware implementation are discussed whereas more detailed stability analysis will be conducted in the following chapter.

4.5.1 Performance and Waveform Analysis. This section presents the comparison of digital control design approach with the results obtained in previous chapter, where conventional analog design was implemented. Output waveforms and FFT analysis are used to compare the two different controllers showing the better performances of the digital approach.

Cascaded configuration of the two power electronic converters is simulated with MATLAB® Simulink, using the mathematical model previously derived. It presents a useful tool for analytical considerations in terms of stability and robustness of the system. Recorded waveforms are then showed and commented in details, both in the steady state and the transient response. Input and output current waveforms are analyzed together with the DC bus voltage and the output current.

It must be mentioned that the following considerations and practical results are explained for the most restrictive case, that is the lowest input voltage corresponding to the highest input current. In this particular application, $V_s = 90\,Vrms$ is used, at the line frequency of $60\,Hz$.

Input current is regulated under average current mode control in order to obtain a near unity power factor and a perfect sinusoidal shape. Using both control techniques good performance is obtained at steady state. In figure 4.9 the two sine

waveforms are compared. Cusp distortion in current waveform at the zero crossing point is minimum and cannot be seen without a very large zoom in the plot (figure 4.10). Using FFT analysis at the steady state the harmonic content of the current signal is shown in figure 4.11. High frequency components are almost zero (figure 4.12) since the regulator tracks the waveform very well and shapes a $60\,Hz$ sine wave with little distortion.

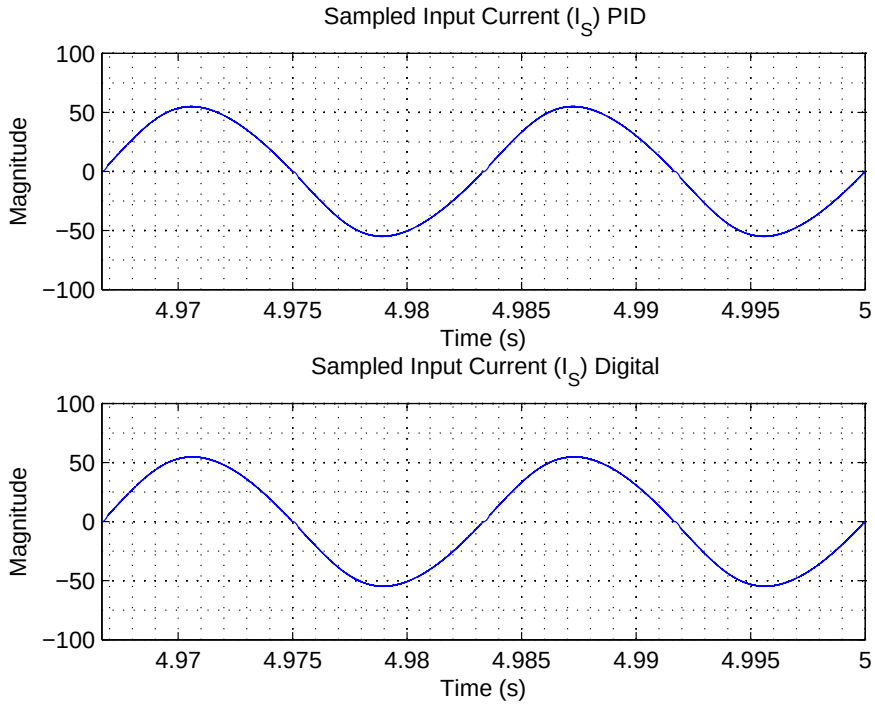

Figure 4.9. Comparison of the input sinusoidal currents.

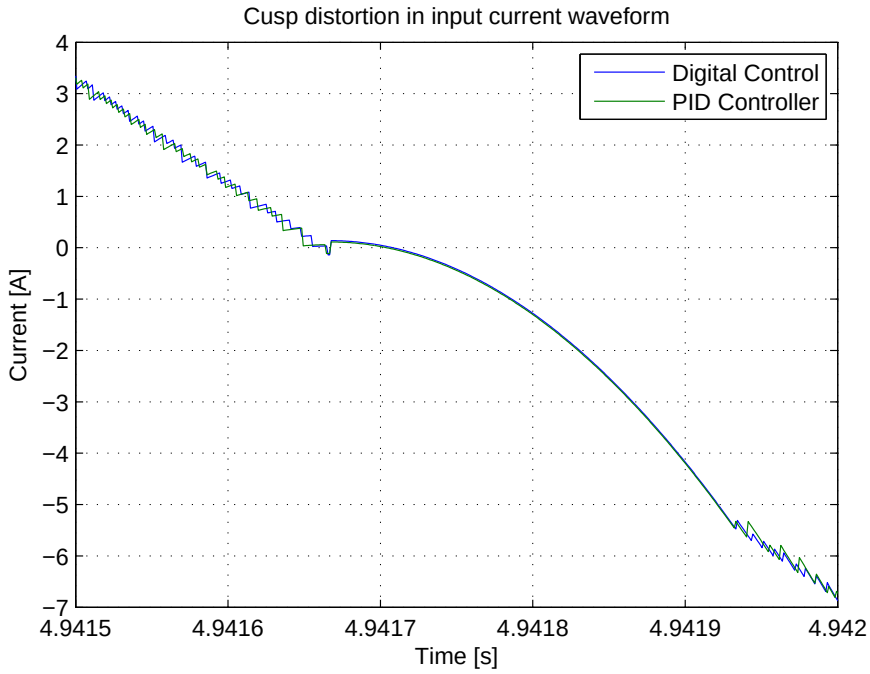

Figure 4.10. Detail of the cusp distortion in the input currents.

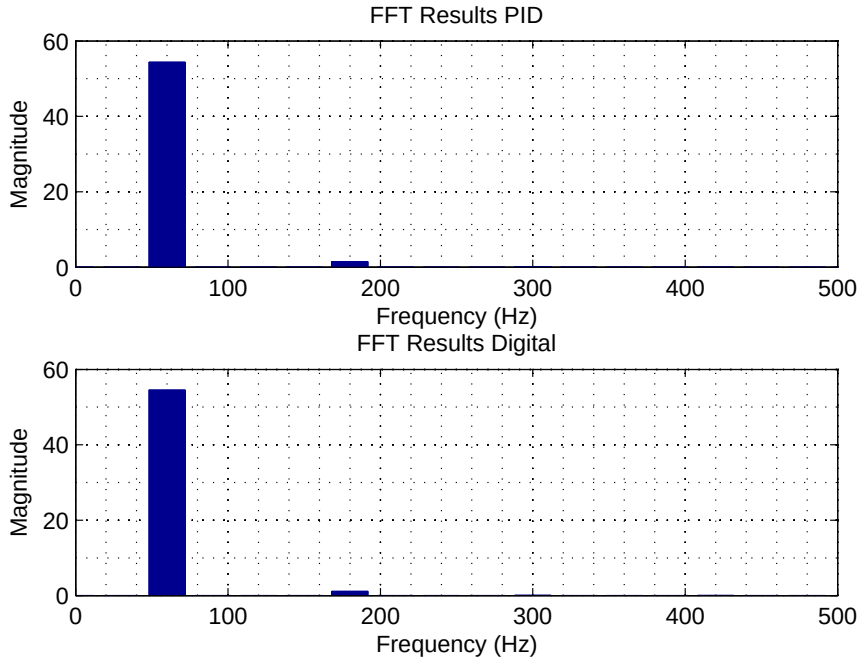

Figure 4.11. Comparison of the FFT analysis of the input current.

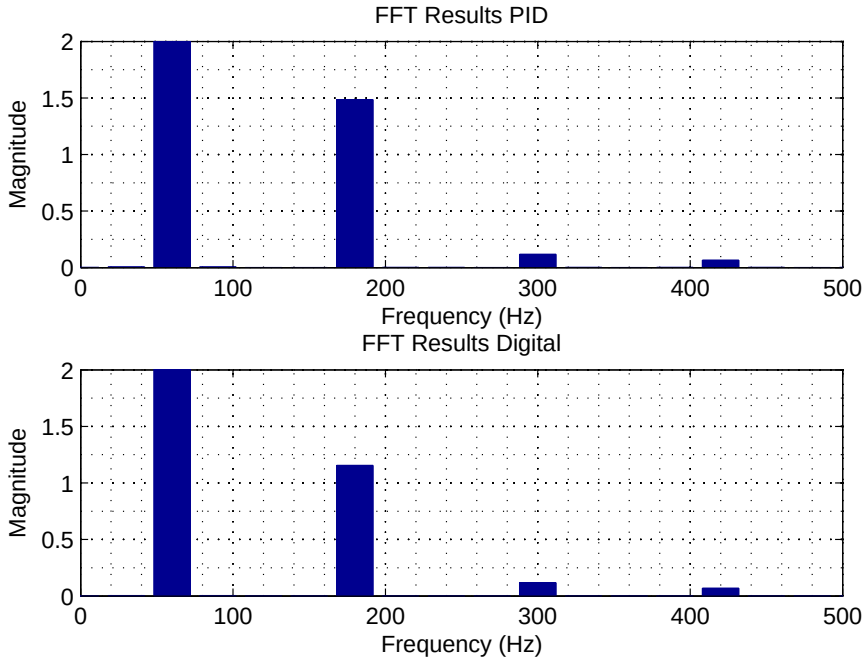

Figure 4.12. Detail of amplitudes of high frequency components on the FFT analysis.

DC bus voltage waveform characteristics have been discussed in previous chapter regarding the design of the PFC circuit. A basic feature is the ripple shown in figure 4.13 at twice the line frequency. Both controllers follow the reference value in the steady state whereas the analog PID controller shows some high oscillations in the transient. A detailed transient analysis will be performed and commented later. A second ripple is present in the DC voltage but can be reduced with a proper design and a good performance of the controllers. As can be seen in figure 4.14 it is not visible and the voltage waveform satisfies the stable operation condition of the PWM boost rectifier.

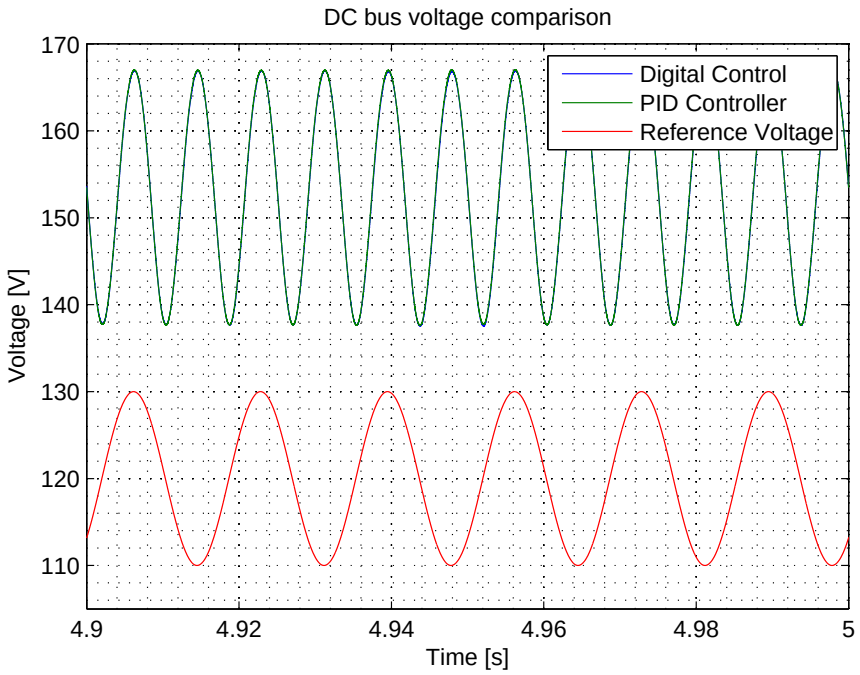

Figure 4.13. Comparison between the two DC bus voltage waveforms and input voltage.

Control for the output current provides a fixed value of $I_L = 62.5\,A$ and performs well in both cases. In fact it provides a value that is nearly constant at the output. Current ripple is minimized through the correct choice of the output capacitor and results in a very small ripple (less than 0.5 %). An oscillation at twice

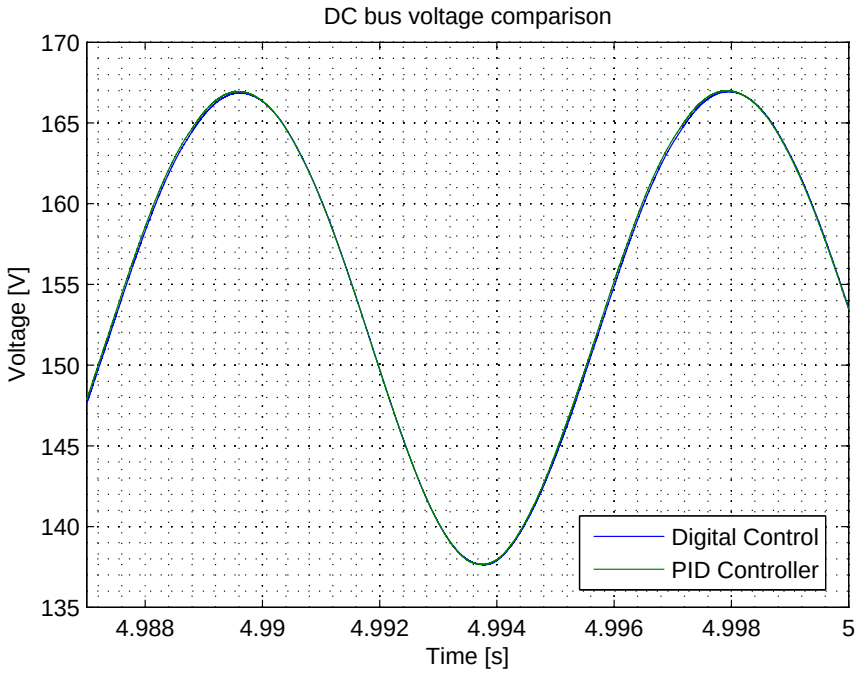

Figure 4.14. Comparison of the two DC bus voltage waveforms.

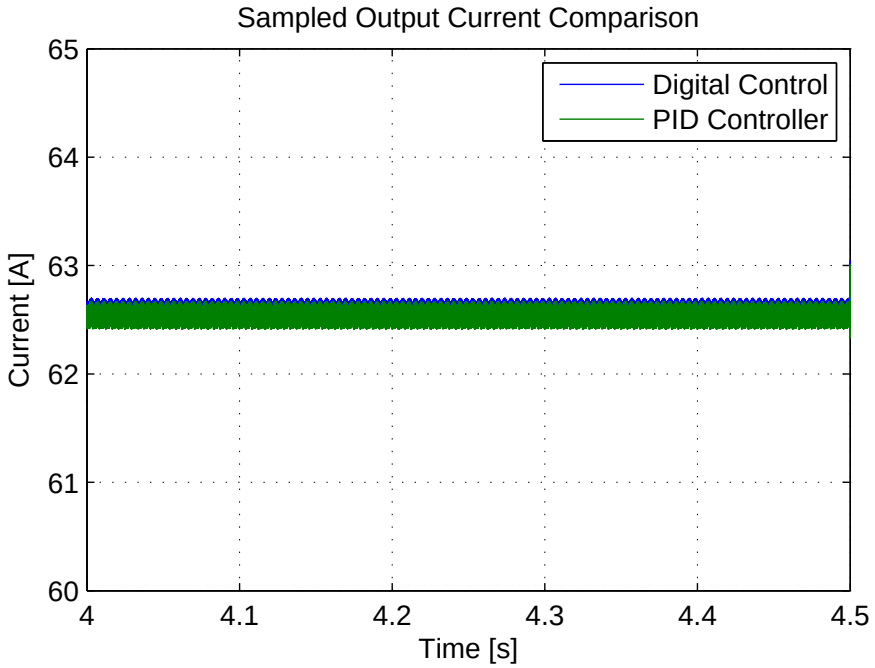

Figure 4.15. Comparison of the two output current waveforms.

the line frequency is seen from the un-rectified bus voltage and can also be observed in the output current. The controller operation drastically reduces its amplitude. Output current waveform of the digital controlled system is compared with the PID controller output in figure 4.15.

A detailed explanation of simulation results has been done for the transient conditions during which the system reaches the steady state operation. In particular, the performance of the digital controller described above results in a much better than the analog PID controller showing a smoother and faster response. As before, input and output waveforms are shown considering also FFT analysis and the DC bus voltage waveform as a quality parameter.

Input sinusoidal current is tracked by the multi-loop controller, either digital or analog, and shaped with a quite fast settling time, of around $0.4\,s$. During this time the error between actual and desired current is almost reset to zero. Most noticeable advantage of the digital controller in this situation is given by its limited current spikes in the transient. This does not require any strict protection system and further simplifies the hardware implementation and the structure of the controller. The amplitude of the first oscillations is shown in figure 4.16.

Better performance of the digital control can also be seen from the DC bus voltage which is an important element in the stability of the circuit. Its waveform is already shown in figure 4.14 for the steady state condition and results in a much more stable operation with the use of the digital control. As can be seen from figure 4.17 digital control reaches the reference signal much faster than the standard PID multi-loop controller thanks to the optimization of the inner loop and the effectiveness of the controller design. In particular, the large oscillations present in the PID-controlled circuit settle fast and a smooth and more stable waveform is reached.

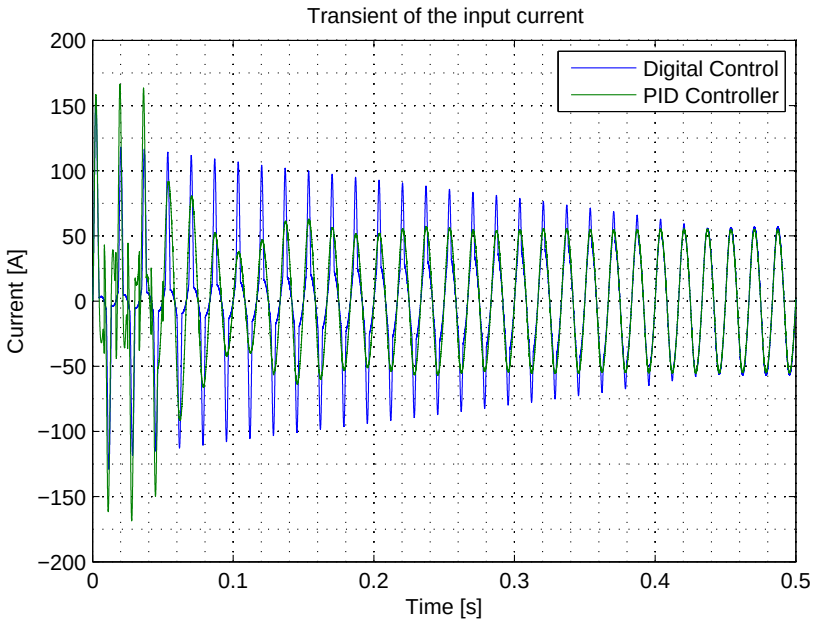

Figure 4.16. Comparison of the two input current transients.

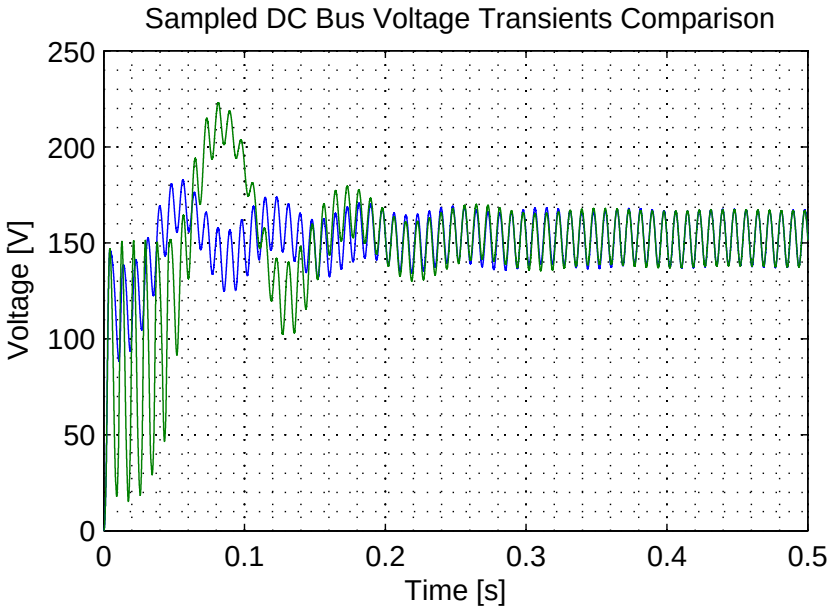

Figure 4.17. Comparison of the two DC bus voltage transients.

Further, improved performance and stability of digital control are also noticeable in the output waveforms. In particular a very fast response and the absence of significant oscillations in the current plot can be observed. Figure 4.18 presents

the current response of the output DC/DC converter. It reaches the reference signal after merely 0.0015 s in the digital-controlled circuit whereas the PID-based design is around 100 times slower. Moreover, analog controller circuit is characterized by large oscillations during transients. A longer settling time is also the result of a slower action of the controller. Large spikes in the current waveform could damage the battery or shorten its life-time without any protection circuit or peculiar design expedient. Thus a more complex design or protection solution is required.

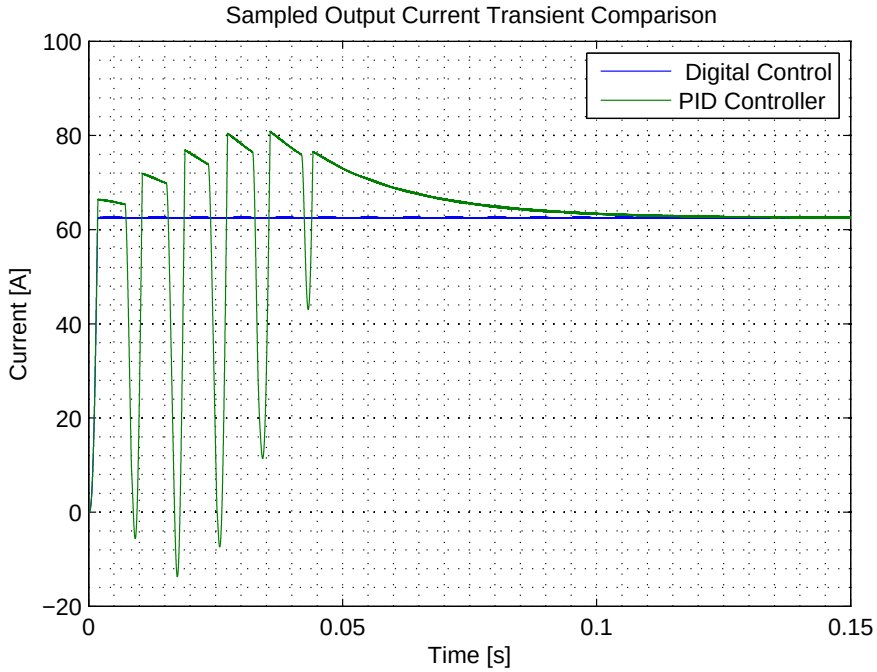

Figure 4.18. Comparison of the two output current transients.

4.5.1.1 Robustness of the Controllers. In this subsection the response of the two compared systems to slight variations of their parameters in the steady state is presented. Using this practical simulation approach, important results can be seen. Robustness of the system to parameter variations and effectiveness of the controller to track desired signal regardless the system modification are shown.

Variation of critical parameters will be performed in the MATLAB® Simulink model, as will be done in following chapter to show stability regions and instabilities phenomena. The output waveforms are shown and obtained results are explained. Two variations are performed in selected components. Starting from optimum and stable case parameters will be changed at instants $t' = 2\,s$ and $t'' = 4\,s$ respectively. All the transient can be observed in the simulation time $T = 5\,s$.

The first set of simulations address a typical series of issues that can happen when the input voltage level is not constant and changes with slight fluctuations of around $5 - 10\%$. This condition is usual in countries like India where amplitude of the utility voltage is not fixed and variations occur. On the other hand, the line frequency usually remains constant. System response is simulated and some considerations about performance and stability issues are done. Input voltage at the nominal value of $90\,Vrms$ is varied to respectively $85.5\,Vrms$ and $81\,Vrms$.

Input waveforms is modified by the voltage drop but shows a very stable behavior especially for the digital-controlled system, as can be seen from figure 4.19. Transitions between different voltage levels are done very fast and without showing significant oscillations. A longer settling time with some dumped oscillations is recorded for the analog-controlled circuit.

On the other hand, DC bus voltage waveform shows more visible effects of the variation of the input voltage. The system is still stable and with a good output

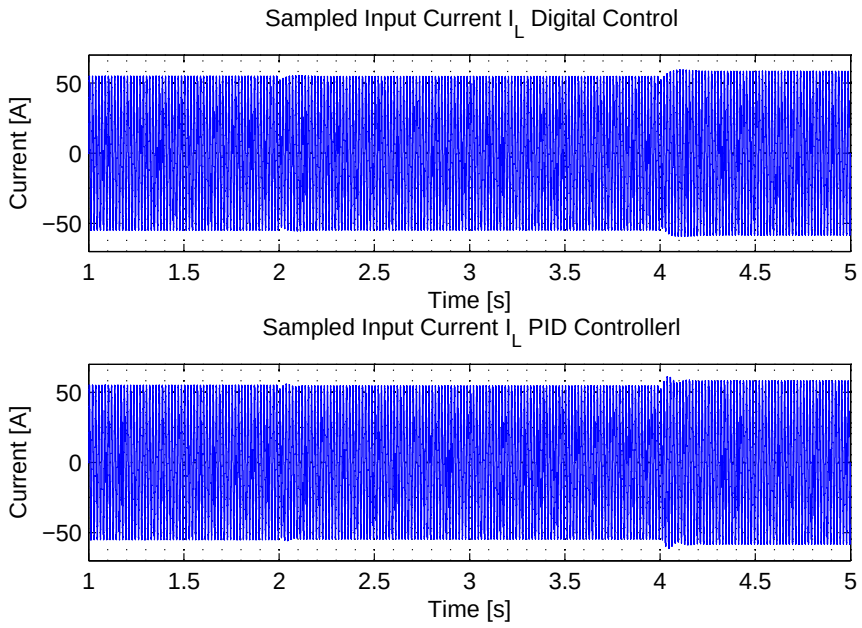

Figure 4.19. Comparison of the two input current waveforms for a change in the input voltage.

response. In particular, digital-controlled system is characterized by unilateral oscillations that lead the waveform to settle after a small time interval. Small voltage peaks of around 15% of the steady state value can also be seen. Analog-controlled circuit shows a better behavior which is probably due to a better tuning of the parameters of the regulator. Waveform variations are shorter and with smaller amplitude. Both responses show anyway a good performance for the overall system (figure 4.20) and the controller seems to work as desired.

Output waveforms are represented in figure 4.21. They also involve the DC/DC converter control section which works very well for both configurations. Only a small variation of the output current in correspondence with the input voltage change can be noticed. In particular, transitions between different levels are smooth even if a small settling time for the PID regulated system can be seen.

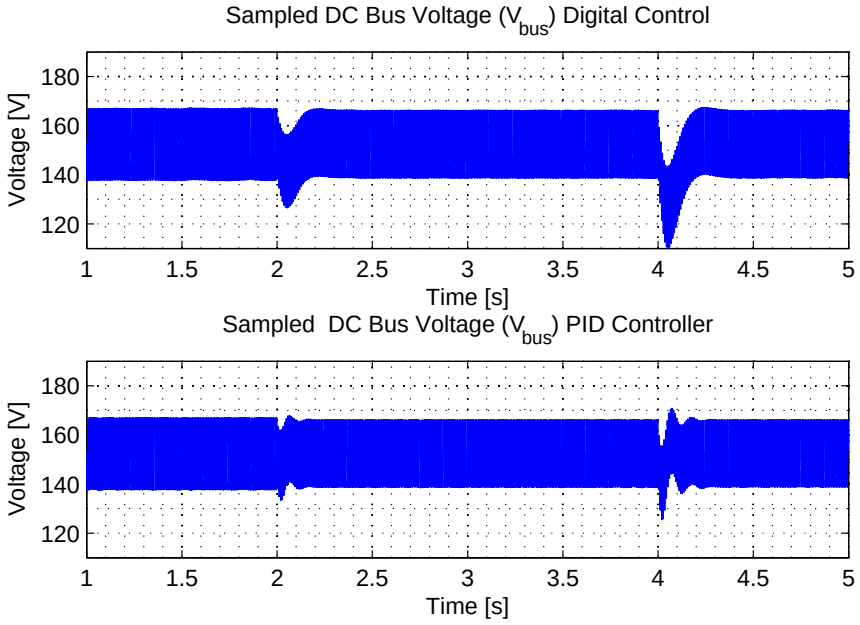

Figure 4.20. Comparison of the two DC bus voltage waveforms for a change in the input voltage.

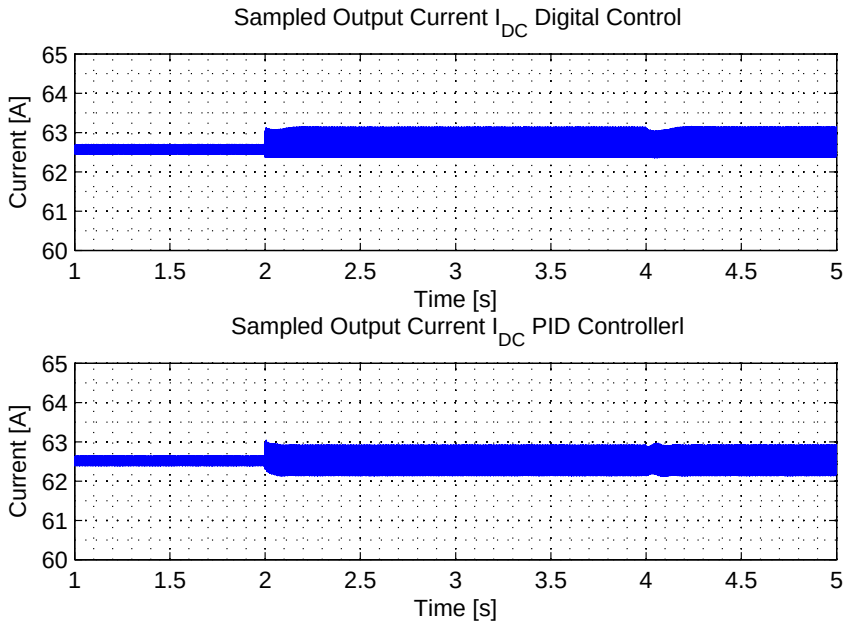

Figure 4.21. Comparison of the two output waveforms for a change in the input voltage.

Second series of simulations has been done considering faulty or un-regular operating conditions, corresponding to a lower voltage in the storage pack, which could be considered as a result of an over-heated battery. In particular, for a typical battery cell at the varying of the temperature rapid changing in the internal equivalent resistor can be seen. Nominal value of the resistor $R_{out} = 0.768\,\Omega$, chosen such as to guarantee a transferred power of $3\,kW$, is decreased to $R'_{out} = 0.7\,\Omega$ and further to $R''_{out} = 0.6\,\Omega$ corresponding to a variation of around -20%. Similarly waveforms and responses of the systems change accordingly to the lower input and controller reaction to these variations is here recorded and explained. As can be seen from figure 4.22, input current is not widely affected by the change in the load and it only shows larger sinusoidal amplitude. Transition between the three different load values results to be smooth with both the control strategies, whereas digital controlled circuit is faster. Some oscillations can be seen in the waveform of the classical PID multi-loop controller system.

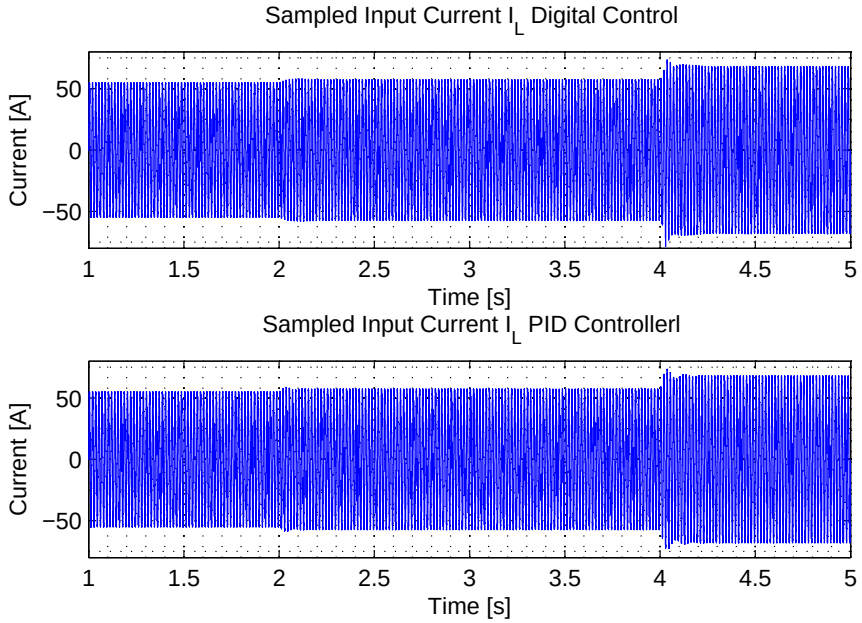

Figure 4.22. Comparison of the input current waveforms for a change in the output load.

DC voltage waveform, measured across the DC side capacitor, is affected by the variation in the output load. It shows a slightly larger ripple at twice the line frequency under stable conditions. Due to the sudden load change, some oscillations can be seen in the figure 4.23. Digital implementation of the controller has a unidirectional and dumped oscillation whereas the classical analog control strategy shows a series of oscillations of smaller amplitude. Both circuits operate under stable conditions, even with a load variation of around 20%.

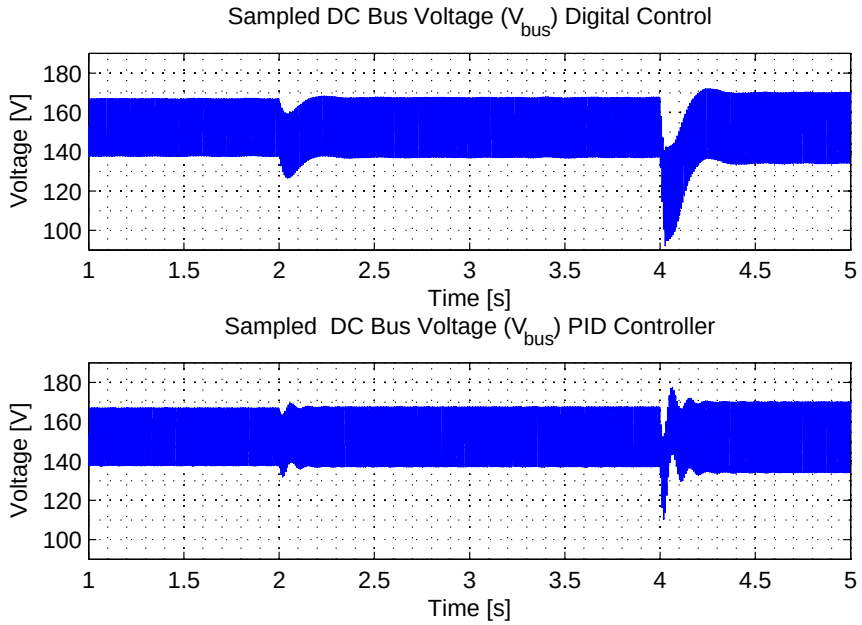

Figure 4.23. Comparison of the two DC bus voltage waveforms for a change in the output load.

Regulated output current is affected by the change of the input load. As it increases linearly rated power also increases. The circuit shows a fair behavior in terms of the variation in the load due to the second stage controller which regulates the output DC level very well. Neither transients nor large settling time can be seen in the waveform of figure 4.24, which shows the comparison between the two control strategies.

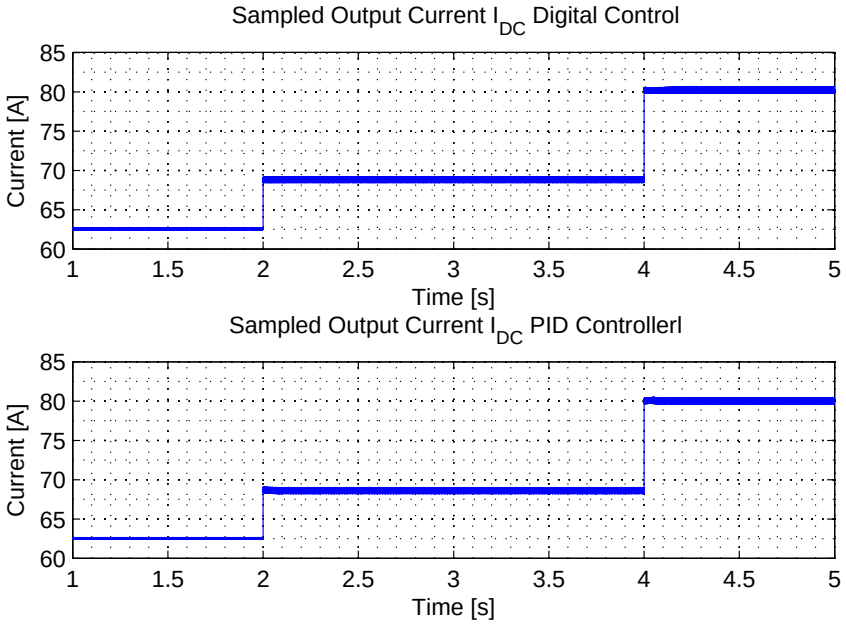

Figure 4.24. Comparison of the two output waveforms for a change in the output load.

CHAPTER 5
STABILITY ANALYSIS AND ISSUES

5.1 System Analysis

The double-stage power electronic converter is characterized by universal voltage input and is a cost effective solution for battery chargers. The proposed circuit provides PFC correction and tight output power regulation either using the conventional PID multi-loop regulator or the novel digital control approach.

Recent studies on the dynamics of switching power converter circuits have revealed the possibilities of several scenarios for unstable operations showing both at fast-scale and slow-scale [43]. Slow-scale instability problem may worsen the harmonic distortion of input current, whereas the fast-scale instability may impose higher current stresses on switching devices [45].

An incorrect design of the components of the system may give rise to such problems, in particular due to an improper choice of parameters such as the DC bus capacitor, input inductor value and the sizing of the battery load. A precise tuning of the parameters of the controller can be done in order to minimize instabilities for all working conditions. However, especially for low voltage and high current inputs instability issues are to be found in the power supply. This chapter also cites examples of several unstable conditions are provided.

5.2 Instability Issues

Different instability conditions can be found in the analysis of the two cascaded converters. They can be divided into different categories based on the waveforms obtained. Several studies [46] and [47] have identified period-doubling bifurcations for input current in certain parameter ranges. Chaotic instability phenomena can also be seen from a non-sinusoidal input inductor current and an unstable DC bus

voltage.

Stable operation for the first stage PFC boost converter is a periodic sinusoidal input current perfectly in phase with the line frequency as shown in figure 5.1. A periodic ripple at twice the line frequency has to be present in the DC bus voltage (figure 5.2). Similarly, instability issues can be seen by the observation of these key waveforms or through the presence of higher harmonics components in FFT analysis. Sinusoidal input current shows bifurcations and cusp distortion for a slight variation of the parameters but reaches a completely non-periodic response for lower values of DC bus capacitor or lighter loads. Also DC bus voltage shows random waveforms under chaotic instability case in this situation.

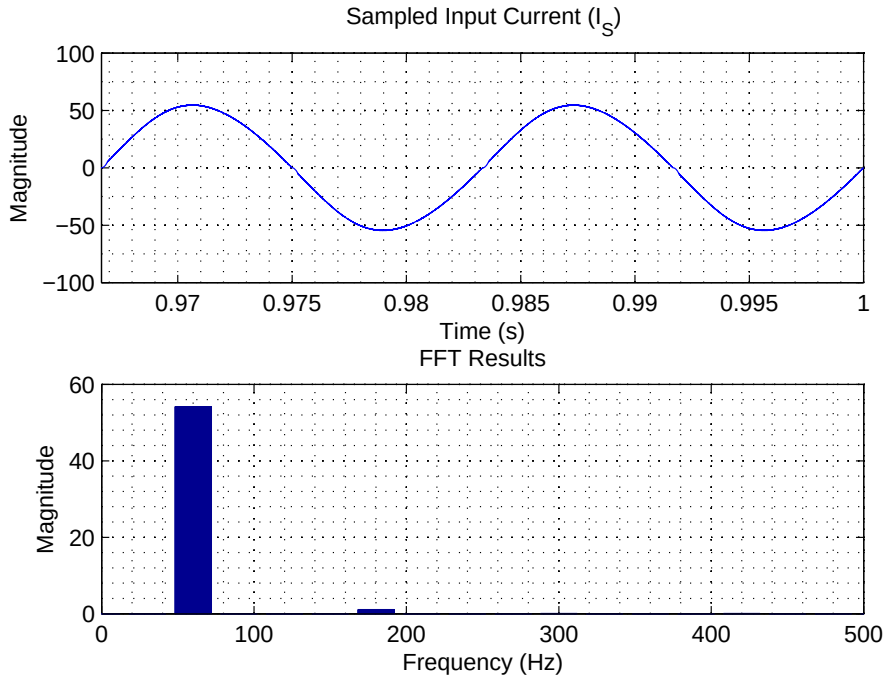

Figure 5.1. Stable mode of operation seen in the sinusoidal input current.

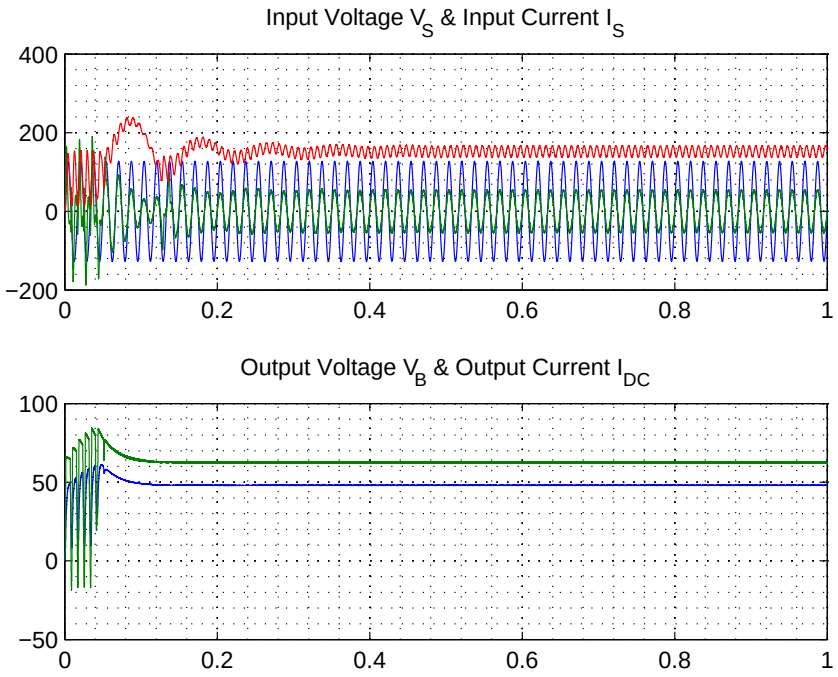

Figure 5.2. Stable mode of operation seen in the DC bus voltage and output current and voltage waveforms.

Similar results indicating stability-instability regions at the varying of the parameters can be identified using the technique of the phase plane trajectories. Phase plane curves, also called Lissajous curves, are a simple method to detect unstable phenomena. These trajectories are drawn between the output voltage ripple on the vertical axis and the input current on the horizontal axis and consider a steady state operation for the circuit. Stable conditions, as well as period-doubling operation and chaotic instability can be easily deduced from these plots. In fact in the stable case, they must show two equal symmetrical loops such as in figure 5.3. Asymmetrical cycles can be seen for period-doubling bifurcation case or chaotic phenomena.

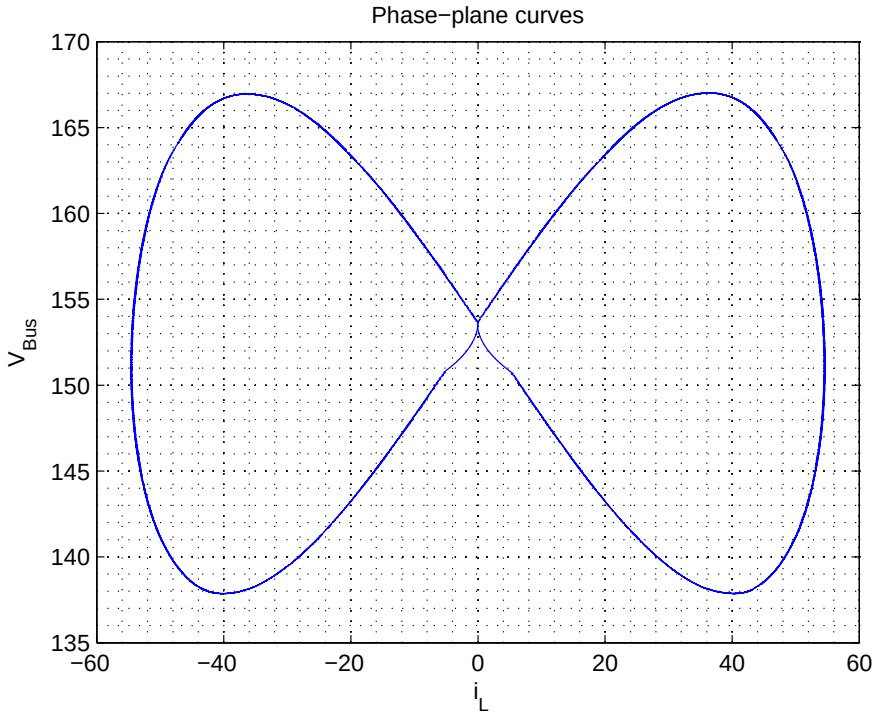

Figure 5.3. Stable mode of operation seen in the DC bus voltage and output current and voltage waveforms.

Phase plane curves form a very powerful tool in the stability analysis of the circuit. A more detailed explanation for particular instabilities conditions as a confirmation of what has been shown through simulation results will be provided later.

5.2.1 Stability Analysis through Circuit Simulations I. In this section a detailed stability analysis will be done considering designed circuit responses. In particular, input inductor current, DC bus voltage and output current waveforms will be analyzed. A series of stability conditions and boundaries will be derived for important parameter of the circuit as well as for different controller parameters and techniques.

All system simulations are done using previously derived state space equations for the combined two-stage converter. The circuit is controlled using the PID analog feedback loop explained in previous chapters. A final comparison with the novel digital control approach is also done in following section. Most strict case of low-voltage high-current input is considered. A n input voltage $V_{in} = 90\,Vrms$, at the line frequency of $60\,Hz$ is used. Component values and controller gains are indicated in tables A.1 and A.2 in Appendix.

Circuit behavior is studied by varying only one parameter at a time and relevant plots will be shown. Then more specific instability issues are empirically derived and will be deeply analyzed with some mathematical references. It must be noted that the AC/DC rectifying operating mode is tested here for the worst case scenario. Instability issues for the charging of the battery from the grid and power factor correction problems for input current are shown.

5.2.1.1 Variation of Load Resistor Value. First study regards variation in the equivalent resistor load R_{out} intended to be internal battery resistor. Its voltage V_{out} remains constant. Current reference signal is changed consequently to maintain constant output voltage for the DC/DC converter when load resistor is changing. Variations in the load resistor will lead to an increase or decrease in drawn power either from the grid or the battery. By the observation of the respective waveforms interesting stability considerations can be made. In particular, optimum operating

point in terms of stability is set to output resistor value of $R_{out} = 0.768\,\Omega$, which corresponds to a nominal $3\,kW$ of power. However, variations around this value can show undesirable behavior for the circuit. An increase in the load resistor corresponds to a decrease in the reference current and in drawn power as shown in figures 5.4 and 5.5. This would not result in instability issues and thus phase plane trajectory shown in figure 5.6 is characterized by a perfect symmetry around the two axes. On the other hand, unstable phenomena can be seen when lighter loads and therefore higher power is applied.

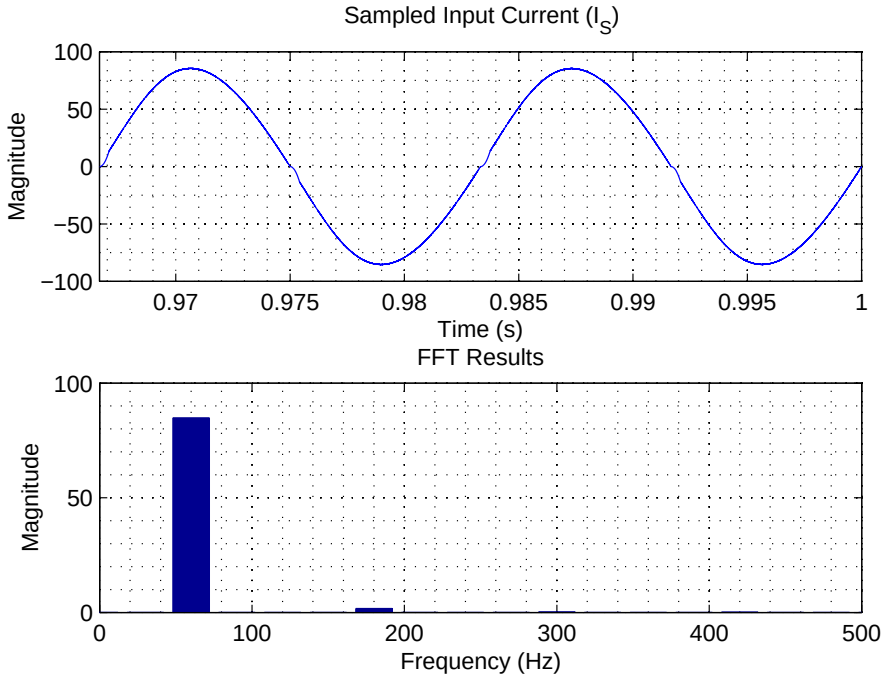

Figure 5.4. Input current waveform and FFT analysis for $R_{out} = 1.2\,\Omega$.

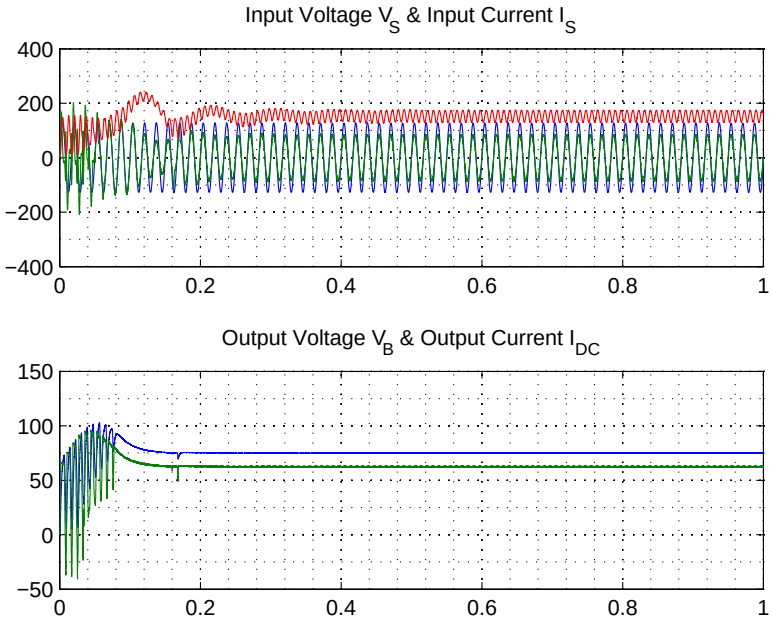

Figure 5.5. DC bus voltage and output current and voltage waveforms for $R_{out} = 1.2\,\Omega$.

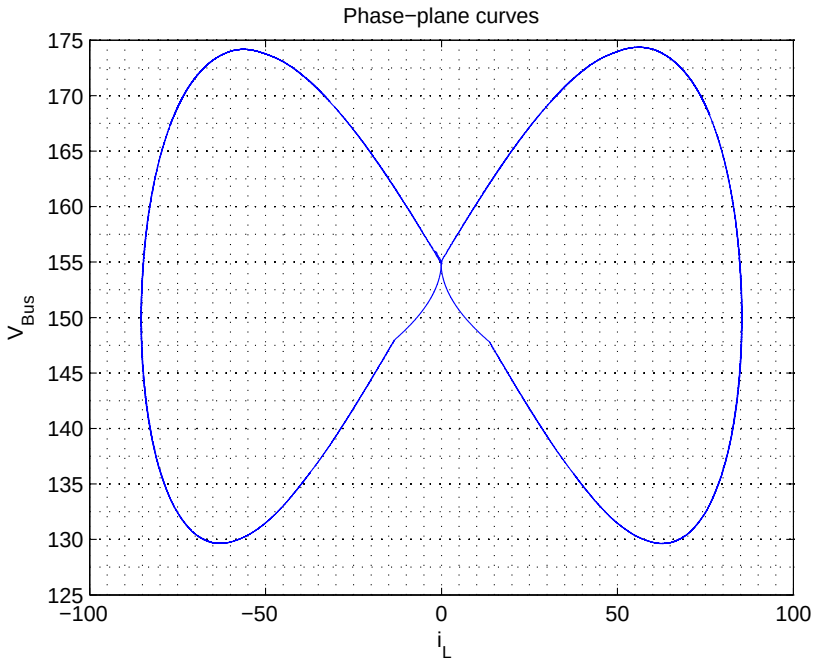

Figure 5.6. Phase plane trajectories for $R_{out} = 1.2\,\Omega$.

Lowering the value of output resistor below a certain threshold will produce a double effect in analyzed plots, as shown in figure 5.8. The presence of undesired oscillations in the DC bus voltage transient which is also characterized by a greater settling time can be recognized. Cusp distortion in the zero-crossing point of the sinusoidal input current is shown in figure 5.7. Similarly, those oscillations will affect the phase plane curve plot (figure 5.9) which will lose its symmetry around horizontal axis. Input inductor current for light load variations of around -25% will still give an almost perfect sinusoidal waveform as can be seen from FFT analysis of figure 5.7.

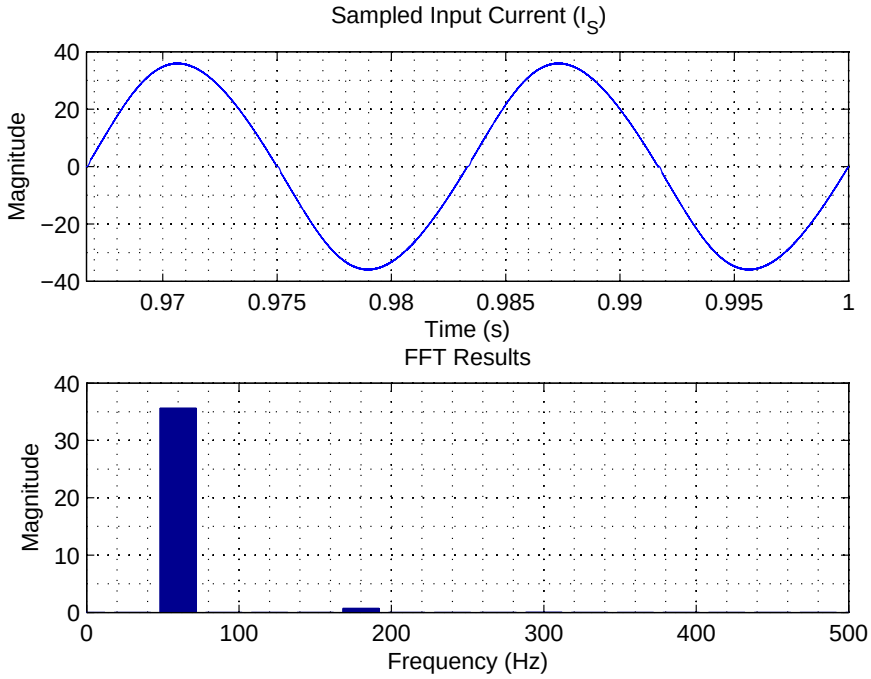

Figure 5.7. Input current waveform and FFT analysis for $R_{out} = 0.5\,\Omega$.

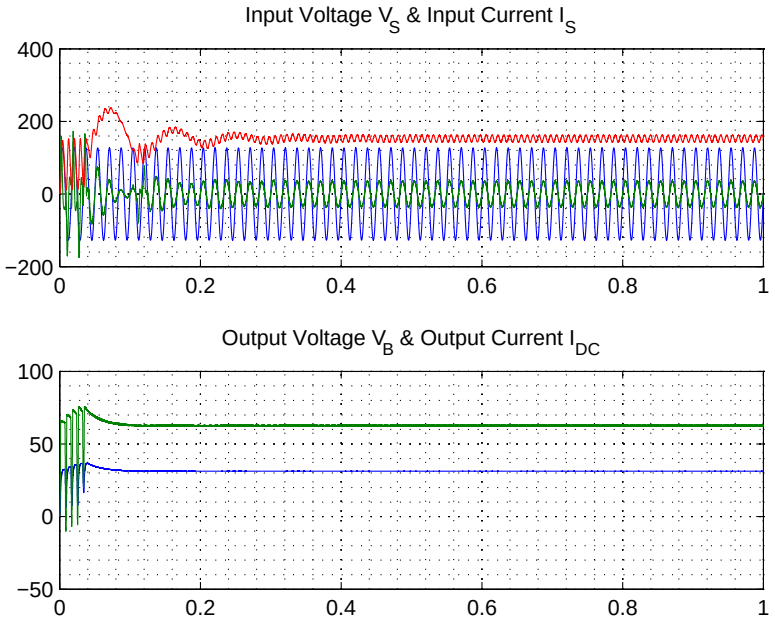

Figure 5.8. DC bus voltage and output current and voltage waveforms for $R_{out} = 0.5\,\Omega$.

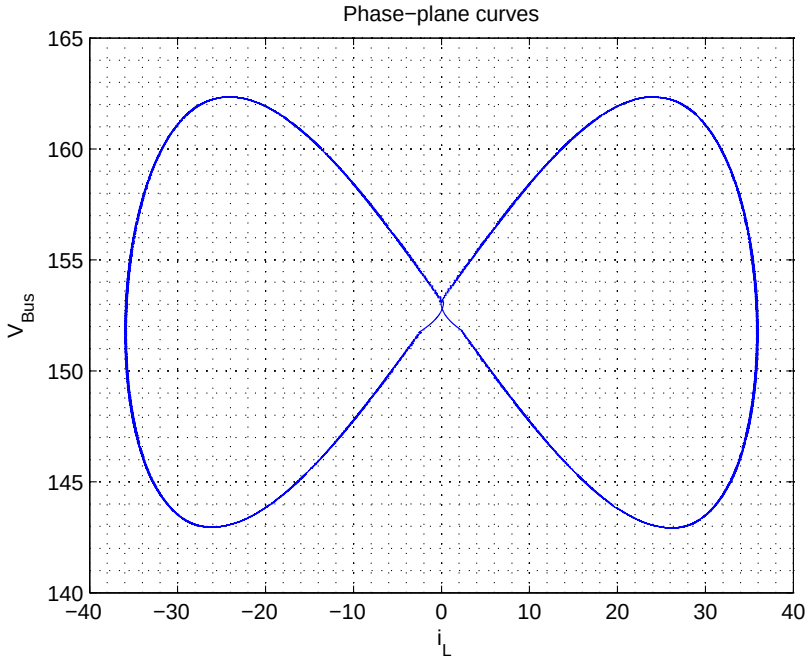

Figure 5.9. Phase plane trajectories for $R_{out} = 0.5\,\Omega$.

For higher variation of the order of -35% or higher effect of instability can be seen. The bifurcation effect is visible in the asymmetrical phase-plane plot (figure 5.12), and larger oscillations in the DC bus voltage waveform (figure 5.11). Also output waveforms are affected by this increasing instability, showing a larger settling time as can be seen in figure 5.11. Input inductor current becomes non-sinusoidal and starts showing the presence of higher frequency harmonics (figure 5.10). Chaotic instability is reached with a completely asymmetrical behavior of the phase-plane curve and the input inductor current with a variation of the load of around -50%.

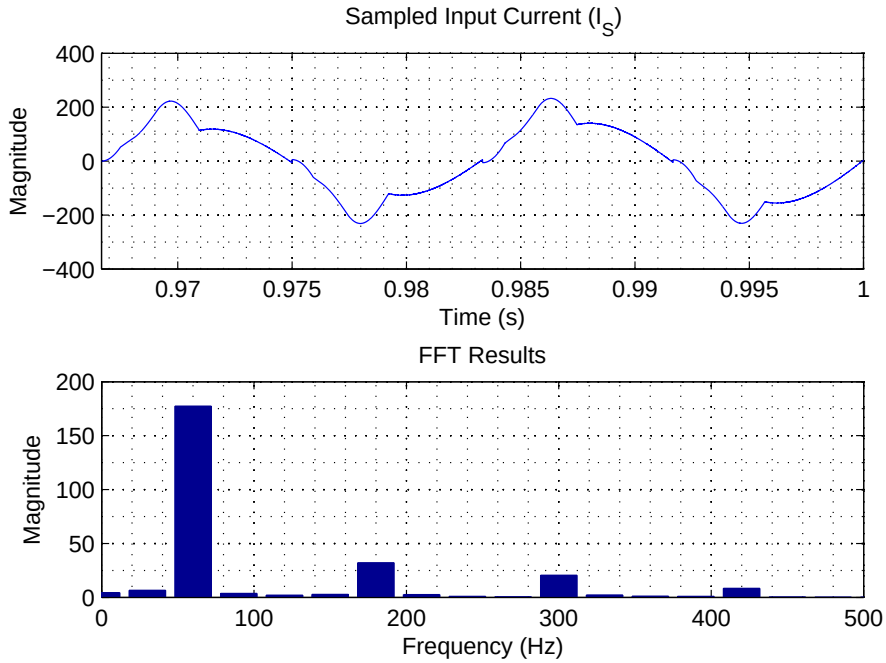

Figure 5.10. Input current waveform and FFT analysis for $R_{out} = 0.3\,\Omega$.

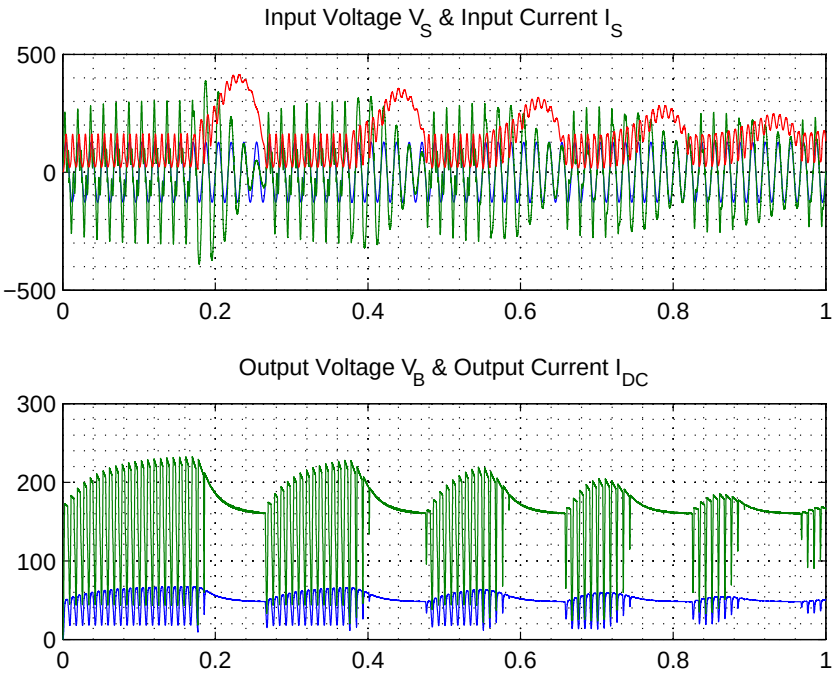

Figure 5.11. DC bus voltage and output current and voltage waveforms for $R_{out} = 0.3\,\Omega$.

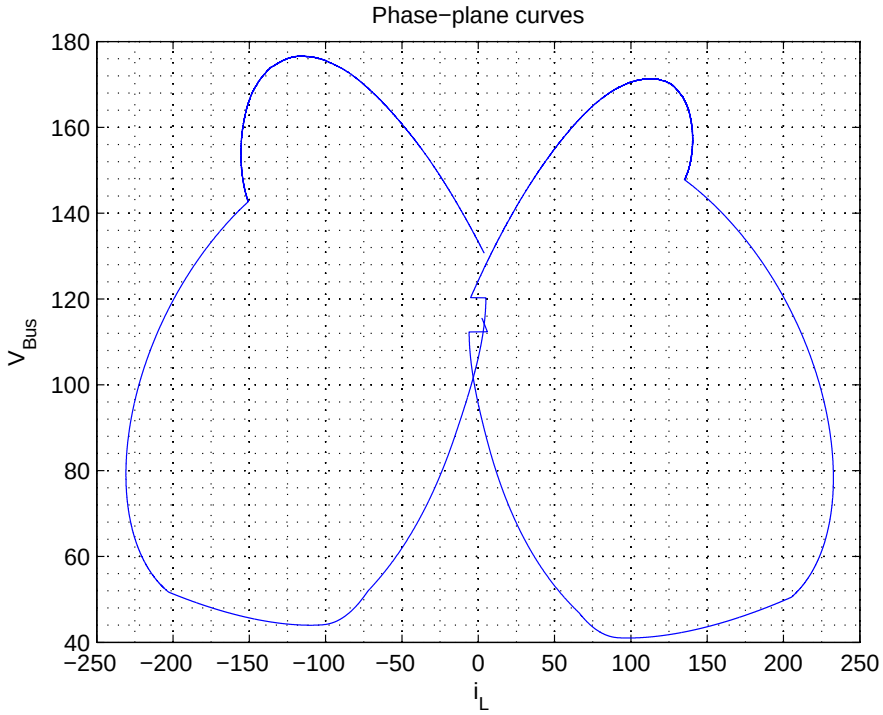

Figure 5.12. Phase plane trajectories for $R_{out} = 0.3\,\Omega$.

5.2.1.2 Variation of Input Inductor Value. The second set of simulations presented regards the variation in the value of the input inductor of the PFC circuit. This very important component has several repercussions in the input inductor current waveform, as well as the DC bus voltage and the output current and voltage. Exactly as before, from the analysis of the phase plane plot and the study of recorded waveforms some instability patterns are recognized.

Inductor value is chosen to be 300 mH in the optimal case and is varied from 50 mH to 1100 mH nominal values. Other components are kept as constant parameters. Two different behaviors are noticed for an increase or decrease in the value and they both affect stability and phase margin for the system. In particular, a decrease in the input inductor value will produce a series of oscillations in the sinusoidal current waveform which can be easily seen from the phase-plane plot. An increase in the parameter value will correspond to some more visible unstable effect which will lead to asymmetrical phase-plane curves and cusp distortion.

For lower values of input inductor, the system is still stable even if a small ripple can be seen in the sinusoidal shape of inductor current (figure 5.13). Also small oscillations around the symmetrical shape of the Lissajous curve (fig. 5.15) and some high frequency components in the FFT analysis (fig. 5.13) are present.

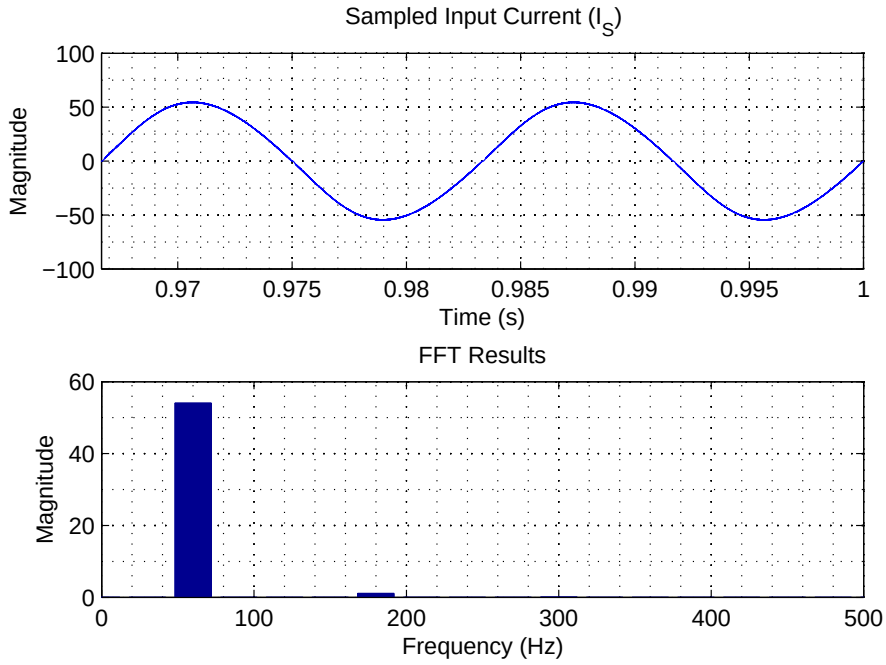

Figure 5.13. Input current waveform and FFT analysis for $L_1 = 150\,\mu H$.

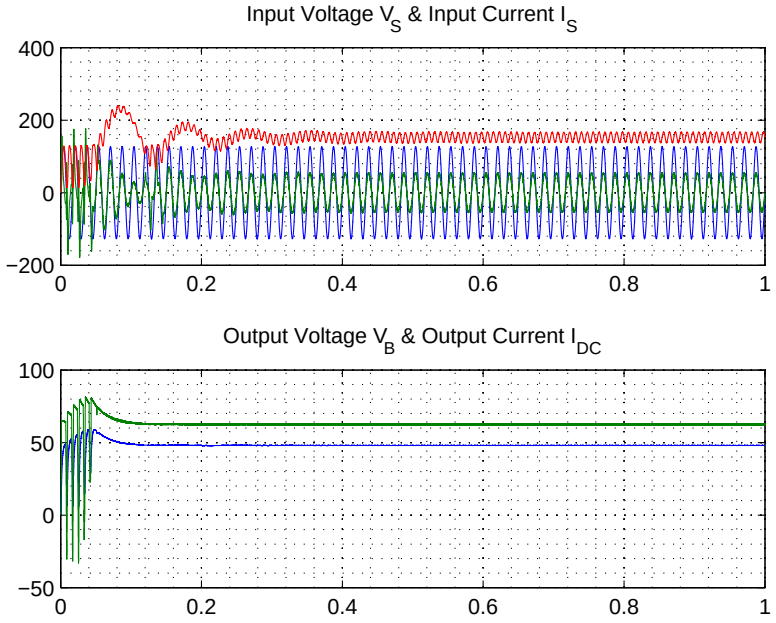

Figure 5.14. DC bus voltage and output current and voltage waveforms for $L_1 = 150\,\mu H$.

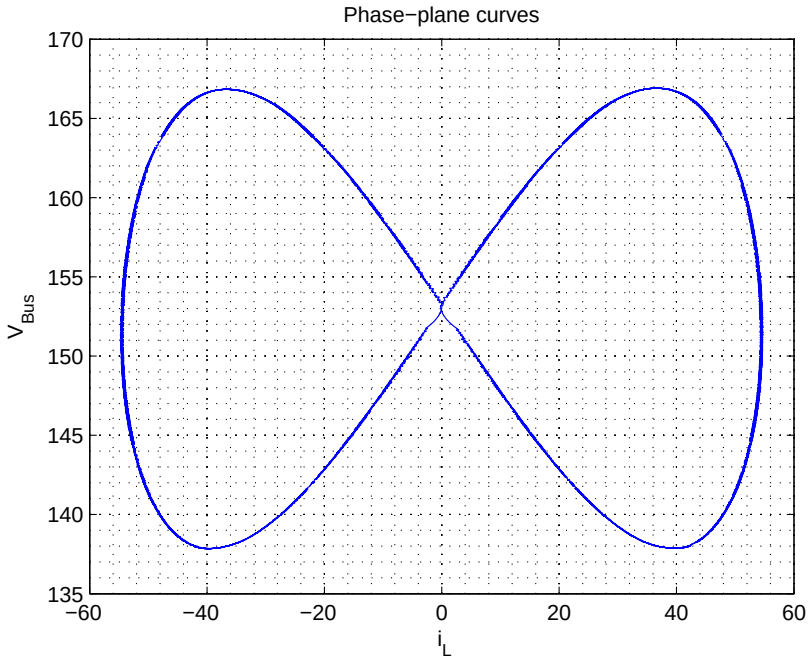

Figure 5.15. Phase plane trajectories for $L_1 = 150\,\mu H$.

For a further decrease in the inductor, this ripple visibly increases leading to lower performance of the system. The circuit will start showing relevant cusp distortion and high frequency harmonics (fig. 5.16) but still a near stable behavior can be seen as verified with the phase-plane plots (figure 5.17).

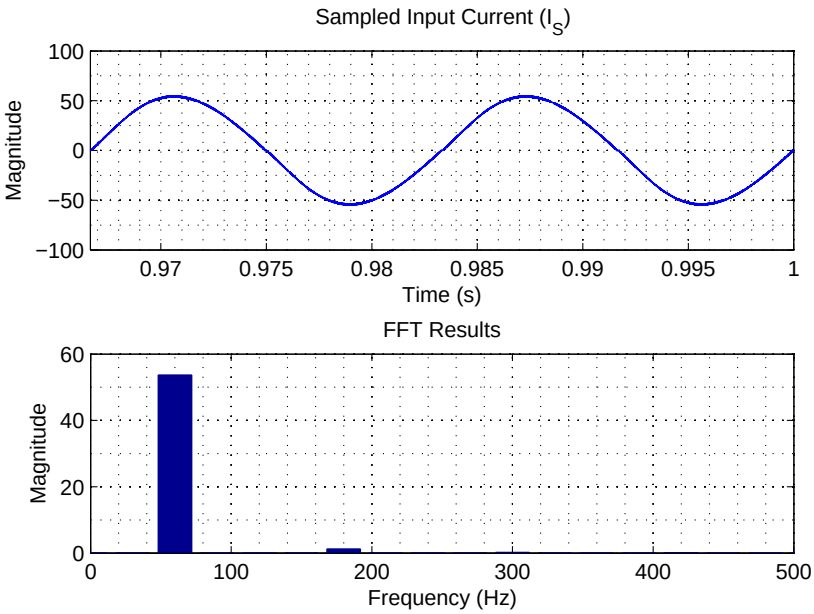

Figure 5.16. Input current waveform and FFT analysis for $L_1 = 50\,\mu H$.

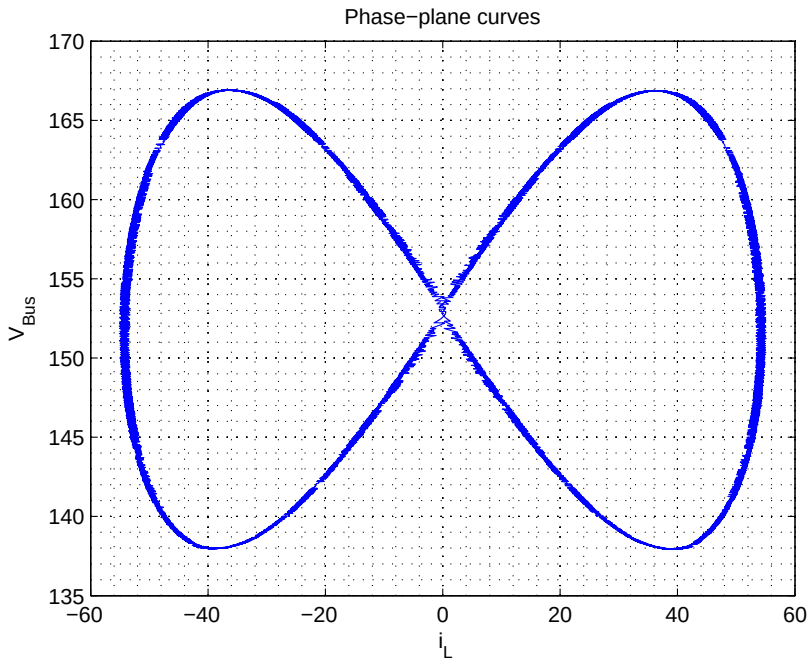

Figure 5.17. Phase plane trajectories for $L_1 = 50\,\mu H$.

A different effect is produced by the increase of the inductor value which will maintain a low ripple in the input current waveform and the absence of high frequency harmonic components. For larger values corresponding to around twice the original value the DC bus voltage response becomes faster and smoother (figure 5.19). Some asymmetrical behavior can be seen in the lower region of the phase-plane plot with the beginning of the cusp distortion phenomena in the sinusoidal waveform (figure 5.18). In correspondence with the zero-crossing point of the current, the cusp distortion effect will cause a non-perfect sine wave. This is due to the fact that right after the input voltage crossover point there is very limited voltage across the boost inductor and a significant magnitude of current. As the result, the inductor current may not be able to follow the reference for a short time period after the zero crossing, causing current distortion. As explained, this effect will increase with the value of the inductance used in the PFC boost converter and with the increasing of the line frequency, which does not represent an extreme issue in this application.

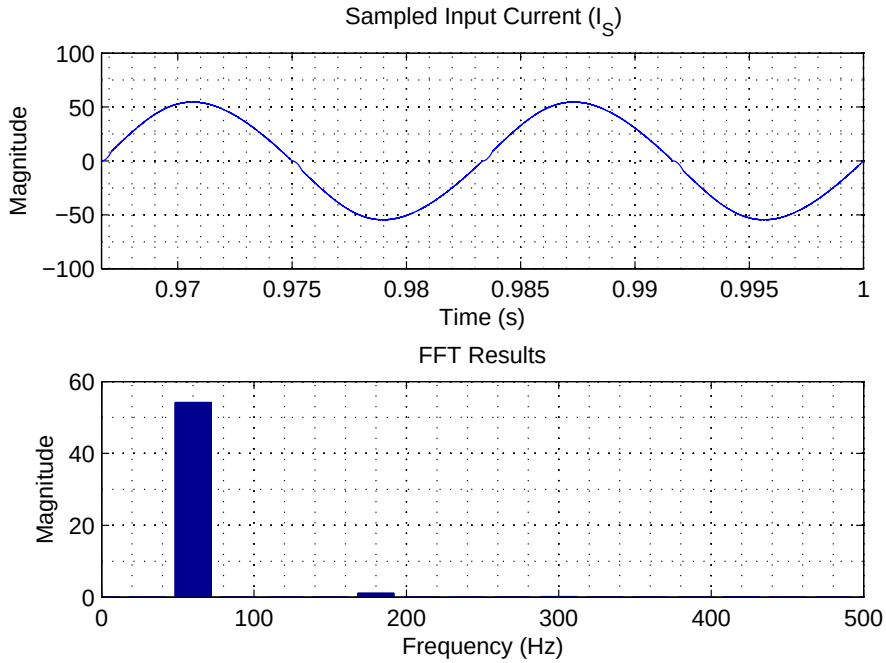

Figure 5.18. Input current waveform and FFT analysis for $L_1 = 500\,\mu H$.

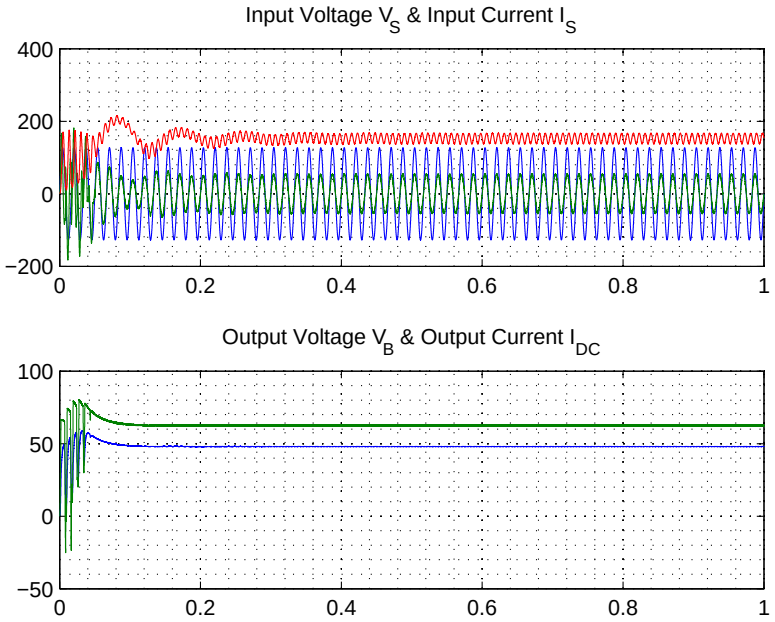

Figure 5.19. DC bus voltage and output current and voltage waveforms for $L_1 = 500\,\mu H$.

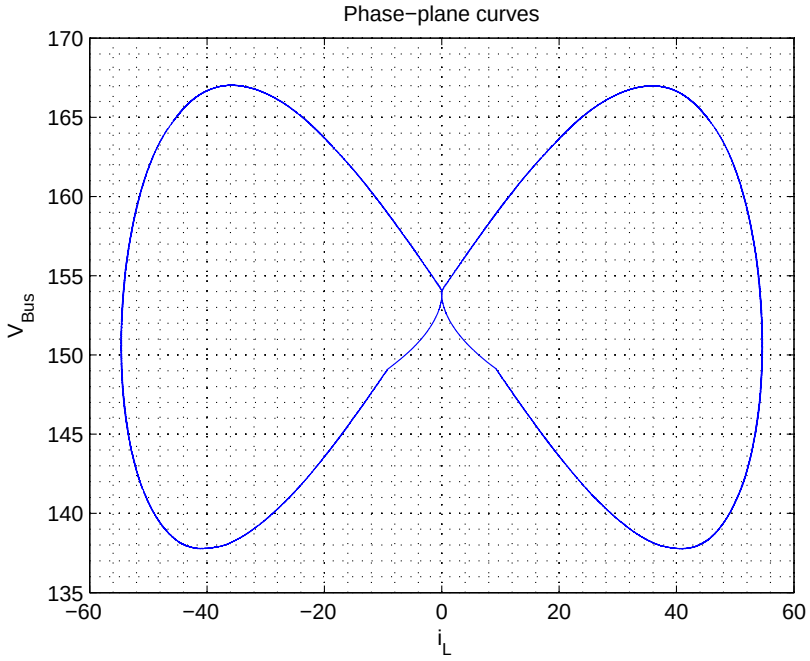

Figure 5.20. Phase plane trajectories for $L_1 = 500\,\mu H$.

Figure 5.22 presents the unstable operation for higher values of the inductor. It can be especially seen from the phase-plane highly asymmetrical curve (fig. 5.23) and from the shape of the input current waveform (figure 5.21). Inductor current is no more sinusoidal and contains high frequency harmonics.

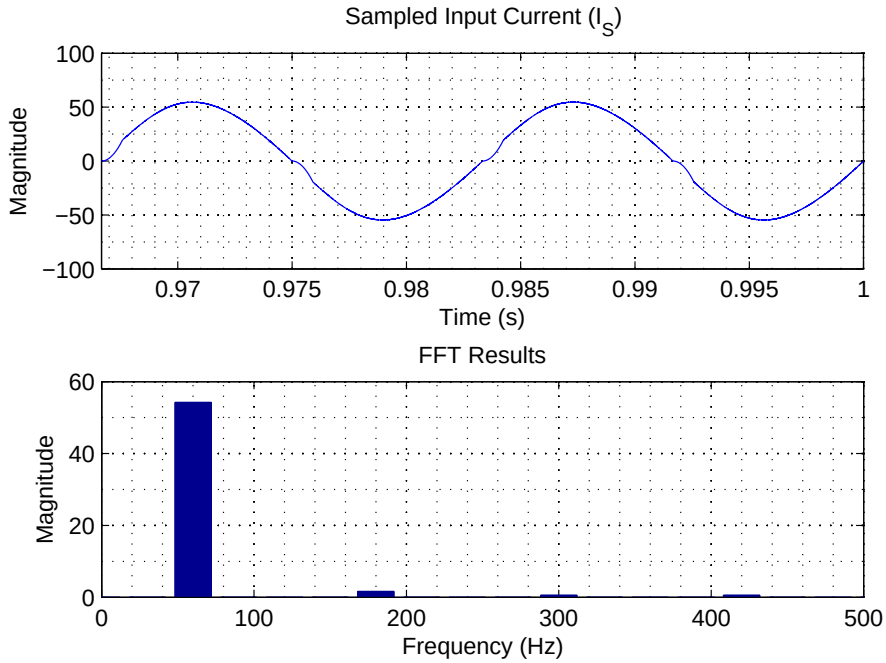

Figure 5.21. Input current waveform and FFT analysis for $L_1 = 1000\,\mu H$.

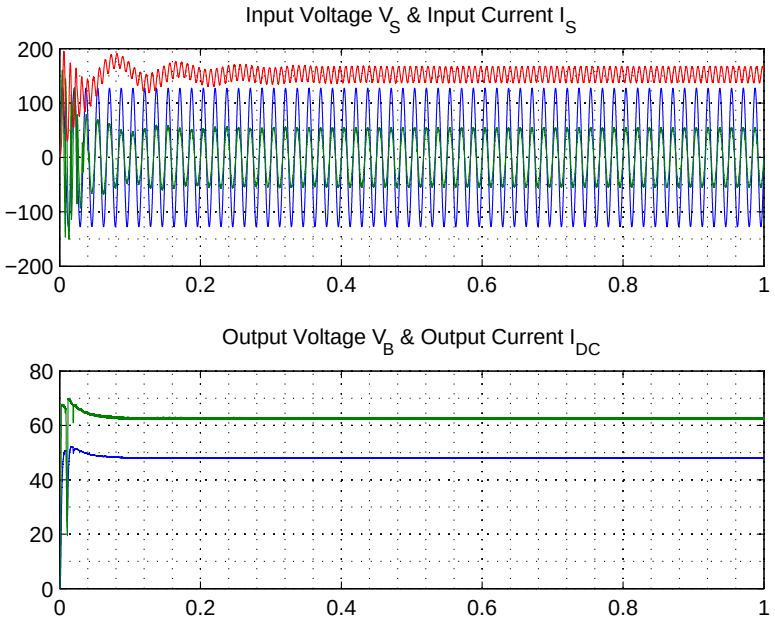

Figure 5.22. DC bus voltage and output current and voltage waveforms for $L_1 = 1000\,\mu H$.

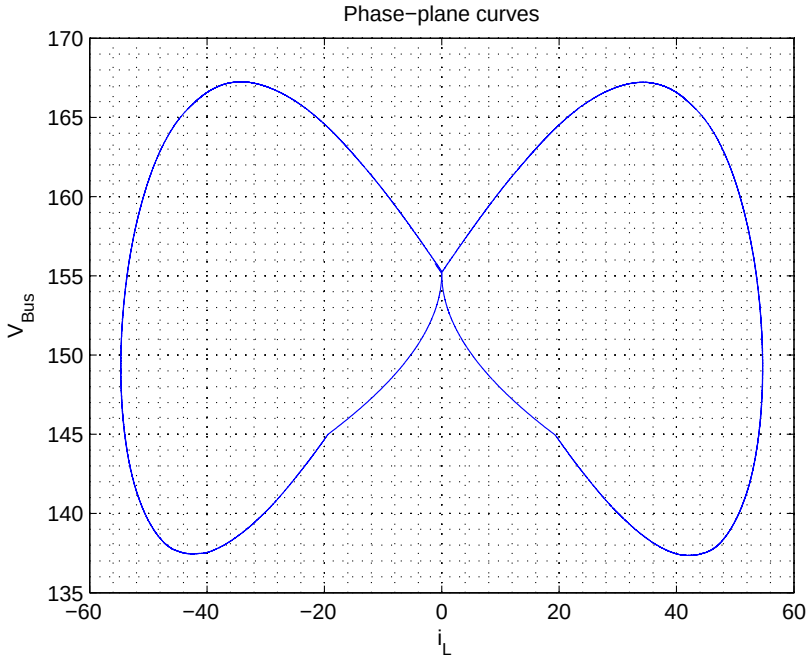

Figure 5.23. Phase plane trajectories for $L_1 = 1000\,\mu H$.

5.2.1.3 Variation of DC Bus Capacitor Value. In this subsection, simulations were run to highlight the effects of the variation of the DC bus capacitor in smoothing the DC voltage bus and shaping the input current. As before, circuit's behavior is simulated in MATLAB® Simulink by varying the value of the capacitor around its nominal value of 2000 μF.

Several different effects can be seen from the analysis of the input current waveform, the DC bus voltage and output current and voltage, as well as with the phase-plane curves. Instability issues for small values of the parameter are shown and design considerations are made. DC link capacitor has to be chosen as a trade-off between size and performances.

As explained, the system becomes unstable for small values of the DC bus capacitor. A highly distorted input current waveform (fig. 5.24) is clearly visible corresponding to a reduction of only 50% from the nominal value. Similarly, smoothing effect of the capacitor is lowered leading to a higher ripple in the DC bus voltage (figure 5.25).

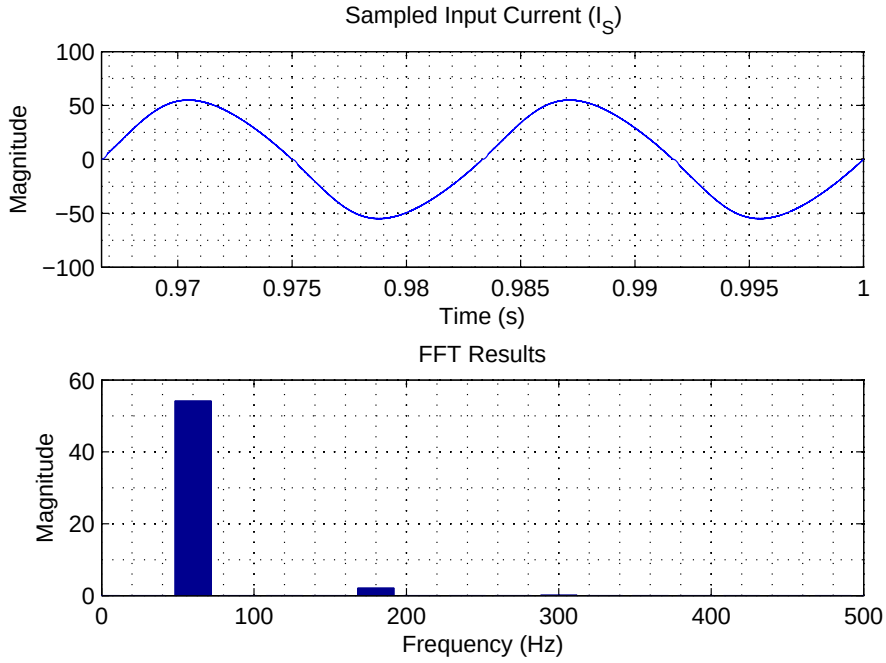

Figure 5.24. Input current waveform and FFT analysis for $C_1 = 1000\,\mu F$.

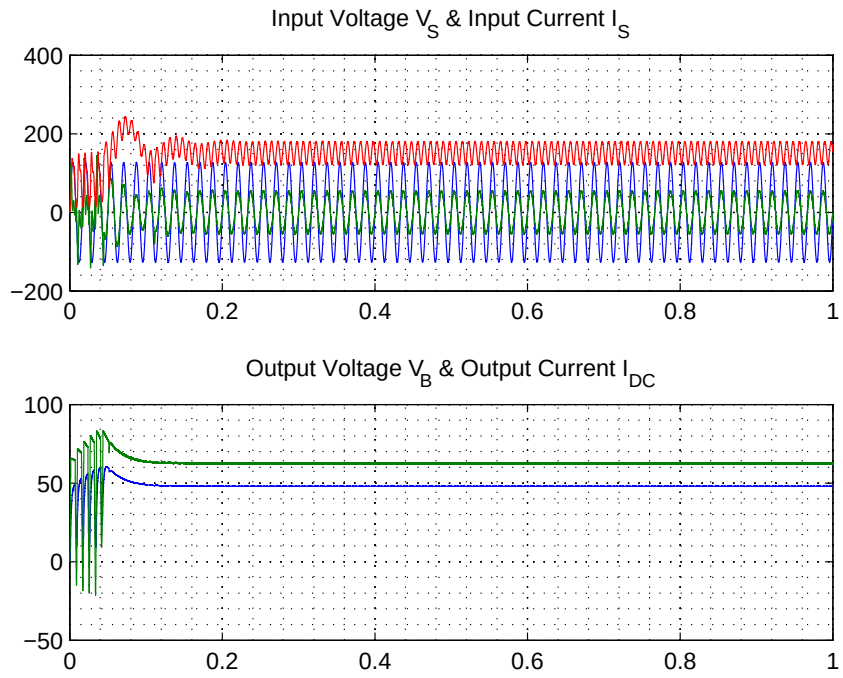

Figure 5.25. DC bus voltage and output current and voltage waveforms for $C_1 = 1000\,\mu F$.

High instability patterns can be recognized for even lower values of the parameter. As a result a highly asymmetrical phase-plane curve and non-sinusoidal input current with high frequency components can be seen in figure 5.28 and 5.26. As before, high ripple is present in the DC voltage bus of figure 5.27.

On the other hand, increasing the value of the capacitor the system remains stable with a smoother DC bus voltage output and a perfectly symmetrical phase-plane curve. Similarly the input current has the sinusoidal shape required to have unity power factor. The only drawback considered is the size of the capacitor; dimension and price increase largely with the capacitance.

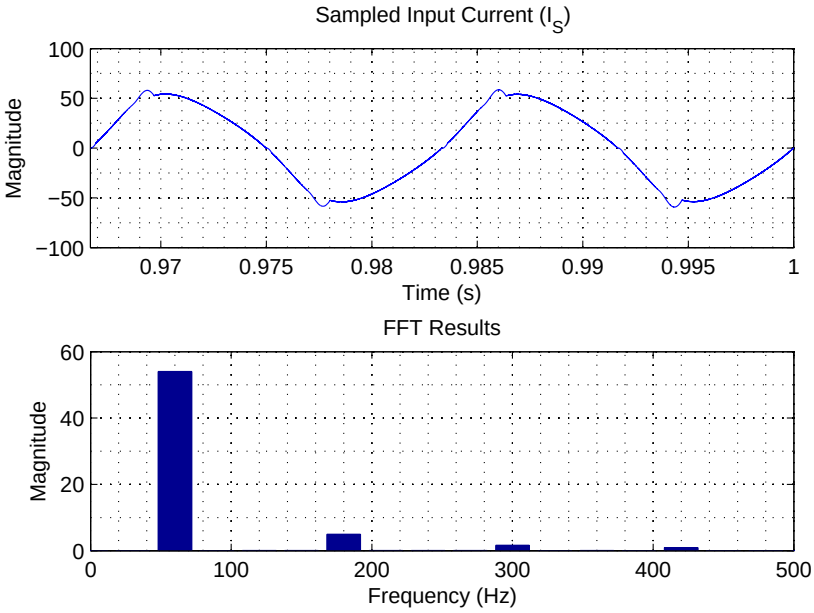

Figure 5.26. Input current waveform and FFT analysis for $C_1 = 500\,\mu F$.

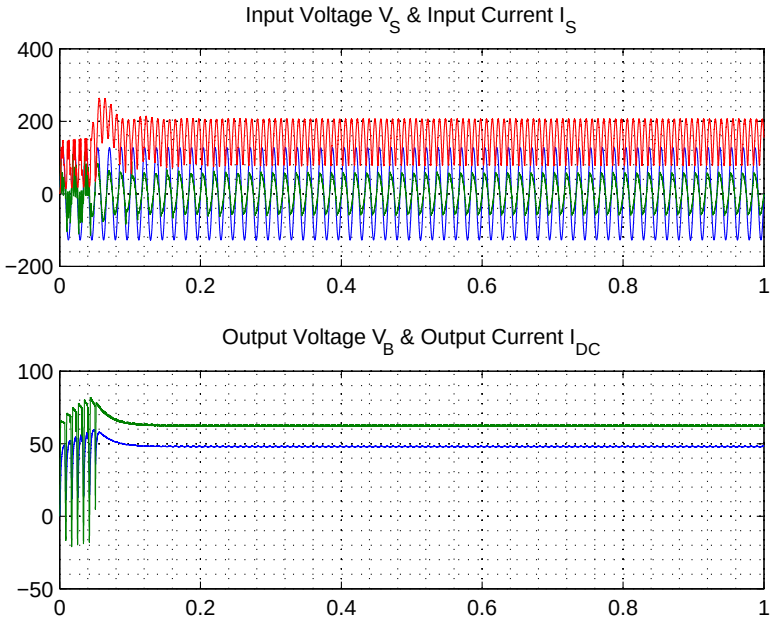

Figure 5.27. DC bus voltage and output current and voltage waveforms for $C_1 = 500\,\mu F$.

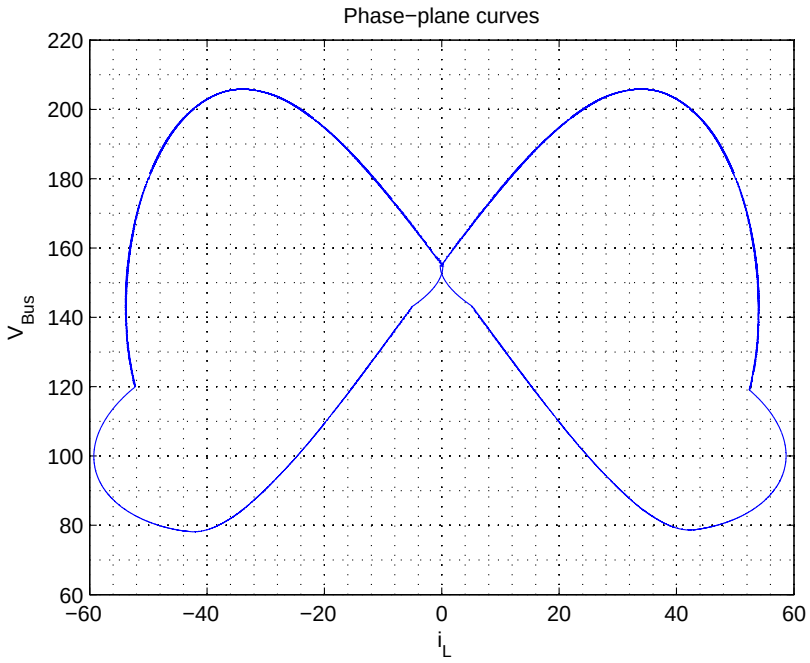

Figure 5.28. Phase plane trajectories for $C_1 = 500\,\mu F$.

5.2.2 Stability Analysis through Circuit Simulations II. Similar to section 5.2.1, stability analysis has been performed in this chapter and some considerations are done for the SimPower System circuit, which is now controlled by the True Digital controller. Circuit response and waveforms are here shown and a detailed comparison is made with respect to the analog PID controller. In particular, input inductor current, DC bus voltage and output current waveforms will be shown and eventual instability issues are commented and explained.

All simulations involve a battery charger circuit implemented with state space equations. They consider a digital feedback loop which uses the designed digital controller. On the other hand, the outer voltage control loop for the PFC boost rectifier still remains a PI controller. Its parameters need to be readjusted with respect to the previous design. $90\,Vrms$ input voltage at the line frequency of $60\,Hz$ is examined, varying one parameter value at a time and showing unstable behaviors.

As a consequence of the digital control structure, a general robustness and better performances are recorded in this case, showing the advantages of this relatively new and simple control technique. Unstable phenomena, even if always present, are usually less strong and are visible only for larger variations in the parameters. All these features of the new control loop will be further discussed in the following paragraphs.

5.2.2.1 Variation of Load Resistor Value. The first set of simulation regards the variation of the equivalent resistor load R_{out} at the output port. Battery voltage has to remain constant and therefore the value of output current reference changes also affecting the power drawn from the circuit.

Stable case corresponds to the nominal value of $R_{out} = 0.768\,\Omega$ and a nominal $3kW$ of power. It shows the desired behavior for the circuit waveforms. In particular, figures 5.30 and 5.29 show that system stability is related to the perfect symmetry of the phase plane plot (figure 5.31), a stable DC voltage and a flat output waveform of current and voltage. Performance of the converters is better than the one described in previous section, both in terms of stability and settling time. In particular, amplitude of the oscillations in the DC bus voltage is less and therefore the settling time is reduced. Also waveforms of output current and voltage have a very short rising time without the oscillations that were present in previous situation. Input inductor current is shaped by the sliding mode controller and results in a perfect sine wave with no high frequency harmonics, as shown in figure 5.29 from the FFT analysis.

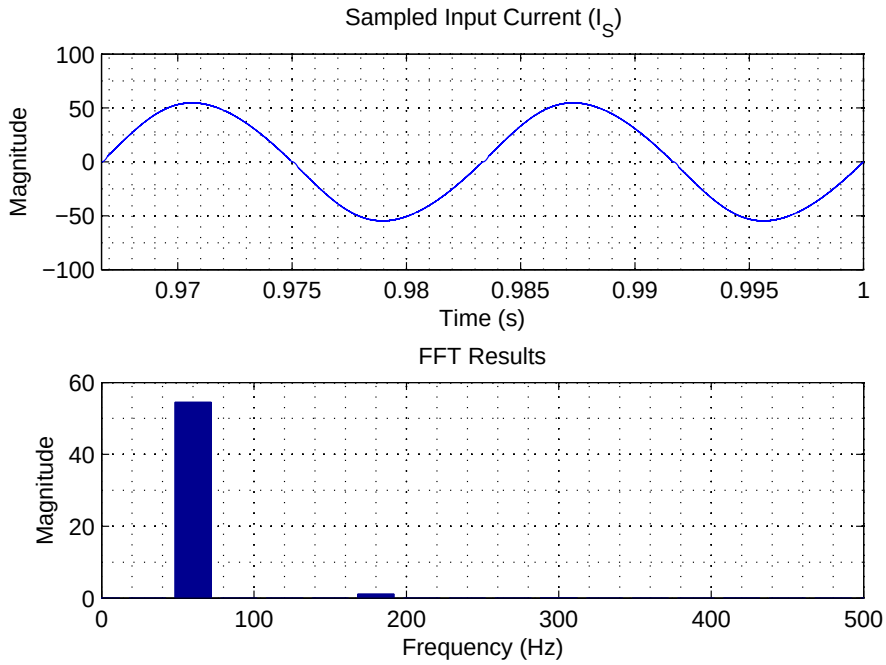

Figure 5.29. Stable mode of operation seen in the sinusoidal input current.

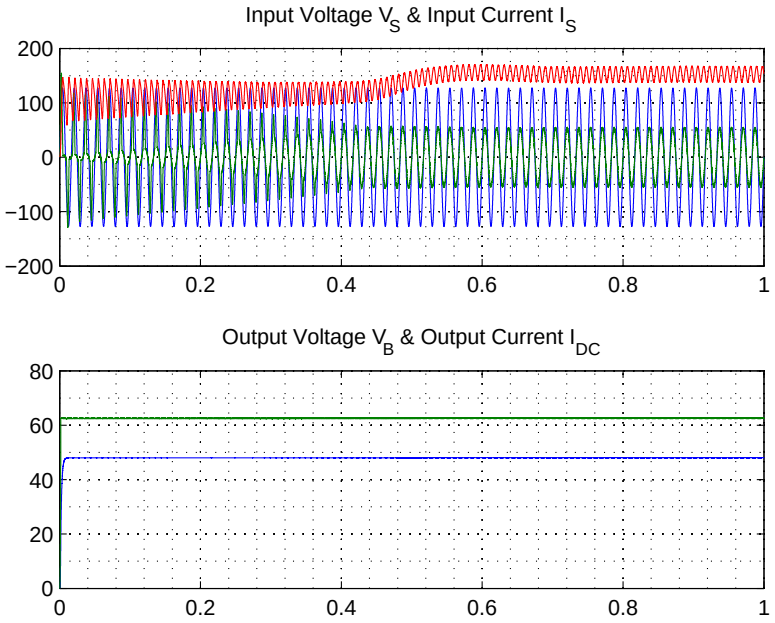

Figure 5.30. Stable mode of operation seen in the DC bus voltage and output current and voltage waveforms.

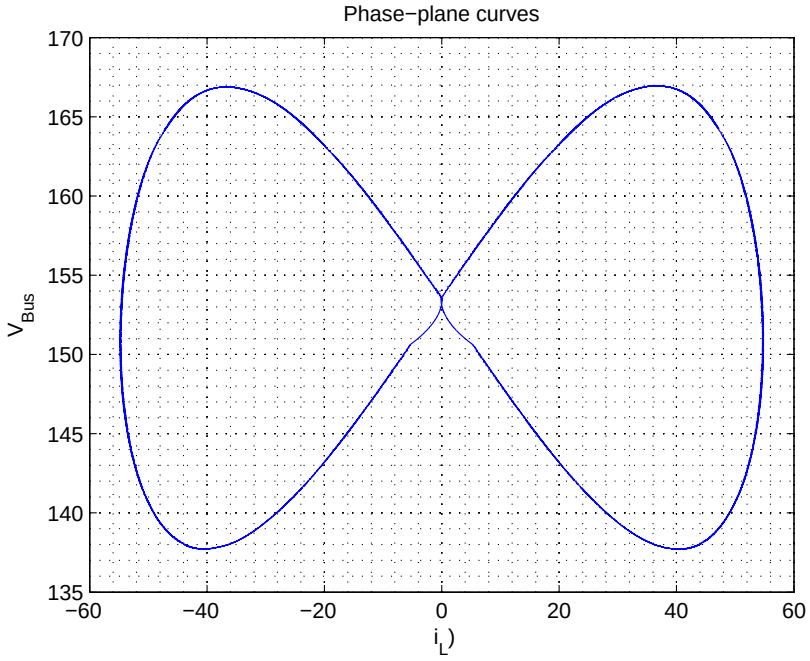

Figure 5.31. Stable mode of operation seen in the DC bus voltage and output current and voltage waveforms.

An increase in the load resistor and a reduction in the current value and power drawn will not lead to instabilities, as can be seen in figures 5.33, 5.32, and 5.34. On the other hand, unstable phenomena can be seen when lighter loads and therefore higher rated power is applied.

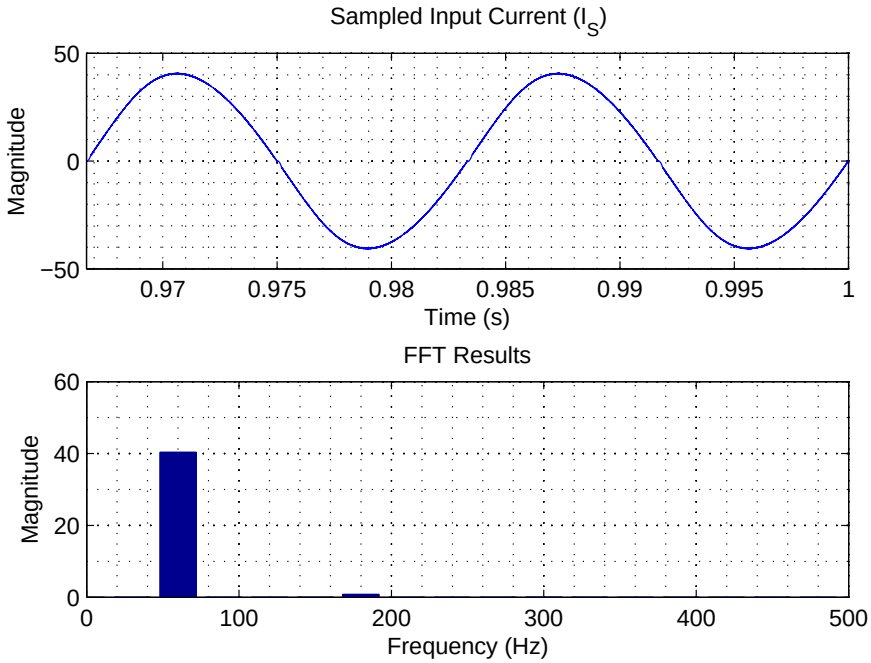

Figure 5.32. Input current waveform and FFT analysis for $R_{out} = 1\,\Omega$.

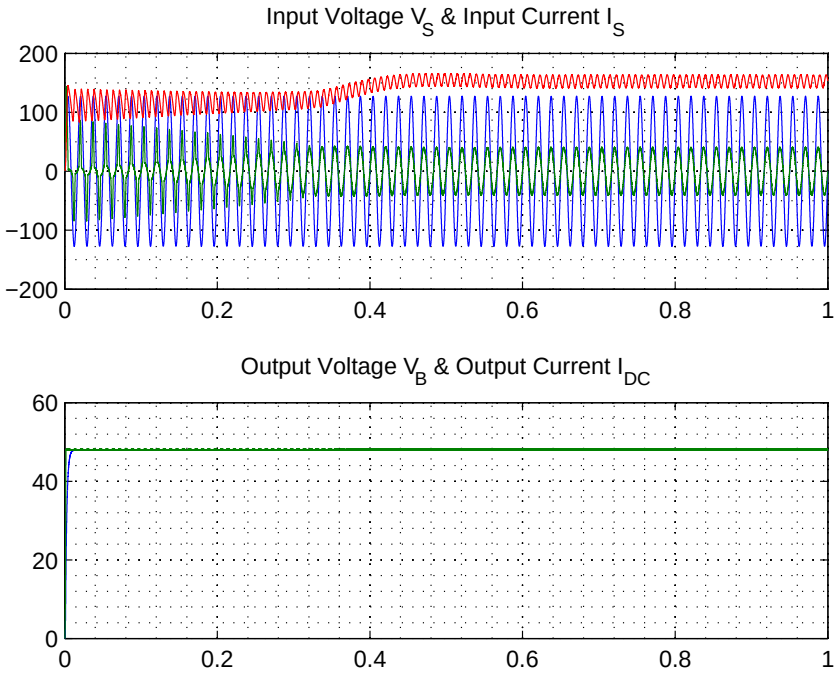

Figure 5.33. DC bus voltage and output current and voltage waveforms for $R_{out} = 1\Omega$.

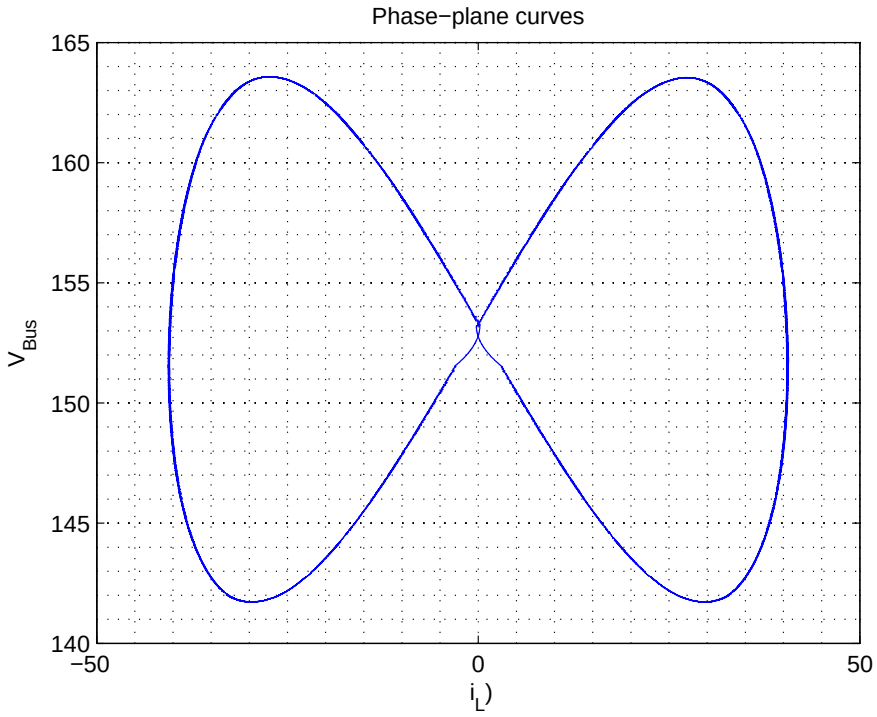

Figure 5.34. Phase plane trajectories for $R_{out} = 1\,\Omega$.

For a lower value of the output resistor, doubling effect and visible oscillations start characterizing the input inductor current and DC bus voltage waveforms respectively (figures 5.35 and 5.36). Oscillations present in the DC bus voltage will cause a non-symmetrical phase-plane curve (fig. 5.37), also for small decrease of the resistor load. Cusp distortion phenomena can be seen in the sinusoidal current waveform, which will show also higher frequency harmonics.

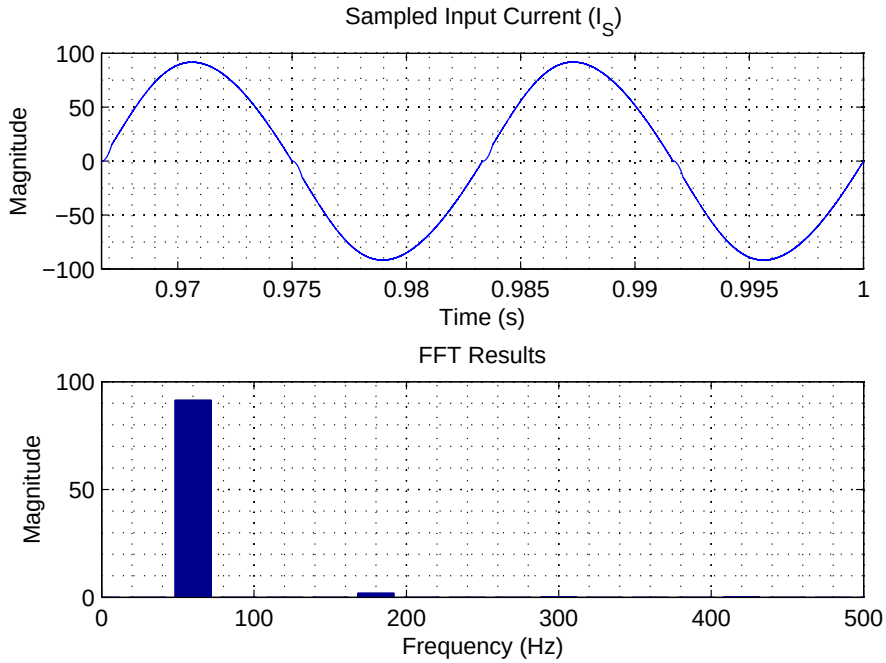

Figure 5.35. Input current waveform and FFT analysis for $R_{out} = 0.5\,\Omega$.

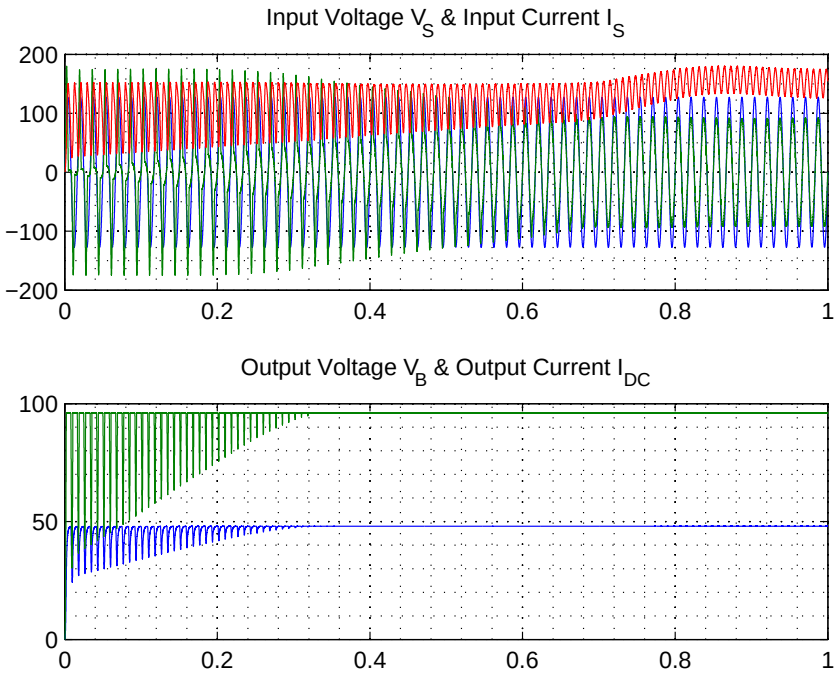

Figure 5.36. DC bus voltage and output current and voltage waveforms for $R_{out} = 0.5\,\Omega$.

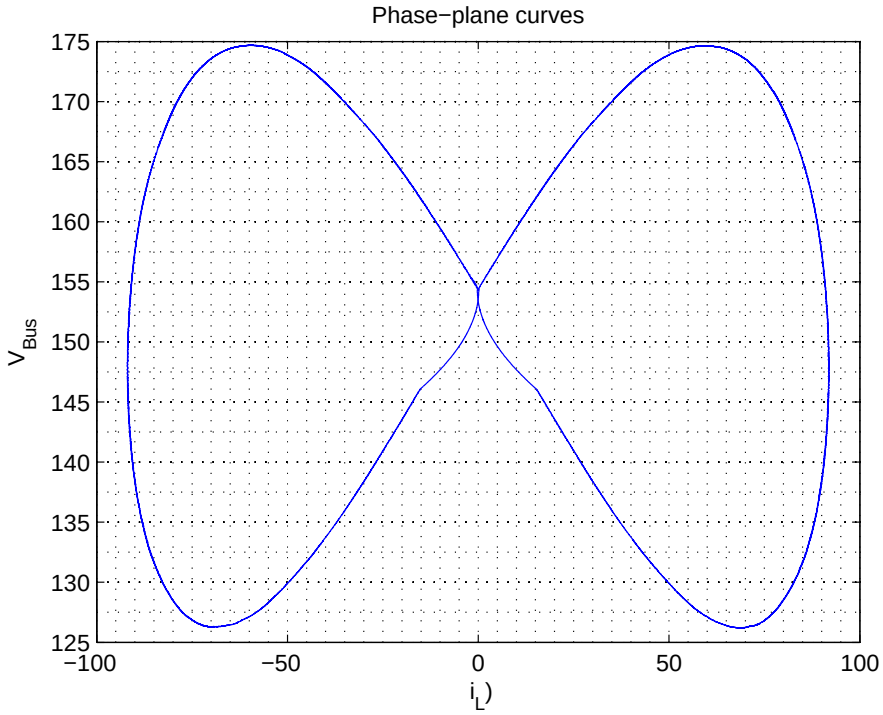

Figure 5.37. Phase plane trajectories for $R_{out} = 0.5\,\Omega$.

Large oscillations are present in the output current and voltage waveforms, which settling time will increase as the parameter value decreases. In particular, for a variation of around -40%, the sinusoidal input current remains stable and the system only requires longer time to reach the steady-state. For higher variations instead, highly asymmetrical phase-plane plots can be seen (figure 5.40). It will also show a more visible cusp distortion in the sinusoidal waveform (fig. 5.38) and higher oscillations for the DC bus voltage (fig. 5.39).

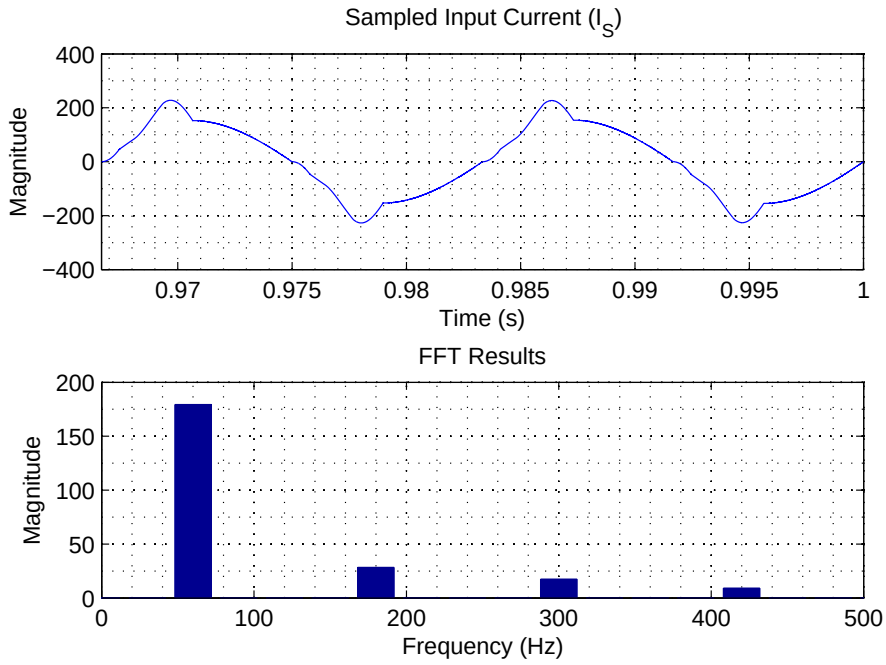

Figure 5.38. Input current waveform and FFT analysis for $R_{out} = 0.3\,\Omega$.

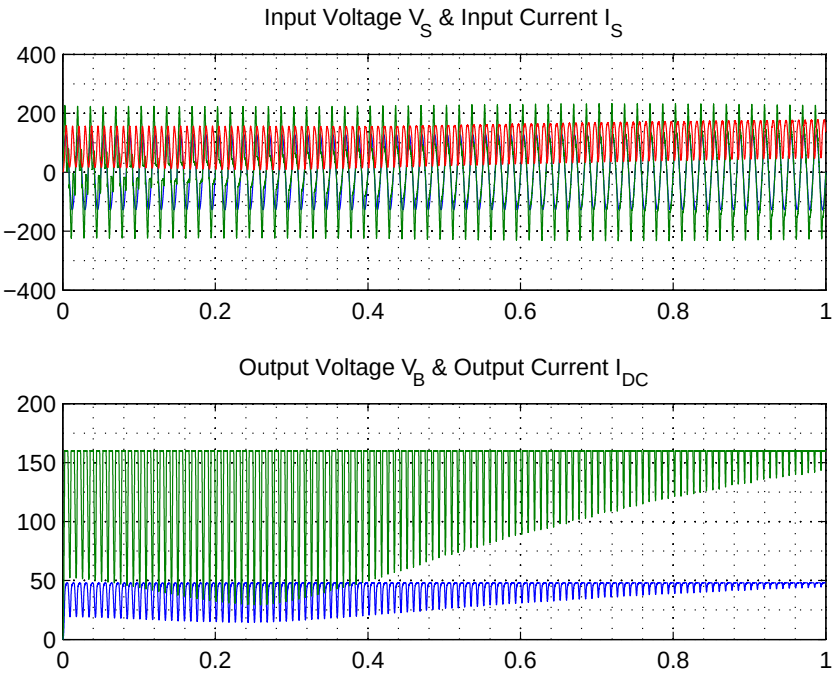

Figure 5.39. DC bus voltage and output current and voltage waveforms for $R_{out} = 0.3\,\Omega$.

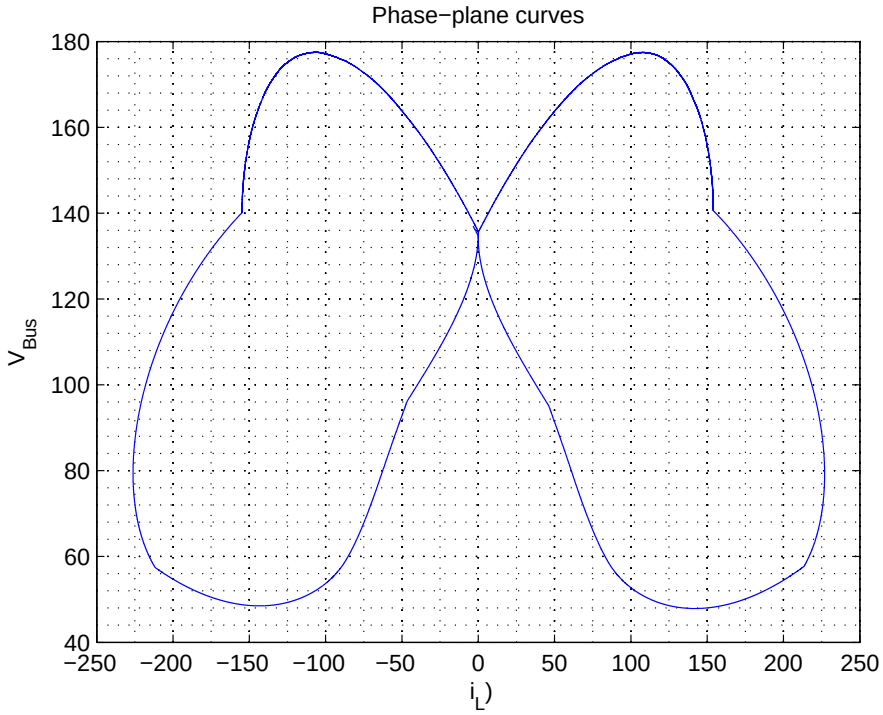

Figure 5.40. Phase plane trajectories for $R_{out} = 0.3\,\Omega$.

5.2.2.2 Variation of Input Inductor Value. Another important parameter in terms of the stability of the system is the input inductor. It largely affects the response of the power factor correction circuit. Instability conditions and boundaries are detected analyzing the phase plane plots and some key waveforms of the circuit simulated in MATLAB® Simulink.

Chosen optimal value of $300\,mH$ is varied as before from $50\,mH$ to $1000\,mH$ nominal values, while other components are maintained constant. Instability issues are present for variations in both directions and lead to different phenomena which anyway result to be less evident than the PI-controlled circuit analyzed before.

A decrease in the inductor value will still maintain a relatively stable behavior, as shown in pictures for a variation of around -80% with respect to the original value. A small ripple is present in the inductor current as can be seen from the picture 5.41. Phase-plane curve (fig. 5.43), even if it is still symmetrical with respect to both axes, shows some ripple which becomes more visible for further variations. On the other hand, even for small values of the inductor, no visible effect of instability can be seen in DC bus voltage waveform, due to the effectiveness of the digital controller which also guarantee a very smooth output current and voltage waveforms like those shown in figures 5.42.

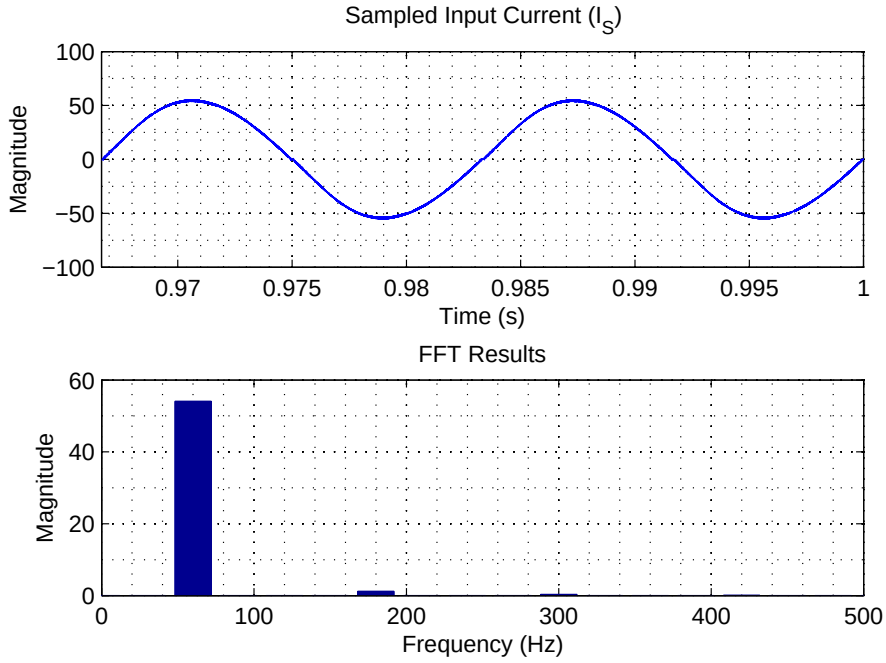

Figure 5.41. Input current waveform and FFT analysis for $L_1 = 50\,\mu H$.

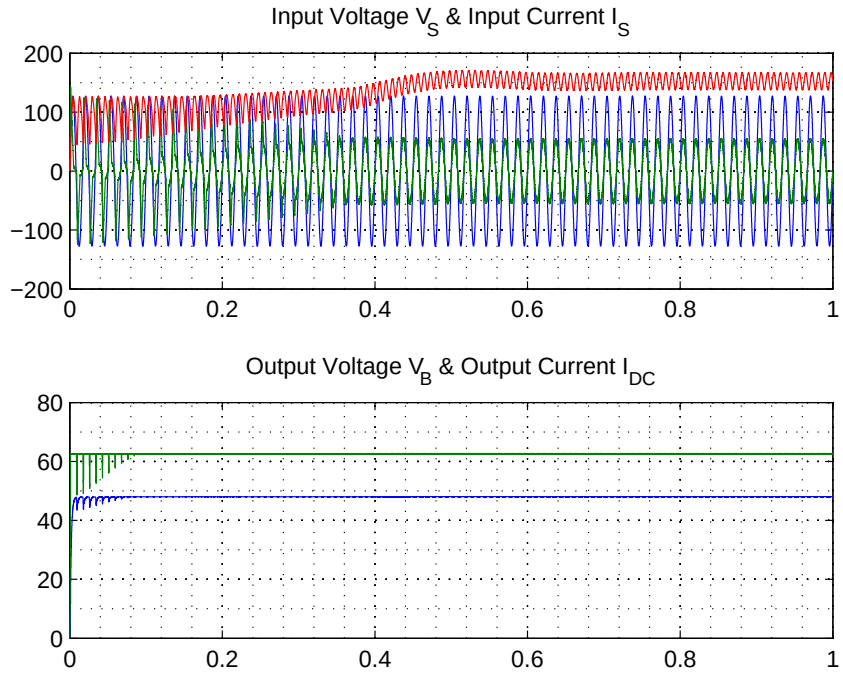

Figure 5.42. DC bus voltage and output current and voltage waveforms for $L_1 = 50\,\mu H$.

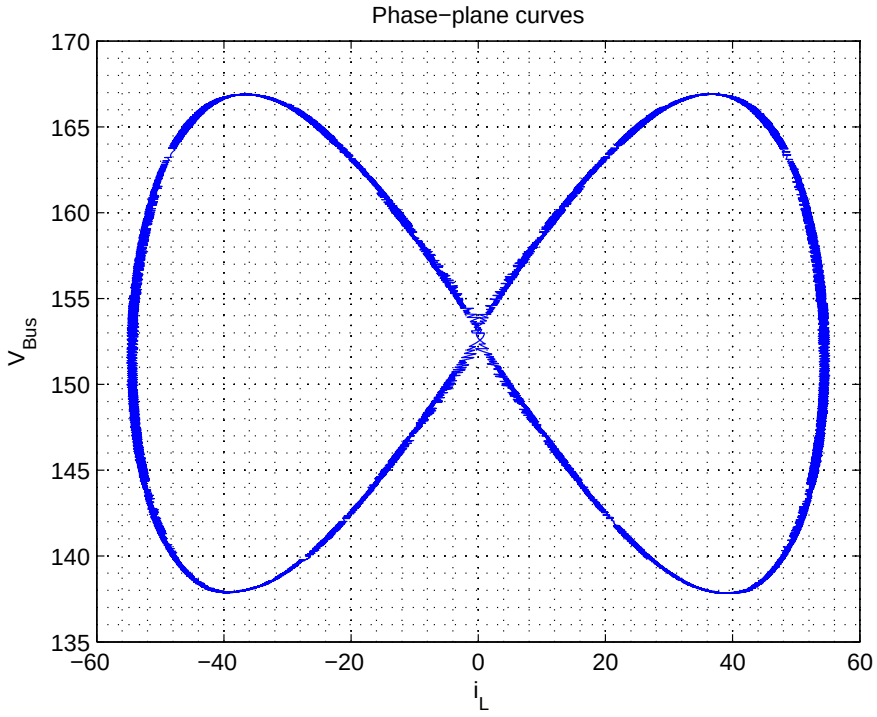

Figure 5.43. Phase plane trajectories for $L_1 = 50\,\mu H$.

If the input inductor value is increased, the bifurcation phenomena can be recognized, together with the cusp distortion problem in the sinusoidal current. DC bus voltage remains almost unmodified showing a slight increase in the ripple and therefore in the settling time (figure 5.45). Most visible effect is the shape of the inductor current and the phase-plane curves. In particular, Lissajous curves start showing a non-symmetrical response with a variation of around 100%. A deformation in the lower part of the plot, that becomes asymmetrical with respect to the horizontal axis, can be recognized in figure 5.46. This effect is mainly due to the presence of the cusp distortion in correspondence of the zero crossing point of the curve. That introduces some high frequency harmonic contents, as can be seen in figure 5.44. Once again, the noticed instability phenomenon is less evident due to the better performance of the digital control loop.

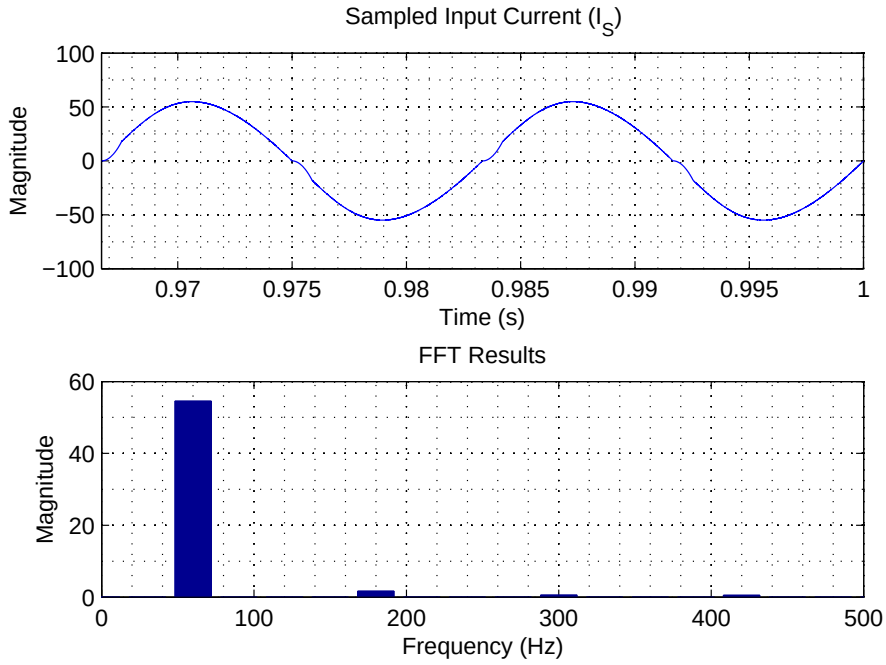

Figure 5.44. Input current waveform and FFT analysis for $L_1 = 1000\,\mu H$.

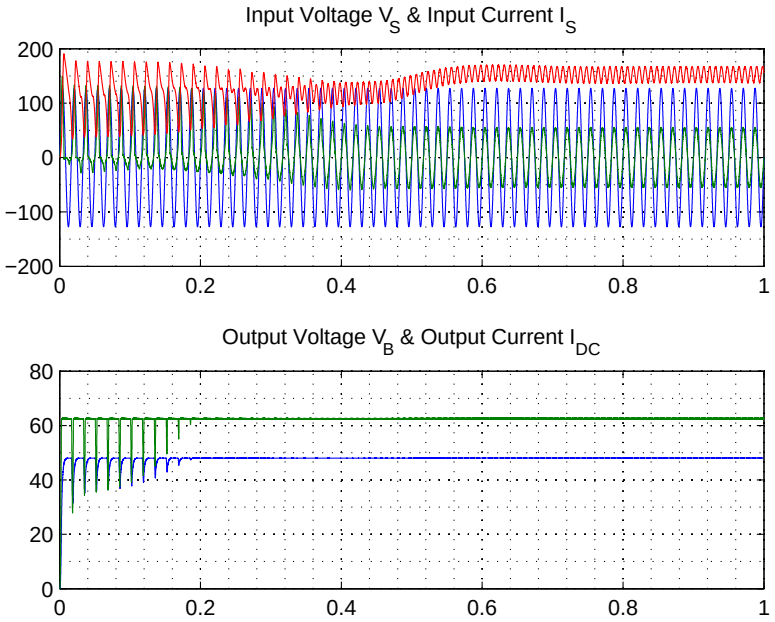

Figure 5.45. DC bus voltage and output current and voltage waveforms for $L_1 = 1000\,\mu H$.

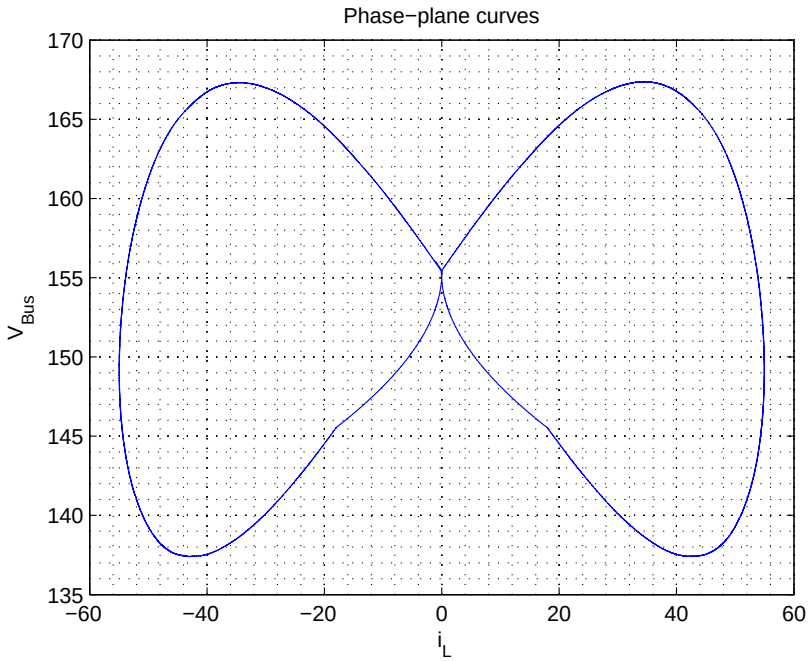

Figure 5.46. Phase plane trajectories for $L_1 = 1000\,\mu H$.

5.2.2.3 Variation of DC Bus Capacitor Value. This subsection presents simulation results and comments to show the effects of the variation in the DC bus capacitor value, with respect to the stability of the system. From a nominal value of $2000\,\mu F$, an increase of the parameter up to 100% and a decrease of -75% will show the presence of evident instability.

In correspondence to a decrease of the DC capacitor value an increase in the ripple in the DC bus voltage can be easily seen in figure 5.48 and it is due to the minor filtering effect of the capacitor. Even if for small variations the system remains stable, quite high oscillations are present in both DC bus voltage waveform and DC outputs. On the other hand, their amplitude is smaller with respect to the standard PID controlled system. Main instability issue is registered for the input inductor current waveform. High frequency harmonics and especially the third harmonic can be seen in both the sinusoidal waveform and the FFT analysis of figure 5.47. Similarly, due to this instability phenomena, the phase-plane curve results to be highly asymmetrical, highlighting the poor power factor correction result (fig. 5.49).

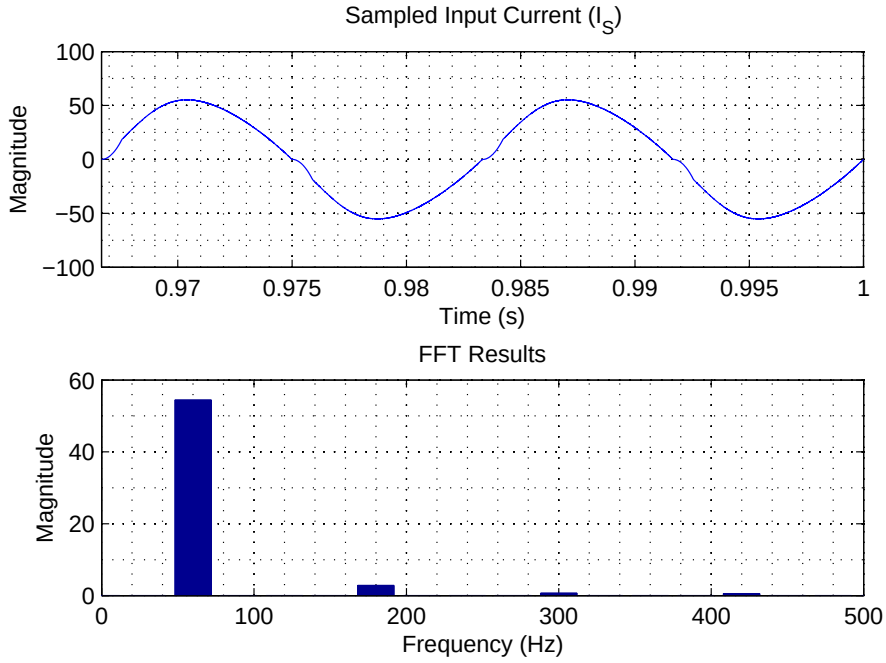

Figure 5.47. Input current waveform and FFT analysis for $C_1 = 1000\,\mu F$.

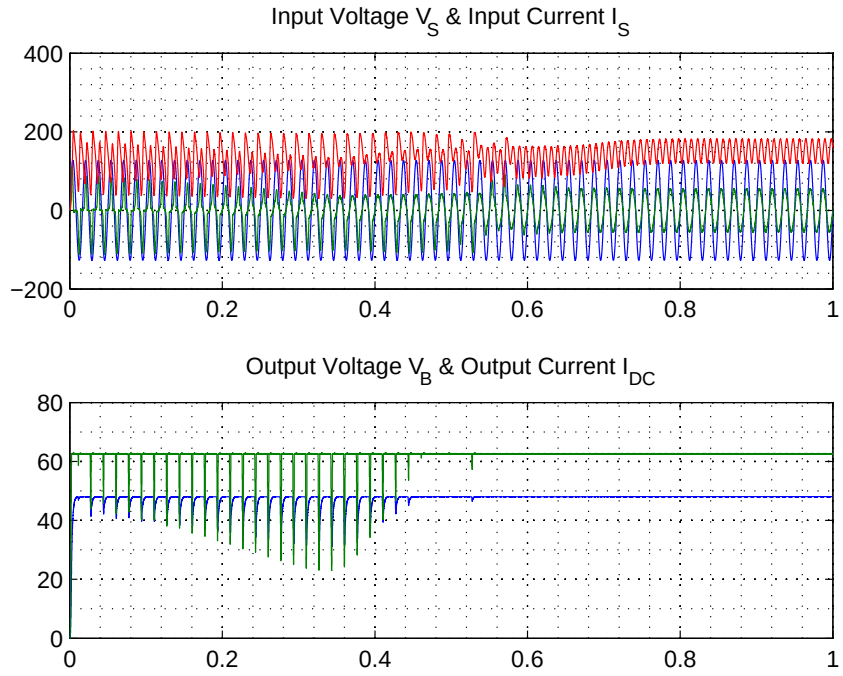

Figure 5.48. DC bus voltage and output current and voltage waveforms for $C_1 = 1000\,\mu F$.

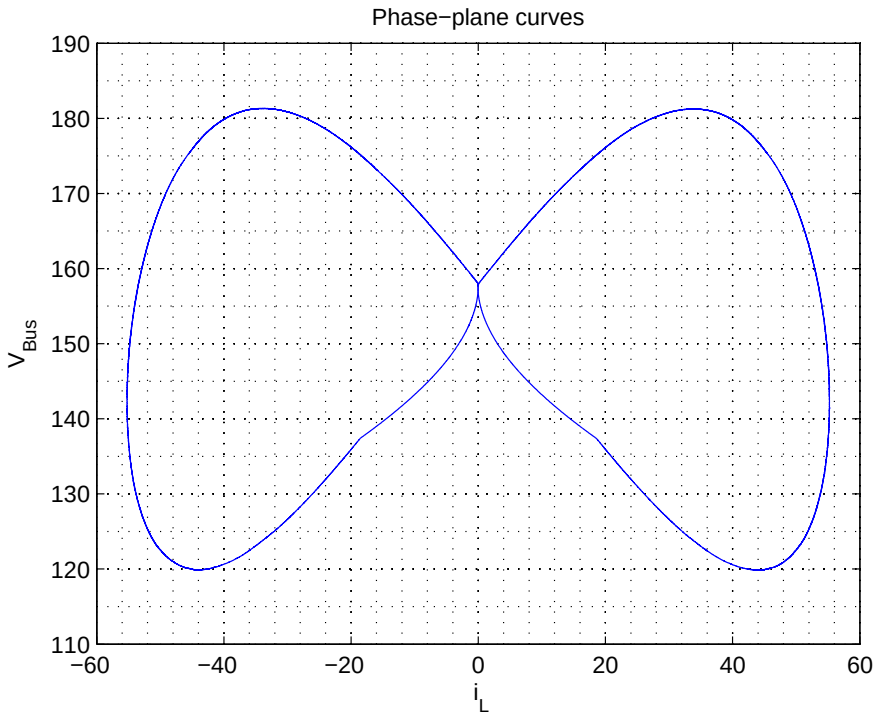

Figure 5.49. Phase plane trajectories for $C_1 = 1000\,\mu F$.

If the DC bus capacitor value is increased, no particular unstable phenomena can be seen, since it filtering effect only smoothes the DC bus voltage waveform. Primary issue in this situation is the size of the capacitor, which drastically increases with its value. Therefore it is chosen to be $2000\,\mu F$ as a compromise between satisfactory circuit response and its dimension and cost.

5.2.3 Cusp Distortion in Input Inductor Current. One of the most important indicators of unstable operation of a PFC converter is cusp distortion. It has been widely observed [21] that the input current in single-phase PFC converters almost always contains some residual distortions. In particular, the zero-crossing distortion is considered one of the primary issues for the meeting of regulatory requirements in mid-high power applications with $50 - 60\,Hz$ input.

High performance is required for power factor correction circuits owing to stringent current harmonics emission limits. Distortion effect increases significantly at higher frequencies and is a crucial aspect in PFC design and control.

Cusp distortion occurs right after the zero-crossing point of the sinusoidal input current waveform. In this situation a very limited voltage can be seen across the boost inductor, and a very high current is required. As a result, the inductor current may not be able to shape the line current which therefore develops distortion. Effect of cusp distortion and thus harmonic content of input current increases with increase in the value of the inductor. It must be noted that discontinuous inductor current or very small amplitude does not necessarily imply the presence of low-frequency input current distortion, especially when the switching frequency is much higher than the line. Rather, the low gain of the current loop controller deteriorates the input current response.

Rigorous mathematical analysis has been done in order to determine the magnitude and the duration of the cusp distortion. In particular in [34], the dependence of the phenomena on circuit parameters is shown. In this context, an alternative control method has been developed to compensate the distortion issue.

On the contrary, for battery charger circuit purposes obtained results are satisfactory. Even if a small cusp distortion is present in the input current, as shown

in figure 5.50, with a precise tuning of the parameters of the controller and proper circuit design, the problem can be minimized.

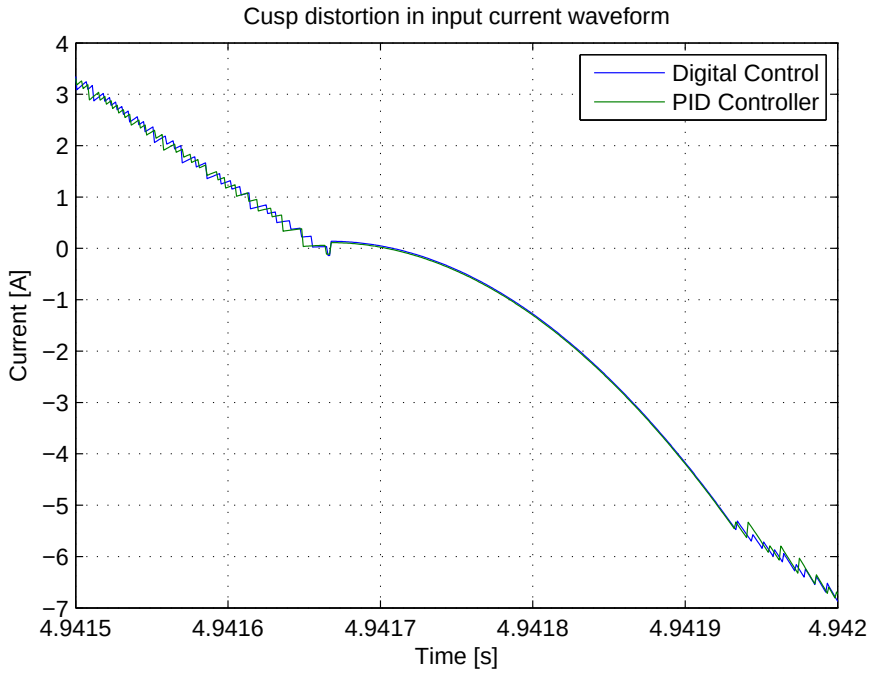

Figure 5.50. Cusp distortion detail in the sinusoidal input current.

As can be seen from previous analysis and simulation results, the phenomenon of cusp distortion constitutes an important element in the performance of the circuit. In particular, the presence of the distortion in the current waveforms comes along with the introduction of higher harmonics in the sinusoidal shape.

In PFC circuits, input current distortion is mainly due to the $3rd$ harmonic arising from two sources. Input current might fail to track perfectly with the sine wave reference signal inside the current control loop. Second disturbance source is given by the second harmonic coming from the DC bus voltage and from the feed-forward voltage.

Input inductor current behavior can therefore be analyzed in terms of cusp distortion providing further stability and performance considerations. Small inductor

choice is also based on the distortion phenomena. Final inductor value is chosen as a trade-off between the presence of the cusp distortion and the higher ripple obtained in the current.

CHAPTER 6

CONCLUSION

Importance of Hybrid Electric Vehicles and Plug-in Electric Vehicles has been growing over the last decades and as a result, these areas have received significant interest. From the power electronics point of view, the power chain has two circuits that have to be designed- the rectifier and the DC/DC converter. The cascaded bi-directional configuration of an AC/DC rectifier with power factor correction and a DC/DC converter is an efficient interfacing circuit that connects the energy storage device of the PHEV to the grid.

The main objective of this research has been to develop an new integrated control strategy using the digital control approach. The motivation for choosing this control strategy was to simplify the hardware structure, reduce complexity of the control algorithm as well as enhance the overall operation of the system.

This thesis describes a simplified version of the multi-loop control for the PFC circuit and the DC/DC converter. It is developed based on the concept of a truly digital control with a fixed switching frequency. Performance of the novel regulator has been verified with respect to standard PID control loop. A complete stability analysis is done to verify the robustness of the system and to identify major stability issues. Operating boundaries are identified investigating various functioning conditions. The design of critical components of the circuit is therefore modified according to obtained results.

Its operating mode is simulated and results are discussed. A complete stability analysis is done to verify the robustness of the system and to identify major stability issues. Operating boundaries are identified investigating various functioning conditions. The design of critical components of the circuit is therefore modified according

to obtained results.

Simulation results indicate that proposed design not only reduces the complexity of the controller but also improve the transient response. Stability and performance of the system, on the other hand, are comparable to the equivalent analog control structure.

CHAPTER 7

FUTURE WORKS

Future works in this area include further simplification of the controller structure for the PFC circuit. Its multi-loop structure can be modified according to recent developments. Inner voltage regulator can be erased and substituted with a sensorless structure. The ripple present in the DC voltage at twice line frequency can also be minimized by using an enhanced control algorithm. Furthermore, digital filtering and other complex control structures can be used to eliminate AC residue in the bus voltage.

Sensor-less controller might be designed in order to further simplify the structure of the circuit. Number of sensors required will also decrease. Soft-switching algorithms can be implemented for the control structure. Performances of the circuit will drastically improve, even if a more complex control section will be required. Future works will consider also a real implementation of the circuit and of the controller. True digital control technique will be implemented in a micro controller and performances of the circuit will be verified. Actual battery charger behavior can be simulated considering State Of Charge of the storage pack, as well as a non-constant voltage.

Important research can be done also in the power electronics field. Bi-directional functioning of the battery charger has to be verified for all possible voltage range. Reverse power flow will need therefore a different DC/DC converter design to accommodate the high voltage step for high input voltages. Practical considerations have been done regarding the boost functioning mode. Voltage boost from the low battery voltage level is not feasible in practice. Therefore an alternative design has to be considered. Electrical isolation can be implemented in this application, with the advantage of an easy step-up of the voltage with a transformer. New bi-directional

isolated converter topology can be designed and investigated for this application.

APPENDIX A

CIRCUIT AND CONTROLLER PARAMETERS

Table A.1. Values of the parameters for the circuit components.

Component	Symbol	Value
Input Inductor	L_1	$300\,\mu H$
Input Inductor Straw Resistor	R_{L_41}	$0.02\,\Omega$
DC Bus Capacitor	C_1	$2000\,\mu F$
DC Bus Capacitor Straw Resistor	R_{C_1}	$0.2\,\Omega$
Diode ON Resistor	R_D	$0.01\,\Omega$
Switch ON Resistor	R_S	$0.01\,\Omega$
Output Inductor	L_2	$100\,\mu H$
Output Inductor Straw Resistor	R_{L_2}	$0.02\,\Omega$
Output Capacitor	C_2	$1500\,\mu F$
Output Capacitor Straw Resistor	R_{C_2}	$0.2\,\Omega$
Output Resistor	R_{out}	$0.768\,\Omega$

Table A.2. Values of the parameters for the controller gains.

Parameter	Symbol	Value
Current Controller for PWM Rectifier		
Proportional Gain	P_1	0.025
Integral Gain	I_1	5
Voltage Controller for PWM Rectifier		
Proportional Gain	P_2	200
Integral Gain	I_2	100000
Feed-Forward Controller for PWM Rectifier		
Proportional Gain	P_4	2.2
Integral Gain	I_4	0
Current Controller for DC/DC Converter		
Proportional Gain	P_3	100
Integral Gain	I_3	5000
Voltage Controller for DC/AC Inverter		
Proportional Gain	P	15
Integral Gain	I	5
Voltage Controller for PWM Rectifier Hybrid Loop		
Proportional Gain	P_1	0.15
Integral Gain	I_1	50

BIBLIOGRAPHY

[1] Bhaskar, K., and D. Czarkowski. 'Bidirectional Buck-Boost Converter with Variable Output.' *IEEE.* (1998).

[2] Biel, D., F. Guinjoan, E. Fossas, and J. Chavarria. 'Sliding-Mode Control Design of a Boost-Buck Switching Converter for AC Signal Generation.' *IEEE Transactions on Circuits and Systems - I: Regular Papers.* 51.8 (August 2004): 1439-1551.

[3] Bilgin, B., A. Emadi, and M. Krishnamurthy. 'Design Considerations for a Universal Input Battery Charger Circuit for PHEV Applications.' *IEEE paper draft.* (2010).

[4] Buso, S., P. Mattavelli, L. Rossetto, and G. Spiazzi. 'Simple Digital Control Improving Dynamic Performance of Power Factor Preregulators.' *IEEE Transaction on Power Electronics.* 13.5 (September 1998): 814-823.

[5] Chu, G., T. Siew-Chong, C. K. Tse, and W. S. Chung. 'General Control for Boost PFC Converter from a Sliding Mode Viewpoint.' *IEEE.* (2008): 4452-4456.

[6] Clare, J., 'High Power Factor Rectifier Circuits.' *The University of Nottingham, School of Electrical and Electronics Engineering.* (November 2003).

[7] Dixon, L., 'Average Current Mode Control of Switching Power Supplies.' *Unitrode Application Note.* 356-369.

[8] Dong, D., S. Li, X. Ma, and C. T. Tse. 'Slow-Scale Instability of Single-Stage Power-Factor-Coorection Power Supplies.' *IEEE Transactions on Circuits and Systems - I: Regular Papers.* 54.8 (August 2007): 1724-1735.

[9] Dranga, O., C. K. Tse, and W. S. Chung. 'Stability Analysis of Complete Two-Stage Power-Factor-Correction Power Supplies.' *IEEE.*

[10] Duvall, M. S., 'Battery Evaluation for Plug-In Hybrid Electric Vehicles.' *IEEE.* (2005): 338-343.

[11] Fanghua, Z., and Y. Yan. 'Novel Forward-Flyback Hybrid Bidirectional DC/DC Converter.' *IEEE TRANSACTIONS ON INDUSTRIAL ELECTRONICS.* (May 2009).

[12] Giri, V., and D. M. Divan. 'Discrete Time Integral Sliding Mode Control for Discrete Pulse Modulated Converters.' *IEEE.* (1990): 67-73.

[13] Grace, C., Siew-Chong Tan, Chi K. Tse, and S. C. Wong. 'General Control for Boost PFC Converter from a Sliding Mode Viewpoint.' *IEEE.* (2008): 4452-4456.

[14] Grace, C., C. K. Tse, and S. C. Wong. 'A Model for Stability of PFC Power Supplies.' *IEEE.* (2007): 1298-1303.

[15] Grace, C., C. K. Tse, and S. C. Wong. 'Line-Frequency Instability of PFC Power Supplies.' *IEEE Transactions on Power Electronics.* 24.2 (February 2009): 469-482.

[16] Hasan, K. N., M. E. Haque, M. Negnevitsky, and K. M. Muttaqi. 'Control of Energy Storage Interface with a Bidirectional Converter for Photovoltaic Systems.' *AUPEC '08.* (2008).

[17] He, Y., X. Weisheng, and W. Hongrun. 'Sliding Mode Control of Single-Phase AC-DC Boost Converter Using Time-Varying Sliding Surface.' *International Conference on Intelligent Computation Technology and Automation.* (2008): 484-487.

[18] Herbert, H. C. I., Y. Zhou, and C. K. Tse. 'Fast Scale Instability in a PFC Boost Converter Under Average Current-Mode Control.' *International Journal of Circuit Theory and Applications.* (April 2003): 611-624.

[19] Horea, B. I., I. Ciocan, and S. Lungu. 'Modeling Transfer Function for Buck Power Converter.' *IEEE* 30^{th} *ISSE.* (2007): 541-544.

[20] Ji, W., A. Emadi, M. J. Duoba, and T. P. Bohn. 'Plug-in Hybrid Electric Vehicles: Testing, Simulations and Analysis.' *IEEE.* (2007): 469-476.

[21] Jian, S., 'On the Zero-Crossing Distrortion in Single-Phase PFC Converters.' *IEEE Transactions on Power Electronics.* 19.3 (May 2004): 685-692.

[22] Jian-ming, H., C. Yuan-rui, and Y. Zi-juan. 'Study and Simulation of One Bi-directional DC/DC Converter in Hybrid Electric Vehicle.' 3^{rd} *International Conference on Power Electronics Systems and Applications.* (2009).

[23] Jianhua, G., C. Zhang, and C. Luo. 'Research of a PWM-Based New Sliding-Mode Controller for the BUCK Converter.' *Second IEEE Conference on Industrial Electronics and Applications.*(2007): 1907-1911.

[24] Khaligh, A., and A. Emadi. 'Pulse Adjustment, a Novel Digital Control Technique, for Control of a DC-DC Buck-Boost Converter Operating in Discontinuous Conduction Mode and Driving Constant Power Loads.' *IEEE.* (2006).

[25] Kroeze, R. C., and P. T. Krein. 'Electrical Battery Model for Use in Dynamic Electric Vehicle Simulations.' *IEEE.*(2008): 1336-1342.

[26] Le Bunetel, J. C., and M. Machmoum. 'Control of Boost Unity Power Factor Correction System.' *IEEE.* (1999).

[27] Liang-Rui, C., C. Neng-Yi, W. Chau-Shing, and L. Ruey-Hsun. 'Design of a Reflex-Based Bidirectional Converter With the Energy Recovery Function.' *IEEE TRANSACTIONS ON INDUSTRIAL ELECTRONICS.* (August 2008).

[28] Martin, C. H. L., C. T. Tse, and L. Yim-Shu. 'A Novel Method for Elimination of Line-Current Harmonics in Single-Stage PFC Switching Regulators.' *IEEE Transaction on Power Electronics.* 13.1 (January 1998): 75-83.

[29] Mehrdad, E., G. Yimin, and J. M. Miller. 'Hybrid Electric Vehicles: Architecture and Motor Drives.' *Proceedings of the IEEE.* (Apr 2007): 719-728.

[30] Miaosen, S., and P. Fang Zheng. 'Converter Systems for Hybrid Electric Vehicles.' *Proceeding of International Conference on Electrical Machines and Systems.* Seoul, Korea (October 2007): 2004-2010.

[31] Middlebrook, R. D., and S. Ćuk. 'A general unified approach to modelling switching-converter power stages.' *IEEE Power Electronic Specialists Conference*. Cleveland, OH. (June 1976): 73-86.

[32] Mikkel, H. C. W., and M. A. E. Andersen. 'Accurate Sliding-Mode Control System Modeling for Buck Converters.' *IEEE*.

[33] Nasiri, A., and A. Emadi. 'Full Digital Control of a Single-Phase Series-Parallel Uninterruptable Power Supply.' *IEEE*. (2004): 443-449.

[34] Natarajan, K., and S. Sivakumar. 'Control of Cusp Distortion in Power Factor Correcting Boost Converter.' *IEEE CCECE '97*. (1997): 650-653.

[35] Nilanga, S. D., and L. D. Dah-Chuan. 'Novel Implementation of Average Current Mode Controlled Power-Factor-Correction Converters.' *Second IEEE Conference on Industrial Electronics and Applications*. (2007): 1468-1472.

[36] Nilkamal, F., and R. T. H. Alden. 'Domain of Stability of AC/DC Power Systems.' *IEEE CCECE 2004 - CCGEI 2004*. Niagara Falls (2004): 433-438.

[37] Olayiwola, A., B. Sock, M. R. Zolghadri, A. Homaifar, M. Walters, and C. Doss. 'Digital Controller for a Boost PFC Converter in Continuous Conduction Mode.' *IEEE ICIEA*. (2006).

[38] Omonowo, M. D., and M. O. Omoiguit. 'An Overwiev of Hybtid Electric Vehicle Technology.' *IEEE*. (2009): 1286-1292.

[39] Orabi, M., and T. Ninomiya. 'Analysis of PFC Converter Stability Using Energy Balance Theory.' *IEEE*. (2003): 544-549.

[40] Orabi, M., and T. Ninomiya. 'Stability Investigation of the Cascade Two-Stage PFC Converter.' *IEICE/IEEE INTELEC*. (October 2003): 565-572.

[41] Orabi, M., and T. Ninomiya. 'Nonlinear Dynamics of Power-Factor-Correction Converter.' *IEEE Transactions on Industrial Electronics*. 50.6 (December 2003): 1116-1125.

[42] Orabi, M., and T. Ninomiya. 'A Simple Criterion to Judge PFC Converter Stability.' *IEEE*. (2003): 260-263.

[43] Orabi, M., and T. Ninomiya. 'A Unified Design of Single-Stage and Two-Stage PFC Converter.' *IEEE*. 2003): 1720-1725.

[44] Orabi, M., and T. Ninomiya. 'An Optimum Design of Boost Power-Factor-Correction Converter.' *IEEE*. (2003): 735-740.

[45] Orabi, M., and Ninomiya. 'Numerical and Experimental Study of Instability Phenomena of a Boost PFC Converter.' *IEEE ICIT*. Maribor, Slovenia (2003): 854-859.

[46] Orabi, M., T. Ninomiya, and C. Jin. 'A Novel Modeling of Instability Phenomena in PFC COnverter.' *IEEE*. (2002): 566-573.

[47] Orabi, M., T. Ninomiya, and C. Jin. 'Novel Developments in the Study of Nonlinear Phenomena in Power-Factor-Correction Circuits.' *IEEE*. (2002): 209-215.

[48] Orabi, M., T. Ninomiya, and C. Jin. 'Nonlinear Dynamics and Stability Analysis of Boost Power-Factor-Correction Circuit.' *IEEE.* (2002): 600-605.

[49] Orabi, M., T. Ninomiya, and C. Jin. 'New Formulation for Stability Analysis of Power Factor Correction Converters.' *IEEE.* (2002): 33-38.

[50] Pandey, A., D. P. Kothari, A. K. Mukerjee, and B. Singh. 'Modeling and simulation of power factor corrected AC/DC converters.' *International Journal of Electrical Engineering Education.* 253-254.

[51] Pepper, M., K. Mansfield, J. Elmes, K. Rustom, R. Kersten, M. Qahwash, and I. Bataresh. 'Bi-Directional DCM DC to DC Converter for Hybrid Electric Vehicles.' *IEEE.* (2008): 3088-3092.

[52] Piyush, C. D., and A. Emadi. 'A Novel Digital Control Technique for Brushless DC Motor Drives: Current Control.' *IEEE.* (2005): 326-331.

[53] Rim, C. T., G. B. Joung, and G. H. Cho. 'A State-Space modeling of non-ideal DC/DC converters.' *IEEE PESC RECORD.* (April 1988): 943-950.

[54] Rodriguez, F., and A. Emadi. 'A Novel Digital Control Technique for Brushless DC Motor Drives.' *IEEE Transaction on Industrial Electronics.* 54.5 (October 2007): 2365-2373.

[55] Rong-Jong, W., and D. Rou-Yong. 'High-Efficiency Bidirectional Converter for Power Sources With Great Voltage Diversity.' *IEEE TRANSACTIONS ON POWER ELECTRONICS.* (September 2007).

[56] Senanayake, T., and T. Ninomiya. 'An Improved Topology of Inductor Switching DC-DC Converter.' *IEEE.* (2003) :36-41.

[57] Shi, L., L. Meintz, and M. Ferdowsi. 'Single-Phase Bidirectional AC/DC Converters for Plug-in Hybrid Electric Vehicle Applications.' *IEEE Vehicle Power and Propulsion Conference (VPCC).* Harbin, China (September 2008).

[58] Siu, K. W., Y. S. Lee, and C. K. Tse. 'Analysis and Experimental Evaluation of Single-Switch Fast-Resposnse Switching Regulators with Unity Power Factor.' *IEEE Transactions on Industry Applications.* 33.5 (September 1997): 1260-1266.

[59] Siu-Chung, W., C. T. Tse, M. Orabi and T. Ninomiya. 'The Method of Double Averaging: an Approach for Modeling Power-Factor-Correction Switching Converters.' *IEEE Transactions on Circuits and Systems - I: Regular Papers.* 53.2 (February 2006): 454-462.

[60] Srdjan, L. M., and A. Emadi, 'State Switching Digital Control Technique for Switched Reluctance Motor Drives.' *IEEE.* (2007): 1332-1337

[61] Stefanutti, W., P. Mattavelli, G. Spiazzi, and P. Tenti. 'Digital Control of Single-Phase Power Factor Preregulators Based on Current and Voltage Sensing at Switch Terminals.' *IEEE Transaction on Power Electronics.* 21.5 (September 2006): 1356-1363.

[62] Stihi, O., and O. Boon-Teck. 'A Single-Phase Controlled-Current PWM Rectifier.' *IEEE Transactions on Power Electronics.* 3.4 (October 1988): 453-456.

[63] Tao, H., A. Kotsopoulos, J. L. Duarte, and M. A. M. Hendrix. 'Family of multiport bidirectional DC/DC converters.' *The Institution of Engineering and Technology.* (May 2006).

[64] Todd, P. C., 'Controlled Power Factor Correction Circuit Design.' *Unitrode Application Note 3.* (1999): 269-288.

[65] Utkin, V. I., 'Sliding Mode Control Design Principles and Applications to Electric Drives.' *IEEE Transactions on Industrial Electronics.* 40.1 (February 1993): 23-36.

[66] Vinada, S., 'Power Factor Correction in Power Conversion Applications Using the dsPIC® DSC.' *Microchip Technology Inc..* (2007): 1-10.

[67] Wai, R. J., C. Y. Lin, L. W. Liu, and Y. R. Chang. 'High-efficiency single-stage bidirectional converter with multi-input power sources.' *The Institution of Engineering and Technology.* (2007).

[68] Wang, H., L. Jinjun, and W. Runxin. 'Stability Issue and Corresponding Design Considerations in A System of Cascaded Bidirectional DC/DC Converters.' *IEEE.* (2008): 2813-2818.

[69] Wenguang, Y., H. Jangang, V. Utkin, and X. Longya. 'Sliding Mode Pulsewidth Modulation.' *IEEE Transactions on Power Electronics.* 23.2 (March 2008): 619-626.

[70] Xiaofeng, Z., W. Chen, and L. Zhengyu. 'Key Technologies of Digital-Current-Controlled Bidirectional DC-DC Converter in the Hybrid Electric Vehicle.' *IEEE.* (2008): 3104-3109.

[71] Xiaoquin, W., C. T. Tse, O. Dranga, and J. Lu. 'Fast-Scale Instability of Single-Stage Power-Factor-Correction Power Supplies.' *IEEE Transaction on Circuits and Systems - I: Regular Papers.* 53.1 (January 2006): 204-213.

[72] Xie, M., L. Bing, D. Wei, and C. Lee Fred. 'Novel Current-Loop Feed-Forward Compensation for Boost PFC Converter.' *IEEE.* (2004) 750-755 .

[73] Young-Joo, and L., A. Emadi. 'Integrated Bi-Directional AC/DC and DC/DC Converter for Plug-in Hybrid Electric Vehicle Conversion.' *IEEE.* (2007): 215-222.

[74] Yu, N., J. Xu. 'Study on Switching Power Converter with Discrete Global Sliding Mode Control.' *IEEE ICIEA.* (2009): 3394-3398.

[75] Zhang, F., J. Xu, Z. Guohua, and Y. Jing. 'Transient Performance Improvement for Digital Control Boost Power Factor Correction Converters.' *IEEE IPEMC.* (2009): 1693-1696.